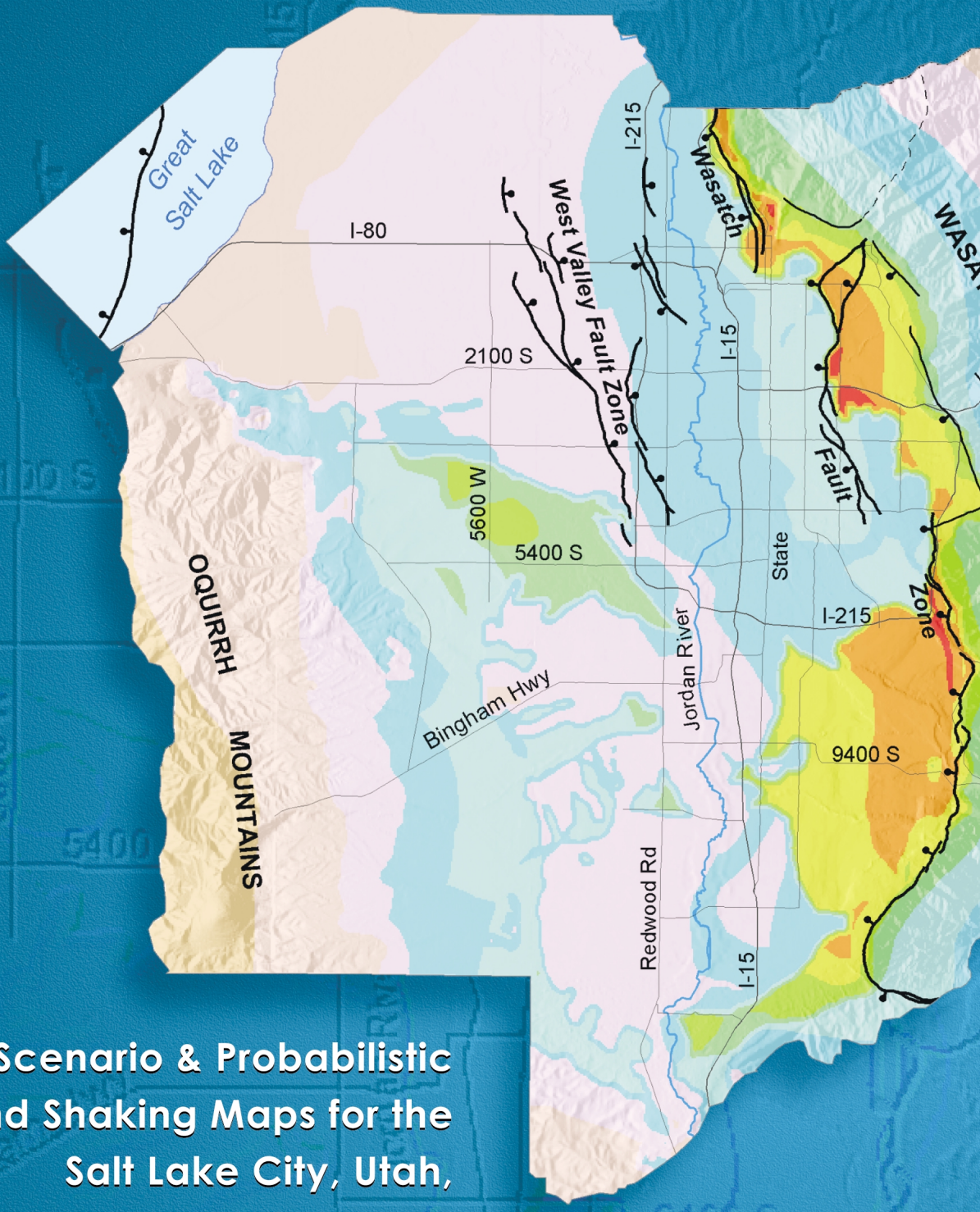

Earthquake Scenario & Probabilistic Ground Shaking Maps for the Salt Lake City, Utah, Metropolitan Area

By:

Ivan Wong, Walter Silva, Susan Olig, Patricia Thomas, Douglas Wright, Francis Ashland, Nick Gregor, James Pechmann, Mark Dober, Gary Christenson, Robyn Gerth

Earthquake Scenario & Probabilistic Ground Shaking Maps for the Salt Lake City, Utah, Metropolitan Area

UGS MP 02-5

Earthquake Scenario and Probabilistic Ground Shaking Maps for the Salt Lake City, Utah, Metropolitan Area

by
Ivan Wong,[1] Walter Silva,[2] Susan Olig,[1] Patricia Thomas,[1] Douglas Wright,[1] Francis Ashland,[3]
Nick Gregor,[2] James Pechmann,[4] Mark Dober,[1] Gary Christenson,[3] and Robyn Gerth[1]

ISBN 1-55791-666-7

Miscellaneous Publication 02-5
UTAH GEOLOGICAL SURVEY
a division of
Utah Department of Natural Resources
2002

[1] Seismic Hazards Group, URS Corporation, 500 12th Street, Suite 200, Oakland, CA 94607
[2] Pacific Engineering & Analysis, 311 Pomona Avenue, El Cerrito, CA 94530
[3] Utah Geological Survey, 1594 . North Temple, Salt Lake City, UT 84116
[4]Seismic Stations, University of Utah, Salt Lake City, UT 84112

UTAH GEOLOGICAL SURVEY

The **UTAH GEOLOGICAL SURVEY** is organized into five geologic programs with Administration and Editorial providing necessary support to the programs. The **ENERGY & MINERAL RESOURCES PROGRAM** undertakes studies to identify coal, geothermal, uranium, hydrocarbon, and industrial and metallic resources; initiates detailed studies of these resources including mining district and field studies; develops computerized resource data bases, to answer state, federal, and industry requests for information; and encourages the prudent development of Utah's geologic resources. The **GEOLOGIC HAZARDS PROGRAM** responds to requests from local and state governmental entities for engineering-geologic investigations; and identifies, documents, and interprets Utah's geologic hazards. The **GEOLOGIC MAPPING PROGRAM** maps the bedrock and surficial geology of the state at a regional scale by county and at a more detailed scale by quadrangle. The **GEOLOGIC INFORMATION & OUTREACH PROGRAM** answers inquiries from the public and provides information about Utah's geology in a non-technical format. The **ENVIRONMENTAL SCIENCES PROGRAM** maintains and publishes records of Utah's fossil resources, provides paleontological and archeological recovery services to state and local governments, conducts studies of environmental change to aid resource management, and evaluates the quantity and quality of Utah's ground-water resources.

The UGS Library is open to the public and contains many reference works on Utah geology and many unpublished documents on aspects of Utah geology by UGS staff and others. The UGS has several computer databases with information on mineral and energy resources, geologic hazards, stratigraphic sections, and bibliographic references. Most files may be viewed by using the UGS Library. The UGS also manages the Utah Core Research Center which contains core, cuttings, and soil samples from mineral and petroleum drill holes and engineering geology investigations. Samples may be viewed at the Utah Core Research Center or requested as a loan for outside study.

The UGS publishes the results of its investigations in the form of maps, reports, and compilations of data that are accessible to the public. For information on UGS publications, contact the Natural Resources Map/Bookstore, 1594 W. North Temple, Salt Lake City, Utah 84116, (801) 537-3320 or 1-888-UTAH MAP. E-mail: nrugs.geostore@state.ut.us and visit our web site at mapstore.utah.gov.

UGS Editorial Staff

J. Stringfellow ..... Editor
Vicky Clarke, Sharon Hamre ..... Graphic Artists
Patricia H. Speranza, James W. Parker, Lori Douglas ..... Cartographers

TABLE OF CONTENTS

TABLES

FIGURES

PLATES

(on CD in pocket)

ABSTRACT

The Salt Lake City metropolitan area is one of the most seismically hazardous urban areas in the interior of the western U.S. because of its location within the Intermountain Seismic Belt and its position adjacent to the active Wasatch fault. The elapsed time since the last large earthquake on the Salt Lake City segment of the Wasatch fault is approaching the mean recurrence interval based on the short-term paleoseismic record. In order to help raise the awareness of the general public and to help reduce earthquake risk in this area, we have developed nine microzonation maps showing surficial ground-shaking hazard. The maps are GIS-based and incorporate the site response effects of the unconsolidated sediments that underlie most of the metropolitan area within Salt Lake Valley. These nine maps, at a scale of 1:75,000, make up three sets, each consisting of three maps that display color-contoured ground motions in terms of (1) peak horizontal acceleration, (2) horizontal spectral acceleration at a period of 0.2 sec (5 Hz) and, (3) horizontal spectral acceleration at a period of 1.0 sec (1 Hz). One set of maps consists of deterministic or "scenario" maps for a moment magnitude (**M**) 7.0 earthquake on the Salt Lake City segment of the Wasatch fault. The two other sets are probabilistic maps for the two return periods of building code relevance, 500 and 2,500 years.

In the probabilistic seismic hazard analysis, a total of 35 faults were characterized in terms of their probability of activity, geometry, rupture behavior (including segmentation), maximum earthquake magnitude, recurrence model, and recurrence rates. Large variations in fault slip rates or recurrence intervals were incorporated into the input wherever appropriate using a variety of approaches, including time-dependent analyses. Background earthquakes ($\mathbf{M} \leq 6\frac{1}{2}$) were also included in the hazard analysis through the use of an areal source zone and Gaussian smoothing of the historical seismicity.

For both the scenario earthquake and the probabilistic analysis, ground motions on rock were calculated using a combination of state-of-the-art empirical attenuation relationships, which were generally applicable to extensional tectonic regimes, and a stochastic numerical modeling approach. Because of Salt Lake City's location in a sedimentary basin, site response effects on ground motions can be significant. To include these effects, five generalized site response units were defined from lithologic characteristics and shear-wave velocities. Based on a suite of *in situ* shear-wave profiles and dynamic material properties for each unit, amplification factors were calculated as a function of input rock motion and thickness of each site response unit. These amplification factors, some of which are less than 1.0 (signifying deamplification), were multiplied by the input rock motions to arrive at the surficial ground motions.

The resulting hazard maps dramatically show the frequency-dependent amplification of unconsolidated sediments in the Salt Lake Valley. The pattern of both amplification and deamplification in the map area is clearly a function of the distribution and thickness of the surficial geologic units. Hanging wall effects are also evident on the hazard maps but are masked to a large extent by the site effects. Peak horizontal accelerations for the scenario earthquake range up to and exceed 1.0 g. For the 500- and 2,500-year return period maps, the maximum peak accelerations are 0.5 and 1.1 g, respectively.

These maps are not intended to be a substitute for site-specific studies for engineering design nor to replace standard maps commonly referenced in building codes. Rather, we hope that these maps will be used as a guide by government agencies, the engineering, urban planning, and emergency preparedness and response communities, and the general public as part of an overall program to reduce earthquake risk and losses in Utah.

Limitations

There are uncertainties associated with earthquake ground motion prediction in Utah due to limited region-specific information and data on the characteristics of seismic sources and ground motion attenuation. Additional uncertainty stems from the characterization of the subsurface geology beneath the map area and the estimation of the associated site response effects on ground motions. Thus the maps should not be used directly for site-specific design or in place of site-specific hazard evaluations.

INTRODUCTION

The Salt Lake City metropolitan area is situated within the southern portion of the Intermountain Seismic Belt (ISB), one of the most seismically active regions in the interior of the western U.S. (Smith and Arabasz, 1991). Additionally, the Salt Lake Valley region includes many faults that have been repeatedly active in the late Quaternary (past 130,000 years) (figure 1). The most significant fault in the region in terms of ground shaking hazard is the Wasatch fault zone. The 343-km-long, westward-dipping Wasatch fault zone consists of several segments that probably rupture independently of each other. The central, more active segments are capable of generating moment magnitude (**M**) 7.0 or larger earthquakes (Machette et al., 1991, 1992). Recent observations from paleoseismic trenches across the southern Salt Lake City segment, which extends along the eastern border of the Salt Lake Valley, suggest that large earthquakes occur more frequently than previously suspected, with an estimated average recurrence interval during the past 6,000 years of 1,350 ± 200 years (Black et al., 1996). The elapsed time since the last large earthquake on this segment is about 1,230 ± 60 years and so this value is approaching the mean recurrence interval. Two other significant faults in the study area are the Oquirrh-East Great Salt Lake and West Valley fault zones (figure 1).

The effects on ground motions from source, path, and site conditions need to be incorporated into any seismic hazard analysis. Near-surface site amplification (Wong and Silva, 1993) and possibly basin amplification (Olsen et al., 1995, 1996) are also significant factors affecting the ground shaking hazard in the Salt Lake Valley. Some empirical observations (e.g., Abrahamson and Silva, 1997) and numerical modeling results (Wong and Silva, 1993; Wong et al., 1995) suggest that near-source effects such as rupture directivity and hanging-wall effects may also be significant in the Salt Lake Valley.

This report provides estimates of strong ground shaking for the Salt Lake City metropolitan area based on the most recent information on seismic sources, crustal attenuation, and near-surface geology. Recent information on Quaternary faulting and a historical earthquake catalog for the Utah region for the period 1962 to 1998 were used in the hazard analysis. Background seismicity not associated with known faults is abundant within this portion of the ISB and thus is also included in the hazard evaluations.

Using both deterministic and probabilistic seismic hazard analyses, we developed a total of nine microzonation maps for earthquake ground shaking hazard. The map area is shown in figure 1. The concept of microzonation used in this study is intended to identify zones, on the order of 500 m and larger (several city blocks), which are characterized by different levels of ground shaking hazard. (An example of macrozonation would be the seismic zones used in the Uniform Building Code.) The maps include (1) earthquake scenario maps for a **M** 7.0 earthquake along the Salt Lake City segment of the Wasatch fault and (2) probabilistic maps for the two return periods of building code relevance, 500 and 2,500 years (10% and 2% probability of exceedance in 50 years, respectively). The GIS-based maps display peak horizontal acceleration (defined at 100 Hz) and horizontal spectral accelerations at periods of 0.2 and 1.0 sec (5 Hz and 1 Hz, respectively) at the ground surface.

These maps are intended to illustrate the intensity and variability of ground shaking within the map area for the scenario earthquake as well as for two annual exceedance probabilities. The maps are intended for a number of uses such as increasing general public awareness of earthquake hazards, urban planning, selecting facility sites, assisting in mitigation planning for lifelines, and aiding emergency preparedness, response, and loss estimation. Although we believe the maps represent the state-of-the-art in ground motion modeling for the area, the maps are not intended to be used directly in engineering design. Various codes such as the Uniform Building Code define minimum design ground motion levels for buildings, bridges, and other structures, and commonly reference other maps to determine these design levels. Our maps do not replace these design maps, but can be used to compare with code-based design, and to evaluate the need for increasing design levels if indicated.

We hope that these maps will be used by all those interested in earthquake hazard mitigation in the Salt Lake City metropolitan area. Although the intended users of these maps and readers of this report will vary considerably in their technical knowledge, the following is a technical description of the approach used in the map development and some important aspects of the resulting maps. For additional details, please contact the authors.

SEISMOTECTONIC SETTING AND HISTORICAL SEISMICITY

The Salt Lake Valley lies in the central Wasatch Front portion of the southern ISB, a region undergoing east-west extension (Zoback, 1983; Bjarnason and Pechmann, 1988). The ISB is a north-south-trending zone of shallow, diffuse, intraplate seismicity that extends from Montana, through central Utah, into southern Nevada and northern Arizona (Smith and Arabasz, 1991). The ISB is further characterized by late Cenozoic normal faulting and episodic surface-faulting earthquakes (**M** 6½ and greater).

The central Wasatch Front straddles the Basin and Range Province to the west and the Middle Rocky Mountains Province to the east, with the Wasatch fault zone marking the physiographic boundary between them. The Wasatch fault is the longest, most active fault in the region (Hecker, 1993), with vertical slip rate estimates ranging from about 0.3 to over 2 mm/yr during the past 20 ka (Machette et al., 1992).

Seismological (Arabasz et al., 1992) and geological (Hecker, 1993) characteristics of the Wasatch Front include: (1) dominantly normal slip on generally north-south-striking Quaternary faults; (2) moderate background seismicity (for comparison, the background seismicity along the Wasatch Front is lower by a factor of four than that along the San Andreas fault system in California); (3) diffuse seismicity that generally does not correlate with mapped Quaternary faults and is typically located at focal depths of less than 15 to 20 km; (4) relatively long and often variable recurrence intervals for surface faulting on individual fault segments (typically more than 1,000 years); (5) vertical slip rates for late

Quaternary faults of typically less than 2 mm/yr; and (6) the historical absence of any surface-faulting earthquake larger than the 1934 **M** 6.6 Hansel Valley earthquake, despite the presence of abundant late-Pleistocene and Holocene fault scarps.

The largest historical earthquake in the Wasatch Front region was the 1934 Hansel Valley earthquake (figure 2). During historical times in the Salt Lake Valley, only three earthquakes have exceeded Richter magnitude (M_L) 5 and none has been greater than M_L 6 - 22 May 1910, M_L 5.7; 22 February 1943, M_L 5.0; and 5 September 1962, M_L 5.2 (Richins, 1979; Arabasz and McKee, 1979; Hopper, 2000) (figure 2). This historical record stands in sharp contrast to the geologic evidence for repeated **M** 7 and greater earthquakes occurring along the Wasatch fault zone. Although the 1910 and 1943 earthquakes occurred in the vicinity of the Wasatch fault, it is arguable whether this fault was the source of these events. In the 1910 earthquake, a maximum Modified Mercalli (MM) intensity of VII was observed in Salt Lake City. The 1910 event damaged several buildings in Salt Lake City, shaking plaster from ceilings and toppling chimneys (Hopper, 2000).

METHODOLOGY AND INPUT TO HAZARD CALCULATIONS

There were six principal tasks in this study: (1) seismic source characterization; (2) definition and characterization of geologic site response categories and assignment of amplification factors; (3) seismic attenuation characterization; (4) scenario and probabilistic ground motion calculations; (5) map development; and (6) production of the final report.

Seismic Source Characterization

The first step in any assessment of earthquake ground-shaking hazards is a characterization of the seismic sources which will produce ground motions of engineering significance at the site or area of interest. Seismic source characterization is concerned with three fundamental elements: (1) the identification, location, and geometry of significant sources of earthquakes; (2) the maximum size distribution of earthquakes for each source; and (3) the rate at which different-size earthquakes occur in each source. For an earthquake scenario analysis, only the characterization of a single seismic source is required. Parameters needed are fault location, geometry, orientation, sense of slip, and maximum earthquake magnitude (M_{max}). No recurrence rate information is used in a scenario analysis.

In a probabilistic hazard assessment of earthquake ground motions, all seismic sources that can generate significant ground shaking at a site (generally those within a distance of 100 to 200 km in the western U.S.) are characterized. The study region for this analysis is shown in figure 1. Two general types of seismic sources were considered in the probabilistic hazard analysis: active or seismogenic faults and an areal source zone.

Uncertainties in the seismic source parameters as described below, which were sometimes large, were incorporated into the probabilistic seismic hazard analysis using a logic tree approach. In this procedure, values of the source parameters are represented by the branches of logic trees with weights that define the distribution of values. A sample logic tree for a fault is shown in figure 3. In general, three values for each parameter were weighted and used in the analysis. Statistical analyses by Keefer and Bodily (1983) indicate that a three-point distribution of 5th, 50th, and 95th percentiles weighted 0.185, 0.63, and 0.185 (rounded to 0.2, 0.6, and 0.2), respectively, is the best discrete approximation of a continuous distribution. Alternatively, they found that the 10th, 50th, and 90th percentiles weighted 0.3, 0.4, and 0.3, respectively, can be used when limited available data make it difficult to determine the extreme tails (i.e., the 5th and 95th percentiles) of a distribution. Note that the weights associated with the percentiles are not equivalent to probabilities for these values, but rather are weights assigned to define the distribution. We generally applied these guidelines in developing distributions for seismic source parameters with continuous distributions (e.g., M_{max}, fault dip, slip rate or recurrence) unless the available data suggested otherwise. Estimating the 5th, 95th, or even 50th percentiles is typically challenging and involves subjective judgement given limited available data.

The following discussion focuses on the seismic source characterization for the probabilistic hazard analysis. The single values used in the scenario ground motion estimation are discussed in the section "Scenario Ground Motions." The source parameters for the significant faults in the study region and the areal source zone representing background earthquakes were estimated and used in the probabilistic analyses. All seismic sources were assigned a maximum seismogenic depth of 13, 15, and 17 km, weighted 0.1, 0.7, and 0.2, respectively (figure 3). This distribution was primarily based on the distribution of well-determined earthquake focal depths in the Wasatch Front region.

This analysis expands on our previous probabilistic hazard studies in the region (Wong et al., 1995; Woodward-Clyde Federal Services, 1998), including recent probabilistic analyses of four U.S. Bureau of Reclamation dams in the back valleys of the Wasatch Front (e.g., Wong et al., 2001a, b).

Quaternary Faults

Below we describe the general attributes of our fault source characterization and our rationale for many of these attributes. We then briefly discuss the most significant faults in the study region: the Wasatch, Oquirrh-East Great Salt Lake, and West Valley fault zones. To update the input from our previous analyses we reviewed fault information from numerous recent studies (e.g., Hylland et al., 1995; Black et al., 1996, 2000; Geomatrix Consultants, 1999; Harty et al., 1997; Solomon, 1996, 1998, 1999; Mohapatra and Johnson, 1998; Coogan and King, 1999; Dinter and Pechmann, 1999, 2000; Olig et al., 1999a, 1999b, 2000). We also contacted numerous geoscientists regarding their unpublished and ongoing work in the region, including: Walter Arabasz, Ann Mattson, and Bob Smith, University of Utah; Bill Black, Jim Coogan, Jon King, Mike Hylland, and Barry Solomon, Utah Geological Survey (UGS); Anke Friedrich, Caltech; Jennifer Helm, AMEC Earth & Environmental; Jim McCalpin, GEO-

HAZ Consulting; and Craig Nelson, URS Corporation. We included 35 potential fault sources in this analysis. Figure 1 shows the location of all the potential fault sources and table 1 summarizes the fault source parameters used in our analysis. Fault nomenclature shown in table 1 and on figure 1 generally follows that used by Hecker (1993) except as noted.

We considered potential Quaternary fault sources as far away as 150 km from the study area. Faults were included that we judged could potentially contribute to the probabilistic hazard because of their activity, length, or proximity to the study area. We included all longer (>5 km) faults suggesting or showing evidence for repeated Quaternary activity that are within 50 km of the study area. We did not include faults ≤ 5 km long as independent sources because they are considered to be accounted for by the areal source zone.

Where the data permit, we have attempted to consider and accommodate the structural variations that are potentially significant to the hazard analysis by including a variety of rupture behavior models and fault geometries in our source characterization (table 1). All faults are dominantly normal-slip faults that we modeled as single planes, zones (multiple planes), or curvilinear surfaces. Most faults are included as single independent (unsegmented) planar sources, unless the available data suggest otherwise. Zones of faults are modeled as multiple fault planes that do not coseismically rupture as in the linked model, but rather have the assigned moment rate distributed evenly among the planes.

The closest and most active faults and fault segments were modeled as curvilinear surfaces and these are shown in italics on table 1. To model the curvilinear nature of normal faults, we digitized the primary, most-active fault trace and projected these curves down-dip using a weighted mean strike. Thus, these simple curvilinear surfaces retain a constant dip and do not accommodate complexities like listric faults (i.e., decreasing dip with depth). All surfaces, planar and curvilinear, extend the full depth of the crust, and so fault dips are averages estimated over the full depth of the seismogenic crust. For most typical range-bounding normal faults, preferred dips are assumed to be 55° unless noted otherwise (table 1, footnote 4).

Alternative rupture behavior models to the single-plane, independent fault model include linked faults, segmented faults, and zones of faults (column 3 of table 1). Potentially linked faults may experience coseismic rupture (either along or across strike), whereas portions of potentially segmented faults may rupture independently of each other. Some faults show compelling evidence for being segmented (e.g., the Wasatch fault zone), where relatively persistent segment boundaries have apparently confined prehistoric surface ruptures to particular sections of the faults (Machette et al., 1991, 1992; Wheeler and Krystnik, 1992). For other faults, the evidence is more ambiguous as to whether persistent rupture segment boundaries exist (e.g., the Stansbury fault). Finally, we note that the rupture behavior of some of the faults in the region is poorly understood and may actually be more complex than our simplifying assumptions, but we have attempted to address uncertainties that are particularly significant to the hazard in the Salt Lake Valley, given the available data.

Preferred M_{max} values (weighted 0.6) were estimated using the empirical relationships of Wells and Coppersmith (1994) for all fault types as noted in footnotes of table 1. Distributions of ± 0.3 (each weighted 0.2) around the preferred M_{max} were included in our analysis to account for the various epistemic uncertainties in determining M_{max} for faults (e.g., dePolo and Slemmons, 1990). These include uncertainties associated with the regression relations used and the input parameters to those relations, insofar as uncertainties in maximum rupture lengths and/or displacements per event were not explicitly included.

In assigning probabilities of activity for each fault source, we considered both the likelihood that it is structurally capable of independently generating earthquakes (seismogenic), and the likelihood that it is still active within the modern stress field. We incorporated many factors in assessing these likelihoods, such as: orientation in the modern stress field, fault geometry (length, continuity, depth extent, and dip), relation to other faults, age of youngest movement, rates of activity, geomorphic expression, amount of cumulative offset, and any evidence for a non-tectonic origin. Faults with definitive evidence for repeated Quaternary activity were generally assigned probabilities of being active and seismogenic of 1.0 (table 1). Exceptions include faults that may be secondary and dependent on other faults (e.g., the Utah Lake faults), faults or suspected fault features that may have a non-seismogenic origin (e.g., scarps associated with the eastern Ogden Valley fault), and faults that may be too short to independently generate large earthquakes (≤ 10 km length). The probability of activity for faults that do not show definitive evidence for repeated Quaternary activity was individually judged based on available data and the criteria explained above. Resulting values range from 0.2 to 1.0 (table 1).

We considered truncated-exponential, characteristic, and maximum-magnitude recurrence models, with weights (see footnote 6 in table 1) depending on the fault length, type of data used to calculate rates of activity, and type of rupture model (as shown in column 3 of table 1). The truncated exponential recurrence model is the traditional Gutenberg-Richter exponential frequency-magnitude relationship (e.g., Arabasz et al., 1992) that is truncated at the maximum magnitude. As defined by Schwartz and Coppersmith (1984), the characteristic recurrence model was based on paleoseismic observations of similar-size displacements per event on faults, implying that surface faulting events more typically exhibited a "characteristic" magnitude rather than a full range of magnitudes, including more frequent moderate-sized (**M** 6 to 7) events, as inferred from extrapolating the historical record of seismicity and using the exponential model. Thus, the characteristic model predicts fewer moderate-size events and generally results in lower hazard than the truncated exponential model. We use the characteristic model of Youngs and Coppersmith (1985). The maximum-magnitude model is an extreme version of the characteristic model and assumes that a fault (or fault segment) only ruptures in its entirety in characteristic-sized events, and smaller events do not occur (e.g., Wesnousky, 1986; Wesnousky et al., 1983).

Observations of historical seismicity and paleoseismic

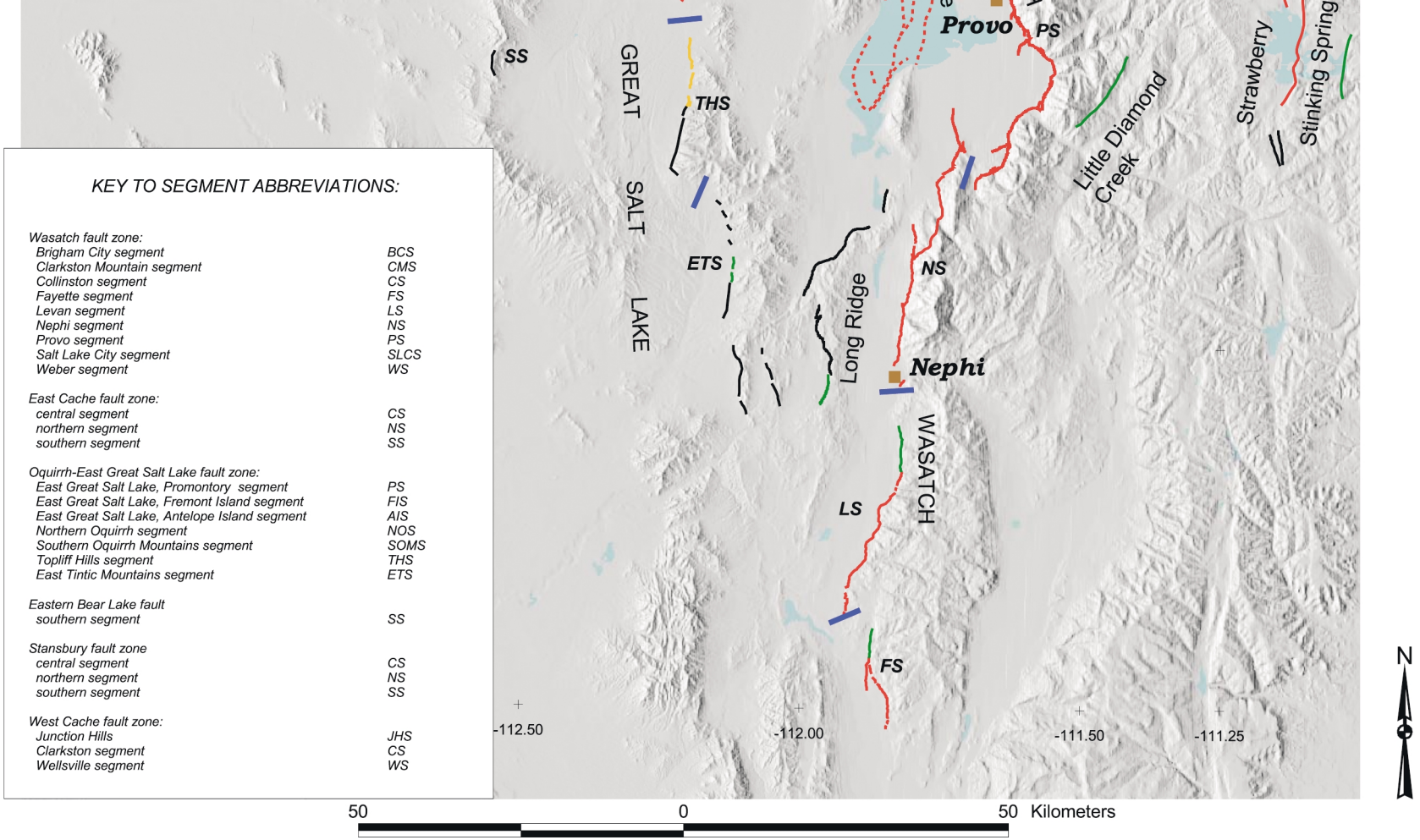

Figure 1. Quaternary faults in the Wasatch Front region included in the probabilistic seismic hazard analysis.

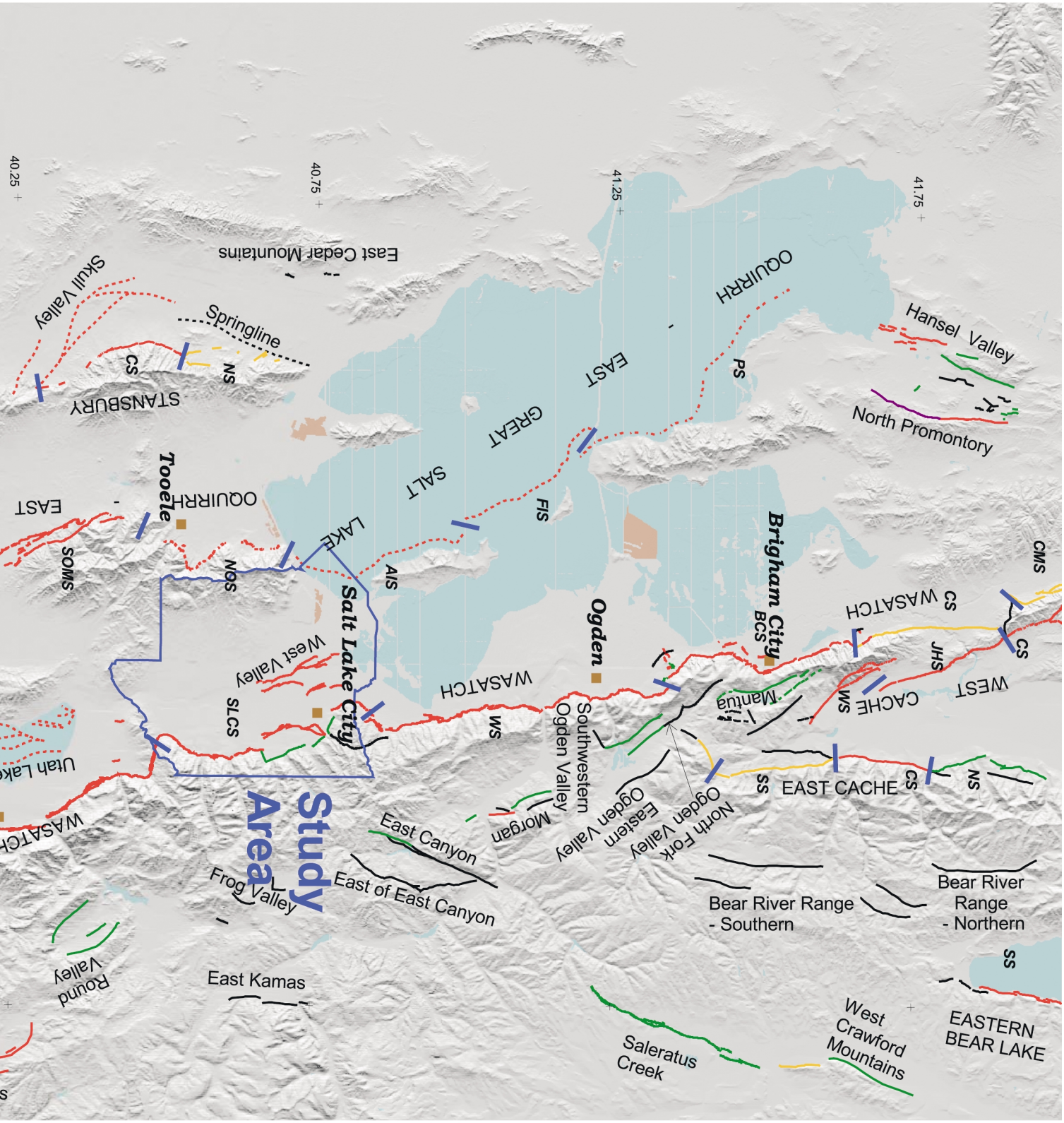
40.25
40.75
41.25
41.75
East Cedar Mountains
Skull Valley
Springline
CS
NS
STANSBURY
Hansel Valley
North Promontory
OQUIRRH
EAST
PS
GREAT
SALT
LAKE
FIS
AIS
SOMS
NOS
Tooele
OQUIRRH
EAST
Brigham City
BCS
CMS
WASATCH
CS
JHS
WEST
CACHE
SM
Salt Lake City
West Valley
SLCS
Ogden
WASATCH
SM
Mantua
Southwestern Ogden Valley
Eastern Ogden Valley
North Fork Ogden Valley
SS
EAST CACHE
CS
NS
Utah Lake
WASATCH
Study Area
Morgan
East Canyon
East of East Canyon
Frog Valley
Bear River Range - Southern
Bear River Range - Northern
SS
Round Valley
East Kamas
Saleratus Creek
West Crawford Mountains
EASTERN BEAR LAKE


Study Area
Salt Lake City
Ogden
Brigham City
Tooele
GREAT SALT LAKE
41.75
41.25
40.75

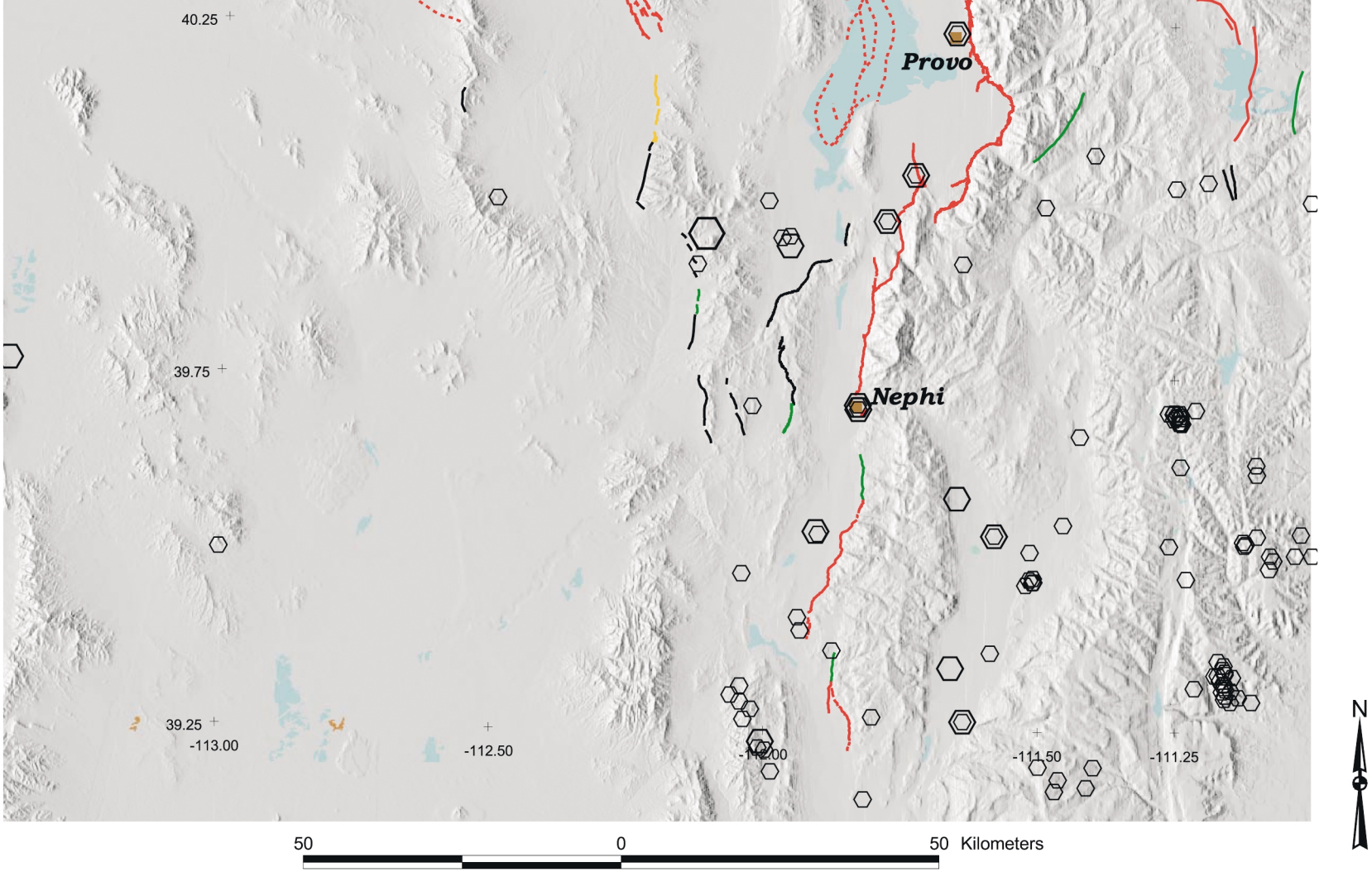

Legend

Fault Age

- Holocene to latest Pleistocene (red) 0 - 30,000 years ago
- Late Pleistocene (orange) 10,000 - 130,000 years ago
- Mid to Late Pleistocene (green) 10,000 - 750,000 years ago
- Early to Mid Pleistocene (purple) 130,000 - 1,650,000 years ago
- Quaternary (black) < 1,650,000 years ago
- Mapped
- Concealed

Magnitude

- 3 - 3.9
- 4 - 4.9
- 5 - 5.9
- 6 - 7

Base Map Data from the Utah Automated Geographic Reference Center (AGRC)

Fault Data Sources: Hecker, 1993; Geomatrix Consultants, 1999; Olig et al., 1999a; Coogan and King, 1999; J.C. Pechmann, written communication, 2000; J.L. Jarva, digital communication, 2000.

Seismicity Data Source: UUSS

*Figure 2. Historical seismicity (**M** ≥ 3.0) of the Wasatch Front region, 1850 to 1998. Only independent mainshocks are plotted.*

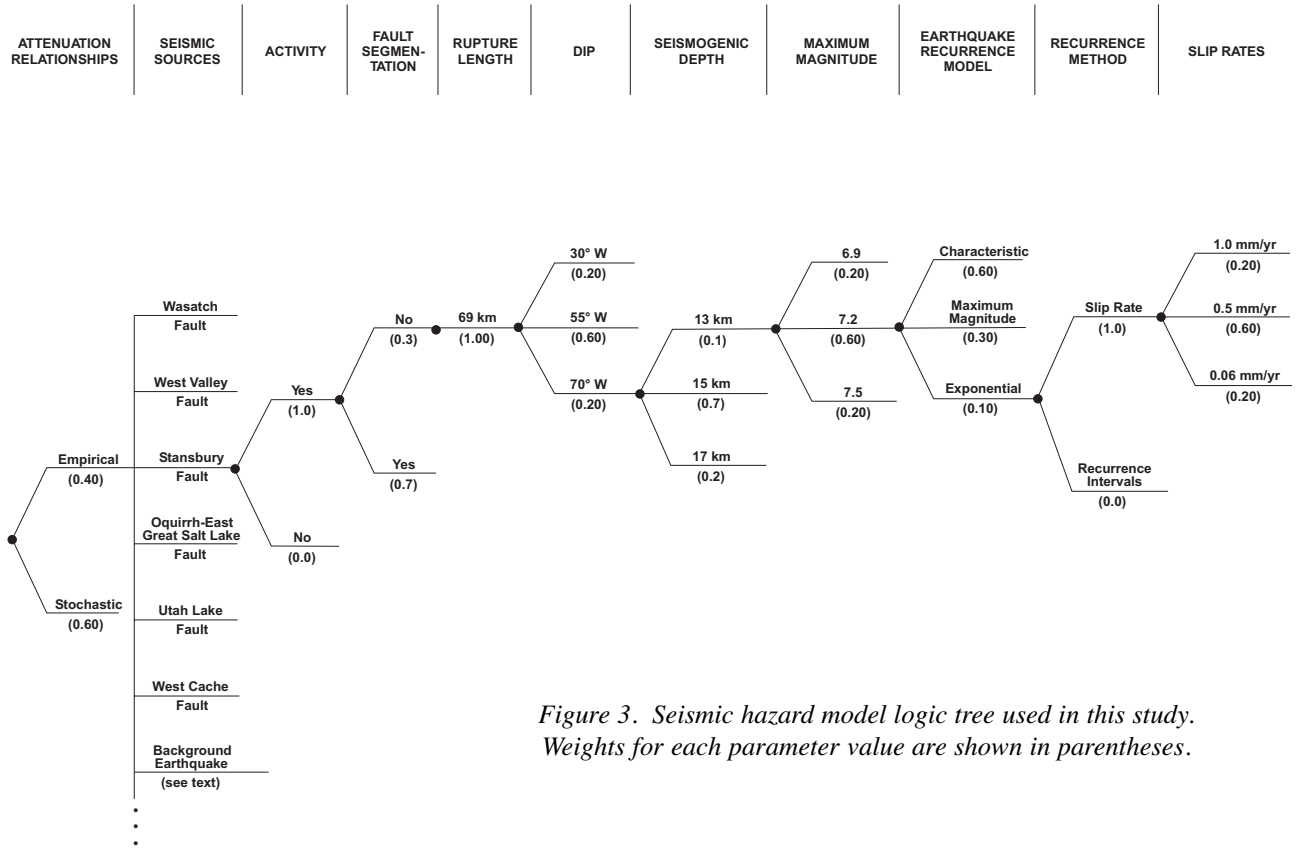

Figure 3. Seismic hazard model logic tree used in this study. Weights for each parameter value are shown in parentheses.

investigations in the Wasatch Front region suggest that characteristic behavior is more likely for individual faults, whereas seismicity in zones best fits a truncated exponential model (Schwartz and Coppersmith, 1984; Arabasz et al., 1992; Hecker, 1993). Therefore, except for zones of faults, we generally favored the characteristic model of Youngs and Coppersmith (1985) for all fault sources by giving it weights of 0.6 to 0.8. We assigned equal weights to the exponential and characteristic models for zones of faults (see footnote 6 of table 1). We assigned a slightly higher weight to the maximum-magnitude model than to the exponential model for longer, segmented faults (0.2 versus 0.1), but for shorter independent faults we assigned both models an equal weight of 0.2. This choice was based on the idea that as faults develop, become longer and eventually segmented, their behavior may evolve to become less exponential and more characteristic (e.g., Wesnousky, 1990, 1994; Stirling et al., 1996). On faults for which recurrence intervals of maximum earthquakes were derived from data of such earthquakes rather than slip rates, we weighted the maximum-magnitude model 0.2 and the exponential model 0.0 (footnote 6, table 1) .

Depending on the quality and time-frame of the available data, we used both slip rates and/or recurrence intervals to characterize rates of activity, generally preferring the latter, based on arguments in Wong and Olig (1998). We incorporated all available intermediate- (≤ 1.6 Ma) and short-term-(≤ 130 ka) data in developing slip rate or recurrence distributions, but we generally preferred short-term data when available. In addition to the time period, we also considered the type and quality of data in determining slip or recurrence rates. We converted vertical slip rates to net (fault parallel) slip rates for most faults by assuming 100% dip slip and the preferred fault dips for each individual fault. Additionally, wherever possible we attempted to calculate or adjust for along-strike average slip rates (e.g., Weber segment of the Wasatch fault). Variations of displacements along strike can significantly affect the calculation of slip rates (Wong and Olig, 1998), but unfortunately very few faults have enough data to calculate average rates for the entire fault. More typically we found only a few data points for one or two sites along the fault or no fault-specific data at all. In the latter case, we assumed slip-rate distributions to be the same as a similar nearby structure, taking into account such factors as style of deformation, geomorphic expression, and age of youngest movement.

Wasatch Fault Zone

The Wasatch fault zone is the most studied Quaternary fault in Utah and the abbreviated information summarized here is primarily from Machette et al. (1991, 1992). However, we also evaluated new data from McCalpin et al. (1994), Black et al. (1996), McCalpin and Nishenko (1996), Harty et al. (1997), Lund and Black (1998), and McCalpin and Nelson (2000) in developing our model. This 343-km-long, west-dipping, range-bounding, normal fault strikes north-south through central Utah, separating the Basin and Range Province to the west from the Wasatch Range of the Middle Rocky Mountains Province to the east (figure 1).

A preponderance of evidence indicates that the fault is separated into segments with relatively persistent segment boundaries between prehistoric surface ruptures (Schwartz and Coppersmith, 1984; Machette et al., 1991, 1992; Wheeler and Krystinik, 1992). Initially, Schwartz and Coppersmith

Table 1. Source parameters for Wasatch Front faults included in the Salt Lake Valley analysis.

FAULT NO. [1]	FAULT NAME	RUPTURE MODEL	MAXIMUM RUPTURE LENGTH[2] (km)	MAXIMUM MAGNITUDE[3] (M)	DIP[4] (degrees)	APPROXIMATE AGE OF YOUNGEST OFFSET	PROBABILITY OF ACTIVITY[5]	RATE OF ACTIVITY[6] (mm/yr)	COMMENTS
12-18	Bear River Fault Zone	Independent (1.0)	40	6.8 (0.2) 7.1 (0.6)[7] 7.4 (0.2)	30 W (0.3) 55 W (0.6) 70 W (0.1)	Holocene	1.0	0.7 (0.2) 1.5 (0.6) 2.0 (0.2)	Preferred slip rate based on an average vertical offset of 3 m per event and a recurrence interval of 2,250 to 2,370 years (West, 1994). Maximum rate is based on analogy with the Wasatch fault zone. Shallower dips were slightly favored based on structural and seismotectonic arguments made by West (1994). Length and location from Plate 1 of West (1994).
11-07	Bear River Range faults – Northern zone	Zone (1.0)	19	6.3 (0.2) 6.6 (0.6) 6.9 (0.2)	30 W (0.2) 55 W (0.6) 70 W (0.2)	Quaternary (?)	0.5	0.03 (1.0)	Very little is known about these inferred Quaternary faults along escarpments in the Bear River Range (Sullivan et al., 1988), so we grouped them into two zones with the maximum magnitude based on the length of the longest individual fault trace in each zone. We assumed a slip rate and p(a) similar to the East Kamas fault.
11-07	Bear River Range faults – Southern zone	Zone (1.0)	22	6.3 (0.2) 6.6 (0.6) 6.9 (0.2)	30 W (0.2) 55 W (0.6) 70 W (0.2)	Quaternary (?)	0.5	0.03 (1.0)	
11-01, 11-02, 11-03, 11-12, 11-13	East Cache fault zone (includes the James Peak and Broadmouth Canyon faults)	Unsegmented (0.3)	84	7.0 (0.2) 7.3 (0.6) 7.6 (0.2)	30 W (0.2) 55 W (0.6) 70 W (0.2)	Holocene	1.0	0.04 (0.2) 0.3 (0.6) 1.0 (0.2)	We modeled the northern end extending into Idaho, as mapped by Westaway and Smith (1989). We included the James Peak and Broadmouth Canyon faults at the southern end as mapped by Nelson and Sullivan (1992). The segmentation model is after McCalpin and Forman (1991). Slip rate distributions based on: (1) 4.2 m of vertical offset of 15.5 ka deposits along the central segment; (2) 1.65 m of vertical offset during the penultimate earthquake cycle (10.3 ky long) on the central segment (McCalpin, 1994); (3) 400 to 500 m of vertical offset of 1 to 2 Ma deposits, and 20 m of vertical offset of 200 to 400 ka deposits along the northern segment (McCalpin, 1994); (4) 10 m of vertical offset of 150 to 1000 ka deposits on the southern segment (McCalpin and Forman, 1991); and (5) 4.2 m of vertical offset of ~140 ka deposits on the James Peak fault (Nelson and Sullivan, 1992). The maximum slip rate (1mm/yr) assumes activity on the East Cache fault zone increases to approach slip rates of nearby faults to alleviate a possible late Pleistocene slip deficit on the East Cache fault zone (McCalpin and Forman, 1991).
		Segmented (0.7)	Northern Segment - 37	6.6 (0.2) 6.9 (0.6) 7.2 (0.2)		Mid Pleistocene	(same for all segments)	0.04 (0.2) 0.2 (0.6) 1.0 (0.2)	
			Central Segment - 18	6.5 (0.2) 6.8 (0.6)[8] 7.1 (0.2)		Holocene		0.04 (0.2) 0.3 (0.6) 1.0 (0.2)	
			Southern Segment - 29	6.6 (0.2) 6.9 (0.6)[9] 7.2 (0.2)		Late Pleistocene		0.04 (0.2) 0.08 (0.6) 1.0 (0.2)	
12-16, 12-17	East Canyon fault (includes northern [12-16] and southern [12-17] sections)	Linked (1.0)	26	6.4 (0.2) 6.7 (0.6) 7.0 (0.2)	30 E (0.2) 55 E (0.6) 70 E (0.2)	Late Quaternary	0.9	0.01 (0.3) 0.04 (0.4) 0.2 (0.3)	We assumed the northern and southern sections are linked based on short lengths and their geometric association (Sullivan et al., 1988). We also assumed a similar slip rate to the Morgan fault based on similar geomorphic expression for the southern section, but assigned a slightly lower p(a) because of the poorer geomorphic expression of the northern section which is likely less active (Sullivan et al., 1988).
7-09	East Cedar Mountains fault	Independent (1.0)	12	6.0 (0.2) 6.3 (0.6) 6.6 (0.2)	55 E (0.3) 70 E (0.4) 80 E (0.3)	Quaternary (?)	0.7	0.1 (0.2) 0.05 (0.6) 0.1 (0.2)	Although Geomatrix Consultants (1999) found no surficial evidence for Quaternary offsets along the east side of the Cedar Mountains, neither could they preclude Quaternary activity. Therefore we included this distant postulated fault for completeness and consistency. However, note that our maximum rupture length is based on Hecker (1993), rather than extending the fault along the entire range front (Geomatrix Consultants, 1999). We assigned rates of activity based on estimates of Geomatrix Consultants (1999). We assumed steeper dips than typical range-bounding faults because of the geometrical constraints necessary if this fault is truly independent of the west-dipping Stansbury fault to the east.

FAULT NO. [1]	FAULT NAME	RUPTURE MODEL	MAXIMUM RUPTURE LENGTH[2] (km)	MAXIMUM MAGNITUDE[3] (M)	DIP[4] (degrees)	APPROXIMATE AGE OF YOUNGEST OFFSET	PROBABILITY OF ACTIVITY[5]	RATE OF ACTIVITY[6] (mm/yr)	COMMENTS
11-08	Eastern Bear Lake fault	Segmented (0.7)	Southern Segment – 32	6.8 (0.2) 7.1 (0.6)[10] 7.4 (0.2)	30 W (0.4) 50 W (0.4) 60 W (0.2)	Late Holocene	1.0	0.4 (0.2) 1.0 (0.6) 2.0 (0.2)	Segmentation model and lengths from McCalpin (1993). Dips based on cross-sections of Evans (1991). Slip rate distribution based on data from McCalpin (1993). Due to the sparcity of data for the central and northern segments, the same slip rates were assumed for all segments and the unsegmented model.
			Central Segment - 26	6.8 (0.2) 7.1 (0.6)[11] 7.4 (0.2)	(same for all segments)	Holocene (?)	1.0	(same for all segments)	
			Northern Segment - 57	6.9 (0.2) 7.2 (0.6)[11] 7.5 (0.2)		Late Quaternary (?)	1.0		
		Unsegmented (0.3)	58 (1.5 times average segment length)	6.9 (0.2) 7.2 (0.6) 7.5 (0.2)		Holocene	1.0		
11-15	Eastern Ogden Valley fault	Independent (1.0)	13	6.1 (0.2) 6.4 (0.6) 6.7 (0.2)	30 E (0.2) 55 E (0.6) 70 E (0.2)	Quaternary (?)	0.5	0.03 (1.0)	Holocene scarps mapped by Sorenson and Crittenden (1979) are likely related to mass-wasting, not fault offset (Sullivan et al., 1988). Based on this, and a range front morphology that suggests an absence of late Quaternary faulting, we assigned a p(a) of 0.5 and a maximum slip rate of 0.03 mm/yr (<3 m vertical offset since 130 ka).
12-11	East Kamas fault	Independent (1.0)	15	6.1 (0.2) 6.4 (0.6) 6.7 (0.2)	30 W (0.2) 55 W (0.6) 70 W (0.2)	Quaternary (?)	0.5	0.03 (1.0)	Deposits estimated to be 130 to 140 ka appear unfaulted and older degraded scarps are more likely related to erosion than fault displacement (Sullivan et al., 1988). Based on this and a more degraded escarpment morphology than the Morgan fault (Sullivan et al., 1988), we assumed a maximum slip rate of 0.03 mm/yr (<3 m vertical offset since 130 ka).
Not Applicable	Fault east of East Canyon	Independent (1.0)	25	6.0 (0.2) 6.2 (0.6) 6.7 (0.2)	30 W (0.2) 55 W (0.6) 70 W (0.2)	Quaternary (?)	0.2	0.03 (1.0)	Fault geometry (including total fault length) based on mapping by Coogan and King (1999) and Bryant (1990). However, the preferred maximum magnitude is based on the length of the suspected Quaternary portion as mapped by Sullivan et al. (1988) for the northern northwesterly trending portion. This is the only portion that shows geomorphic expression or suggestive evidence for Quaternary activity (J. King, UGS, personal communication, 4-3-00; J. Coogan, UGS affiliate, personal communication, 4-3-00). Due to a lack of slip rate data, we assumed a distribution similar to the East Kamas fault. The low p(a) for this suspected Quaternary fault is based on its relatively poor geomorphic expression and lack of associated scarps, the possibility that it may be antithetic to the East Canyon fault, and that proprietary seismic lines which indicate that it soles into a salt bed within the Pruess Formation between 4 to 5 km depth (J. Coogan, personal communication, 4-3-00).

FAULT NO. [1]	FAULT NAME	RUPTURE MODEL	MAXIMUM RUPTURE LENGTH[2] (km)	MAXIMUM MAGNITUDE[3] (M)	DIP[4] (degrees)	APPROXIMATE AGE OF YOUNGEST OFFSET	PROBABILITY OF ACTIVITY[5]	RATE OF ACTIVITY[6] (mm/yr)	COMMENTS
12-09, 12-10, 12-15	Frog Valley and nearby faults (Bald Mountain fault [12-15] and Parleys Park faults [12-10])	Zone (1.0)	14	6.1 (0.2) 6.4 (0.6) 6.7 (0.2)	55 W (0.4) 90 (0.3) 55 E (0.3)	Late Quaternary (?)	0.7	0.01 (0.3) 0.04 (0.4) 0.2 (0.3)	Due to their short individual lengths (5 km or less), we grouped these faults together as a zone. Sullivan et al. (1988) inferred late Quaternary activity primarily based on the geomorphic expression of bedrock scarps. During a more recent reconnaissance of these faults, a potential Holocene fault scarp was identified along the Frog Valley fault (F.X. Ashland, UGS, written communication, 3-20-00). Based on this, and the possibility that the Frog Valley fault may represent initiation of normal, Quaternary slip reactivated along an older thrust fault (F.X. Ashland, UGS, written communication, 3-20-00), we assigned a p(a) of 0.7 despite the short individual trace lengths and odd geometries for some of the faults in this zone. Due to a lack of slip rate data, we assumed a distribution similar to the Morgan fault based on the somewhat similar geomorphic expression of the Frog Valley fault.
6-01, 6-04	Hansel Valley fault (includes the east Hansel Mountains fault)	Linked (1.0)	27	6.6 (0.2)[12] 6.8 (0.6)[13] 7.1 (0.2)	30 E (0.2) 55 E (0.6) 70 E (0.2)	Historic (1934)	1.0	0.07 (0.2) 0.18 (0.7) 0.7 (0.1)	Although the **M** 6.6 1934 event was roughly only 10 km long and did not rupture the east Hansel Mountains fault, large (2.6 m) displacements per event for prehistoric ruptures of the Hansel Valley fault (McCalpin et al., 1992) imply longer maximum rupture lengths than 10 km. Based on this, their along-strike association, and similar dip direction, we linked these faults. Slip rate distribution based on data from McCalpin et al. (1992).
12-13	Little Diamond Creek fault	Independent (1.0)	20	6.3 (0.2) 6.6 (0.6) 6.9 (0.2)	30 E (0.2) 55 E (0.6) 70 E (0.2)	Late Quaternary (?)	0.8	0.01 (0.3) 0.04 (0.4) 0.2 (0.3)	Baker (1976) and Young (1978) suggested little or no late Cenozoic activity on this fault but Sullivan et al. (1987) found it to be similar in geomorphic expression and other respects to many "back valley" faults with inferred late Quaternary offset. Based on this we assigned a p(a) of 0.8 and assumed a slip rate distribution similar to the Morgan fault. Note that we modeled the geometry and length after Sullivan et al. (1987, figure 3) rather than Hecker (1993).
13-03, 13-04	Long Ridge faults	Linked (1.0)	34	6.6 (0.2) 6.9 (0.6) 7.2 (0.2)	30 W (0.2) 55 W (0.6) 70 W (0.2)	Mid to late Quaternary	1.0	0.05 (0.3) 0.1 (0.4) 0.3 (0.3)	Due to their along-strike association, similar dip, individual short lengths, and for simplicity, we assumed the west (13-3) and northwest (13-4) faults of Hecker (1993) were linked. Based on the presence of scarps on middle to late Quaternary alluvium (Meibos, 1983), we assigned a p(a) of 1.0. Slip rate data are lacking so we assumed a slip rate distribution similar to the East-Tintic segment of the Oquirrh-East Great Salt Lake fault zone (segmentation model A).
11-10	Mantua faults	Independent (1.0)	23	6.4 (0.2) 6.7 (0.6) 7.0 (0.2)	55 E (0.3) 90 (0.4) 55 W (0.3)	Late Quaternary (?)	0.9	0.01 (0.3) 0.04 (0.4) 0.2 (0.3)	Length based on Solomon (1999). Sullivan et al. (1988) inferred the existence and late Quaternary activity on these faults primarily based on basin and range-front morphology, and drainage patterns. Subsequent mapping by Solomon (1999) corroborates their existence and supports late-Quaternary activity, although he also did not find any associated scarps on unconsolidated deposits along the faults. Therefore, we assumed a slip rate distribution similar to the Morgan fault, but assigned a p(a) of 0.9 because rates are likely lower based on comparison of geomorphic expression.
11-17, 11-18, 11-19	Morgan fault (includes northern [11-17], central [11-18], and southern [11-19] sections)	Linked (1.0)	17	6.4 (0.2) 6.7 (0.6)[14] 7.0 (0.2)	30 W (0.2) 55 W (0.6) 70 W (0.2)	Holocene	1.0	0.01 (0.3) 0.04 (0.4) 0.2 (0.3)	We grouped the northern, central, and southern sections defined by Sullivan and Nelson (1992) based on: (1) short section lengths; (2) along-strike patterns of topographic profiles; and (3) similar geomorphic expression (Sullivan et al., 1988). Slip rates based on data of Sullivan and Nelson (1992) and Sullivan et al. (1988).

FAULT NO. [1]	FAULT NAME	RUPTURE MODEL	MAXIMUM RUPTURE LENGTH[2] (km)	MAXIMUM MAGNITUDE[3] (M)	DIP[4] (degrees)	APPROXIMATE AGE OF YOUNGEST OFFSET	PROBABILITY OF ACTIVITY[5]	RATE OF ACTIVITY[6] (mm/yr)	COMMENTS
11-14	North Fork fault of Ogden Valley	Independent (1.0)	22	6.3 (0.2) 6.6 (0.6) 6.9 (0.2)	30 E (0.2) 55 E (0.6) 70 E (0.2)	Late Quaternary (?)	0.9	0.01 (0.3) 0.04 (0.4) 0.2 (0.3)	We assumed the North Fork fault is independent from the southwestern margin faults of Ogden Valley (11-16 of Hecker [1993]) for simplicity, and because of a 2-km gap or step-over between the faults and differences in geomorphic expression and apparent younger age of activity for the southwestern margin faults (Sullivan et al. 1988). We assumed similar slip rates to the Morgan fault but assigned a slightly lower p(a) based on comparisons of geomorphic expression (Sullivan et al., 1988).
6-02	North Promontory fault	Independent (1.0)	26	6.5 (0.2) 6.8 (0.6)[15] 7.1 (0.2)	30 W (0.2) 55 W (0.6) 70 W (0.2)	Latest Quaternary	1.0	0.02 (0.2) 0.25 (0.6) 1.0 (0.2)	Slip rate distribution based on data in McCalpin et al. (1992)
6-08, 7-15, 7-14, 7-07, 8-16	Oquirrh-East Great Salt Lake fault zone (after Wong et al., 1995; includes the East Great Salt Lake, Oquirrh, South Oquirrh Mountains, Topliff Hills, and East Tintic faults)	Unsegmented (0.3)	64 (1.5 times weighted-mean segment length)	6.9 (0.2) 7.2 (0.6) 7.5 (0.2)	30 W (0.2) 45 W (0.6) 70 W (0.2)	Holocene	1.0	0.1, *0.5* (0.2) 0.2, *0.9* (0.6) 1.0, *1.7* (0.2)	Rupture lengths and segmentation models A, B, and C modified from Wong et al. (1995) based on preliminary data from Dinter and Pechmann (1999, 2000) and Olig et al. (1999b, 2000). Note that the South Oquirrh Mountains fault includes the Mercur fault (No. 7-14 of Hecker, 1993) as well as other associated Quaternary faults as mapped by Olig et al. (1999a). Mapping of the East Great Salt Lake fault based on recent seismic reflection studies (J.C. Pechmann, UUSS, written and digital communication, 2000). Shallower dips considered for the East Great Salt Lake fault (i.e., the Promontory, Antelope Island, and Fremont Island segments) based on seismic reflection and drill-hole data (Pechmann et al., 1987; Vivieros, 1986; Smith and Bruhn, 1984; Mohapatra and Johnson, 1998). Slip rates based on data in Pechmann et al. (1987), Olig et al. (1994), Barnhard and Dodge (1988), Everitt and Kaliser (1980), Olig et al. (1999b and 2000), and Dinter and Pechmann (1999, 2000). However, data from Olig et al. (1999b and 2000) and Dinter and Pechmann (1999, 2000) are preliminary, pending final age estimates. We used two slip rate distributions for the unsegmented model, with the higher rates (shown in italics) applying to the more active portion along the Antelope Island, Fremont Island, and Promontory segments. Recurrence intervals (in years, and shown in bold) based on seismic and drill hole data along the East Great Salt Lake fault that indicates at least 3 events occurred since 13,500 (± 500) cal yr B.P. along both the Antelope and Fremont Island segments (Dinter and Pechmann, 2000).
		Segmented (0.7)	**Segmentation Model A (0.2):**						
			Promontory Segment-50	6.7 (0.2) 7.0 (0.6) 7.3 (0.2)	30 W (0.3) 40 W (0.4) 50 W (0.3)	Latest Quaternary	1.0	**3250 (0.3)** **4500 (0.4)** **7000 (0.3)**	
			Antelope – Fremont Island Segment-61	6.9 (0.2) 7.2 (0.6)[16] 7.5 (0.2)	30 W (0.3) 40 W (0.4) 50 W (0.3)	Holocene	1.0	**3250 (0.3)** **4500 (0.4)** **7000 (0.3)**	
			Northern Oquirrh Segment-32	6.7 (0.2) 7.0 (0.6) [17] 7.3 (0.2)	30 W (0.2) 55 W (0.6) 70 W (0.2)	Holocene	1.0	0.1 (0.3) 0.2 (0.4) 0.4 (0.3)	
			South Oquirrh-Topliff Hills Segment-49	6.8 (0.2) 7.1 (0.6)[18] 7.4 (0.2)	30 W (0.2) 55 W (0.6) 70 W (0.2)	Holocene	1.0	0.1 (0.3) 0.2 (0.4) 0.4 (0.3)	
			East Tintic Segment-40	6.6 (0.2) 6.9 (0.6) 7.2 (0.2)	30 W (0.2) 55 W (0.6) 70 W (0.2)	Mid to late Pleistocene	1.0	0.05 (0.3) 0.1 (0.4) 0.3 (0.3)	
	Oquirrh-East Great Salt Lake fault zone (continued)		**Segmentation Model B (0.5):**						
			Promontory Segment-50	6.7 (0.2) 7.0 (0.6) 7.3 (0.2)	30 W (0.3) 40 W (0.4) 50 W (0.3)	Latest Quaternary	1.0	**3250 (0.3)** **4500 (0.4)** **7000 (0.3)**	
			Fremont Island Segment-30	6.8 (0.2) 7.1 (0.6)[19] 7.4 (0.2)	30 W (0.3) 40 W (0.4) 50 W (0.3)	Holocene	1.0	**3250 (0.3)** **4500 (0.4)** **7000 (0.3)**	
			Antelope Island Segment-35	6.8 (0.2) 7.1 (0.6)[20] 7.4 (0.2)	30 W (0.3) 40 W (0.4) 50 W (0.3)	Holocene	1.0	**3250 (0.3)** **4500 (0.4)** **7000 (0.3)**	
			N. Oquirrh-S. Oquirrh Segment-54	6.8 (0.2) 7.1 (0.6) [18] 7.4 (0.2)	30 W (0.2) 55 W (0.6) 70 W (0.2)	Holocene	1.0	0.1 (0.3) 0.2 (0.4) 0.4 (0.3)	

FAULT NO. [1]	FAULT NAME	RUPTURE MODEL	MAXIMUM RUPTURE LENGTH[2] (km)	MAXIMUM MAGNITUDE[3] (M)	DIP[4] (degrees)	APPROXIMATE AGE OF YOUNGEST OFFSET	PROBABILITY OF ACTIVITY[5]	RATE OF ACTIVITY[6] (mm/yr)	COMMENTS
			Topliff Hills-East Tintic Segment-63 **Segmentation Model C (0.3):** Promontory Segment - 50 Fremont Island Segment - 30 *Antelope Island* *Segment* - 35 Northern Oquirrh Segment - 32 South Oquirrh Mountains Segment - 25 Topliff Hills Segment - 25 East Tintic Segment - 40	6.9 (0.2) 7.2 (0.6) 7.5 (0.2) 6.7 (0.2) 7.0 (0.6) 7.3 (0.2) 6.8 (0.2) 7.1 (0.6)[19] 7.4 (0.2) 6.8 (0.2) 7.1 (0.6)[20] 7.4 (0.2) 6.7 (0.2) 7.0 (0.6)[17] 7.3 (0.2) 6.6 (0.2) 6.9 (0.6)[18] 7.2 (0.2) 6.4 (0.2) 6.7 (0.6) 7.0 (0.2) 6.6 (0.2) 6.9 (0.6) 7.2 (0.2)	30 W (0.2) 55 W (0.6) 70 W (0.2) 30 W (0.3) 40 W (0.4) 50 W (0.3) 30 W (0.3) 40 W (0.4) 50 W (0.3) 30 W (0.3) 40 W (0.4) 50 W (0.3) 30 W (0.2) 55 W (0.6) 70 W (0.2) 30 W (0.2) 55 W (0.6) 70 W (0.2) 30 W (0.2) 55 W (0.6) 70 W (0.2) 30 W (0.2) 55 W (0.6) 70 W (0.2)	Late Pleistocene Latest Quaternary Holocene Holocene Holocene Holocene Late Pleistocene Mid to late Pleistocene	1.0 1.0 1.0 1.0 1.0 1.0 1.0	0.1 (0.3) 0.2 (0.4) 0.4 (0.3) **3250 (0.3)** **4500 (0.4)** **7000 (0.3)** **3250 (0.3)** **4500 (0.4)** **7000 (0.3)** **3250 (0.3)** **4500 (0.4)** **7000 (0.3)** 0.1 (0.3) 0.2 (0.4) 0.4 (0.3) 0.1 (0.3) 0.2 (0.4) 0.4 (0.3) 0.1 (0.3) 0.2 (0.4) 0.4 (0.3) 0.05 (0.3) 0.1 (0.4) 0.3 (0.3)	
11-20	Porcupine Mountain faults	Independent (1.0)	36	6.6 (0.2) 6.9 (0.6) 7.2 (0.2)	30 W (0.2) 55 W (0.6) 70 W (0.2)	Late Quaternary	1.0	0.01 (0.3) 0.04 (0.4) 0.2 (0.3)	Fault geometry and length from Coogan and King (1999) and Bryant (1990). This fault offsets young (Holocene-latest Pleistocene?) alluvial fans (J. King, UGS, personal comm., 4-3-00). Due to a lack of slip rate data, we assumed a distribution similar to the Morgan fault.
Not Applicable	Reactivated Section of the Absaroka thrust fault	Independent (1.0)	15	6.1 (0.2) 6.4 (0.6) 6.7 (0.2)	30 W (0.3) 55 W (0.6) 70 W (0.1)	Holocene	0.7	0.4 (0.3) 0.7 (0.6) 1.5 (0.1)	Length and location based on mapping of West (1994), which includes the Martin Ranch scarp. We assigned a slightly lower p(a) to account for the possibility that this structure may not be seismogenic and capable of independent rupture from the Bear River fault zone, as suggested by West (1994). Preferred slip rate based on West's (1994) 0.5 to 0.7 mm/yr vertical estimate, even though this is not for a complete seismic cycle.
12-14	Reactivated Section of the Darby-Hogsback thrust fault	Independent (1.0)	55	6.8 (0.2) 7.1 (0.6) 7.4 (0.2)	30 W (0.3) 55 W (0.6) 70 W (0.1)	Middle to late Pleistocene	0.5	0.1 (0.2) 0.4 (0.6) 0.7 (0.2)	Length and location based on mapping of West (1994), which includes the Elizabeth Ridge scarps (12-14 of Hecker, 1993). West (1994) speculates that normal slip on the Darby-Hogsback fault may have been abandoned, and so we assigned a lower p(a). Based on geomorphic relations near Bigelow Bench, West (1994) infers as much as 200 m of vertical separation since initiation of faulting about 600 ka, which is the basis for our preferred slip rate.
12-12	Round Valley faults	Linked with the Deer Creek fault (0.15) Not Linked (0.85)	35 15	6.6 (0.2) 6.9 (0.6) 7.2 (0.2) 6.1 (0.2) 6.4 (0.6) 6.7 (0.2)	30 W (0.2) 50 W (0.6) 70 W (0.2) See comments	Mid to late Quaternary (?)	0.6 0.9	0.01 (0.3) 0.04 (0.4) 0.2 (0.3)	Due to their along-strike proximity, mapping uncertainties, and their proximity to Deer Creek Dam (Wong et al., 2001b), we considered the possibility that rupture of the Round Valley faults may extend farther northwest along the Deer Creek fault, but assigned a low weight due to the lack of evidence for Quaternary activity on the Deer Creek fault and evidence that Round Valley faults may not have been active when the Deer Creek fault was most active. The location and geometry of the Deer Creek fault is from Plate 1b of Sullivan et al. (1988). For the not-linked model, we considered three equally weighted possibilities as to which of the faults is dominant (northern, central, or southern). with preferred dips of 55° SW, 90°, 55° NE, respectively. Due to the lack of slip rate data, rates of activity were assumed to be similar to the Morgan fault.

FAULT NO. [1]	FAULT NAME	RUPTURE MODEL	MAXIMUM RUPTURE LENGTH[2] (km)	MAXIMUM MAGNITUDE[3] (M)	DIP[4] (degrees)	APPROXIMATE AGE OF YOUNGEST OFFSET	PROBABILITY OF ACTIVITY[5]	RATE OF ACTIVITY[6] (mm/yr)	COMMENTS
11-06	Saleratus Creek fault	Independent (1.0)	29	6.5 (0.2) 6.8 (0.6) 7.1 (0.2)	30 W (0.2) 55 W (0.6) 70 W (0.2)	Mid to late Quaternary (?)	0.7	0.01 (0.4) 0.04 (0.3) 0.2 (0.3)	Length and geometry based on Coogan and King (1999). Although Everitt (1995) found equivocal evidence for the existence of a normal fault and disagreed with Hecker's (1993) interpretation of probable Quaternary offsets, Coogan and King (1999) found more convincing geomorphic and stratigraphic evidence for this down-to-the-west normal fault along a portion of the Crawford thrust system. Based on this, we assigned a p(a) of 0.7. We assumed a slip rate distribution similar to the Morgan fault but modified weights based on the maximum long-term vertical rate from Everitt (1995).
Not Applicable	Skull Valley faults (includes East and West mid-valley faults of Geomatrix Consultants, 1999)	Linked (1.0)	32	6.5 (0.2) 6.8 (0.6) 7.1 (0.2)	30 W (0.2) 55 W (0.6) 70 W (0.2)	Latest Quaternary	0.9	0.06 (0.2) 0.3 (0.6) 0.5 (0.2)	For simplicity these faults were modeled as a single, linked plane. Similar to the Springline fault, these faults may be dependent on the Stansbury fault. Therefore, a slightly lower p(a) was assigned although Geomatrix Consultants (1999) found definite evidence for repeated late Pleistocene offsets. Lower bound slip rate is based on analogy with the Stansbury fault. Other rates are based on late Pleistocene vertical slip rates of 0.2 (±0.1) and 0.06 (±0.01) mm/yr for the East and West faults, respectively (Geomatrix Consultants, 1999).
11-16	Southwestern margin faults of Ogden Valley	Independent (1.0)	16	6.2 (0.2) 6.5 (0.6) 6.8 (0.2)	30 E (0.2) 55 E (0.6) 70 E (0.2)	Late Quaternary (?)	0.9	0.01 (0.3) 0.04 (0.4) 0.2 (0.3)	We assumed similar slip rates to the Morgan fault but assigned a slightly lower p(a) based on comparisons of geomorphic expression (Sullivan et al., 1988).
Not Applicable	Springline fault (of Helm, 1995)	Independent (1.0)	18	6.2 (0.2) 6.5 (0.6) 6.8 (0.2)	30 W (0.2) 55 W (0.6) 70 W (0.2)	Quaternary (?)	0.7	0.06 (0.2) 0.2 (0.6) 0.5 (0.2)	Although this postulated fault may actually be dependent on the Skull Valley faults (East and West faults of Geomatrix Consultants, 1999), and/or the Stansbury fault, for simplicity and because of its distance, we considered it only as an independent source and assigned a relatively lower p(a). Geometry, location, and slip rates based on data and estimates of Geomatrix Consultants (1999).
7-10	Stansbury fault	Unsegmented (0.3)	69	6.9 (0.2) 7.2 (0.6)[21] 7.5 (0.2)	30 W (0.2) 55 W (0.6) 70 W (0.2)	Holocene (?)	1.0	0.06 (0.2) 0.5 (0.6) 1.0 (0.2)	Segmentation model modified after Helm (1995) and Geomatrix Consultants (1999). Maximum rupture lengths measured on Plate 6 of Geomatrix Consultants (1999). Slip rate distribution based on long-term (Miocene) vertical slip rates of 0.07 (± 0.02) mm/yr (Helm, 1995), late-Pleistocene vertical slip rates of 0.4 (±0.1) mm/yr (Geomatrix Consultants, 1999), and comparison with the Oquirrh-East Great Salt Lake fault for the maximum.
		Segmented (0.7)	Northern Segment-24 (Sec. A, Geomatrix Consultants, 1999)	6.4 (0.2) 6.7 (0.6) 7.0 (0.2)	(same for all segments)	Late Pleistocene (?)	(same for all segments)	0.06 (0.2) 0.5 (0.6) 1.0 (0.2)	
			Central Segment-29 (Sec. B and C, Geomatrix Consultants, 1999)	6.7 (0.2) 7.0 (0.6)[21] 7.3 (0.2)		Holocene (?)		0.06 (0.2) 0.5 (0.6) 1.0 (0.2)	
			Southern Segment-17 (Sec. D, Geomatrix Consultants, 1999)	6.2 (0.2) 6.5 (0.6) 6.8 (0.2)		Quaternary		0.06 (0.2) 0.2 (0.6) 1.0 (0.2)	
12-05	Stinking Springs fault	Independent (1.0)	11	6.0 (0.2) 6.3 (0.6) 6.6 (0.2)	30 W (0.2) 55 W (0.6) 70 W (0.2)	Late Quaternary	1.0	0.04 (0.2) 0.2 (0.6) 1.0 (0.2)	We assumed a slip rate distribution similar to the Strawberry fault based on a similar geomorphic expression (Nelson and Martin, 1982).
12-04	Strawberry (normal) fault	Independent (1.0)	32	6.7 (0.2) 7.0 (0.6)[21] 7.3 (0.2)	30 W (0.2) 55 W (0.6) 70 W (0.2)	Holocene	1.0	0.04 (0.2) 0.2 (0.6) 1.0 (0.2)	Maximum rupture length includes the southernmost suspected Quaternary fault trace of Hecker (1993). Slip rate distribution based on data in Nelson and Van Arsdale (1986), with vertical offsets of 1 to 2 m per event and average recurrence of 5,000 to 15,000 years during the latest Quaternary, and longer-term late Quaternary vertical slip rates of 0.03 to 0.06 mm/yr. Maximum (95th percentile) value assumes the maximum rate calculated for a subsidiary fault (2 m in 5,000 years) is one-half the rate for the main fault (adjusted to net slip for a 55° dip).

FAULT NO. [1]	FAULT NAME	RUPTURE MODEL	MAXIMUM RUPTURE LENGTH[2] (km)	MAXIMUM MAGNITUDE[3] (M)	DIP[4] (degrees)	APPROXIMATE AGE OF YOUNGEST OFFSET	PROBABILITY OF ACTIVITY[5]	RATE OF ACTIVITY[6] (mm/yr)	COMMENTS
12-19	Utah Lake faults	Zone (1.0)	31	6.5 (0.2) 6.8 (0.6) 7.1 (0.2)	55 W (0.4) 90 (0.3) 55 W (0.3)	Latest Pleistocene to Holocene (?)	0.7	0.1 (0.3) 0.35 (0.4) 0.5 (0.3)	This complex anastamosing system of east- and west-dipping faults generally strikes north-south, but individual fault traces are poorly located. Because of this, we modeled the Utah Lake faults as a zone. Although seismic airgun surveys suggest offset of <2 to 5 m of Lake Bonneville deposits (Brimhall and Merritt, 1981), we assigned a slightly lower p(a) to account for the possibility that the Utah Lake faults rupture dependently on the Provo segment of the Wasatch fault zone, given the geometric and possible seismogenic relation of the faults. Slip rates are based on < 2 to 5 m of vertical offset of regressive Lake Bonneville deposits (Machette, 1992) (assumed to be 12 to 14.5 ka for these elevations).
6-05, 6-06, 6-16, 11-22, 12-03, 12-06, 13-21, 13-22, 13-23	Wasatch fault zone (includes the Malad City, Clarkston Mountain, Collinston, Brigham City, Weber, Salt Lake City, Provo, Nephi, Levan, and Fayette segments)	Segmented (0.8)	Malad City Segment-17 Clarkston Mountain Segment-17 Collinston Segment-30 *Brigham City Segment*-36 *Weber Segment*-56	6.2 (0.2) 6.5 (0.6) 6.8 (0.2) 6.2 (0.2) 6.5 (0.6) 6.8 (0.2) 6.5 (0.2) 6.8 (0.6) 7.1 (0.2) 6.7 (0.2) 7.0 (0.6)[23] 7.3 (0.2) 6.8 (0.2) 7.1 (0.6)[24] 7.4 (0.2)	30 W (0.2) 55 W (0.6) 70 W (0.2) (same for all segments)	Late Pleistocene Late Pleistocene Late Pleistocene Holocene Holocene	1.0 (same for all segments)	0.05 (0.3) 0.2 (0.4) 0.5 (0.3) 0.05 (0.3) 0.2 (0.4) 0.5 (0.3) 0.05 (0.3) 0.2 (0.4) 0.5 (0.3) **720, *280* (0.2)** **1870, *700* (0.6)** **6850, *1120* (0.2)** 0.5 (0.2) 1.5 (0.6) 3.5 (0.2)	Segmentation model from Machette et al. (1992). Maximum rupture lengths are from table 2 (straight line) in Machette et al. (1992), except the Levan segment where we considered a longer length, extending to the southern end of the Nephi segment. This allows for continuous extension along the range front and accounts for the possibility that the fault is buried along the range front within this apparent gap between surface traces. For the Salt Lake City segment, our model includes possible coseismic rupture of the antithetic West Valley fault zone during large (characteristic) events (see comments for West Valley fault zone entry). Slip rates and recurrence based on data in Machette et al. (1992), Nelson and Personius (1993), Black et al. (1996), McCalpin and Nishenko (1996), and McCalpin and Nelson (2000). Due to the limited recurrence data, we only used slip rates to characterize rates of activity on the end segments (Fayette, Collinston, Clarkston Mountain, and Malad City). Recurrence intervals (in years) are shown in bold.
	Wasatch fault zone (continued)		*Salt Lake City Segment*-39 (not linked with the West Valley fault zone-0.3) *Salt Lake City Segment*-39 (linked with the West Valley fault zone-0.7) *Provo Segment*-59 Nephi Segment-38 Levan Segment-36 Fayette Segment-11	6.7 (0.2) 7.0 (0.6)[25] 7.3 (0.2) 6.7 (0.2) 7.0 (0.6)[26] 7.3 (0.2) 6.9 (0.2) 7.2 (0.6)[23] 7.5 (0.2) 6.7 (0.2) 7.0 (0.6)[23] 7.3 (0.2) 6.7 (0.2) 7.0 (0.6)[27] 7.3 (0.2) 6.0 (0.2) 6.3 (0.6) 6.6 (0.2)		Holocene Holocene Holocene Holocene Holocene Latest Pleistocene		**610 (0.2)** **1400 (0.6)** **4090 (0.2)** (same as not linked above) **720 (0.2)** **1870 (0.6)** **6850 (0.2)** **890 (0.2)** **2800 (0.6)** **15750 (0.2)** **3500 (0.3)** **7000 (0.4)** **10,000 (0.3)** 0.05 (0.3) 0.2 (0.4) 0.5 (0.3)	Except for the Weber segment, the recurrence approach was solely used for the central segments because recurrence data are good and slip rate data are more variable in quality (particularly in regard to constraining along-strike variations and net slip across entire zones), and inherently depend on fault geometry in the analysis (see Wong and Olig [1998] for discussion). For the Weber segment, hundreds of surface offset measurements provide well-constrained displacement profiles for various time periods over the past 15 ka (Nelson and Personius, 1993). In addition, uncertainties in identifying and correlating some events between trench sites introduces more uncertainty in using recurrence interval data for this segment. Therefore, we also used slip rate data from Nelson and Personius (1993), supplemented by trench data, for the Weber segment (weighted 0.5). Recurrence distributions are based on McCalpin and Nishenko's (1996) segment-specific Poisson model, which is weighted 0.5 in our analysis, except for the Brigham City segment (weighted 0.2). For this segment, we also included a time-dependent lognormal mode1, weighted 0.3. This recurrence distribution is shown in italics and was calculated using covariances of 0.3 to 0.7, and data from McCalpin and Nishenko (1996). We also included McCalpin and Ninshenko's group or fault-specific poisson model for all the central segments (weighted 0.5), which

FAULT NO. [1]	FAULT NAME	RUPTURE MODEL	MAXIMUM RUPTURE LENGTH[2] (km)	MAXIMUM MAGNITUDE[3] (M)	DIP[4] (degrees)	APPROXIMATE AGE OF YOUNGEST OFFSET	PROBABILITY OF ACTIVITY[5]	RATE OF ACTIVITY[6] (mm/yr)	COMMENTS
									has the same recurrence distribution for each segment except the Levan segment: 1150 yrs (0.3) 7000 yrs (0.4) Levan 15000 yrs (0.3) 1150 yrs (0.2) 1750 yrs (0.6) All Other Central Segments 2790 yrs (0.2)
	Wasatch fault zone (continued)	Unsegmented (0.2)	68 (2 times the average segment length)	6.9 (0.2) 7.2 (0.6) 7.5 (0.2)	30 W (0.2) 55 W (0.6) 70 W (0.2)	Holocene	1.0	0.05, *0.5* (0.2) 0.2, *1.5* (0.6) 0.5, *3.5* (0.2)	This model assumes that the rate of activity for the five central segments is similar and a composite recurrence distribution best characterizes activity rates. One advantage to this model is that the composite dataset provides a larger sample size, yielding more stable and likely more robust results. For the unsegmented model two different slip rate distributions were used, with the larger values for the five central segments (shown in italics) and the smaller values for the other segments.
6-13, 6-15, 11-11, 11-21	West Cache fault zone	Unsegmented (0.3) Segmented (0.7)	80 (includes the Hyrum fault) Clarkston Segment -37 Junction Hills Segment - 33 Wellsville Segment - 20	7.0 (0.2) 7.3 (0.6) 7.6 (0.2) 6.7 (0.2) 7.0 (0.6)[28] 7.3 (0.2) 6.8 (0.2) 7.1 (0.6)[29] 7.3 (0.2) 6.6 (0.2) 6.9 (0.6)[30] 7.2 (0.2)	30 E (0.2) 55 E (0.6) 70 E (0.2) (same for all segments)	Holocene Holocene Early Holocene Holocene	1.0 (same for all segments)	0.04 (0.2) 0.3 (0.6) 1.0 (0.2) 0.04 (0.2) 0.6 (0.6) 1.0 (0.2) 0.04 (0.2) 0.2 (0.7) 1.0 (0.1) 0.04 (0.2) 0.2 (0.6) 1.0 (0.2)	Seismic reflection data indicate that the West Cache fault zone has significantly less cumulative offset than the East Cache fault zone (Evans, 1991; Evans and Oaks, 1996), suggesting that the former is antithetic to the latter (Sullivan et al., 1988). However, subsequent detailed mapping and trenching studies have shown that the latest Quaternary behavior of the two faults is distinctly different, implying generally independent behavior (Black et al., 2000). Therefore, we assigned a p(a) of 1.0. Fault trace geometry modified after Solomon (1999). Segmentation model after Black et al. (2000). We included the Hyrum fault as a southern extension of the Wellsville segment (Black et al., 2000; figure 1). Slip rate distributions based on: (1) 9 m of vertical offset since 16.8 ka on the Clarkston segment (Solomon, 1999); (2) 2.9 m of vertical offset since 22.5 ka (Black et al., 2000), and 600 to 1200 m of vertical offset since the Miocene (Evans, 1991) on the Junction Hills segment; and (3) 13.2 m of vertical offset of 100 to 200 ka deposits, and 4.4 m of vertical offset since 15.1 to 25 ka on the Wellsville segment (Black et al., 2000). Maximum rates are based on similar arguments to those made for the East Cache fault zone.
11-04	West Crawford Mountains fault (or Leefe fault of Ott, 1980)	Independent (1.0)	33	6.5 (0.2) 6.8 (0.6) 7.1 (0.2)	30 W (0.2) 55 W (0.6) 70 W (0.2)	Late Quaternary	1.0	0.01 (0.3) 0.04 (0.4) 0.2 (0.3)	Length includes scarps on alluvium south of the Bear River based on observations and interpretations of Everitt (1995). Due to a lack of data, we assumed a slip rate distribution similar to the Morgan fault.

FAULT NO. [1]	FAULT NAME	RUPTURE MODEL	MAXIMUM RUPTURE LENGTH[2] (km)	MAXIMUM MAGNITUDE[3] (M)	DIP[4] (degrees)	APPROXIMATE AGE OF YOUNGEST OFFSET	PROBABILITY OF ACTIVITY[5]	RATE OF ACTIVITY[6] (mm/yr)	COMMENTS
12-07, 12-08	*West Valley fault zone* (includes the Granger [12-7] and Taylorsville [12-8] faults)	Independent (0.3) Linked with the Salt Lake City Segment of the Wasatch fault zone (0.7)	16 See the Salt Lake City Segment entry of Wasatch fault zone for all parameters	6.4 (0.2) 6.7 (0.6)[31] 7.1 (0.2)	55 E (0.3) 70 E (0.4) 80 E (0.3)	Holocene	1.0	0.03 (0.2) 0.2 (0.6) 0.7 (0.2)	Due to their close proximity, similar dip, and for simplicity, we assumed that the Granger and Taylorsville faults of the West Valley fault zone merge at a shallow depth and that the primary moment release occurs on the Granger fault as it appears to have the greatest cumulative offset (Keaton et al., 1993). The West Valley fault zone is antithetic to, and lies 3 to 13 km west of, the more active Salt Lake City segment of the Wasatch fault zone. We allowed for both independent and dependent (linked or coseismic) rupture of the West Valley fault zone with the Salt Lake City segment of the Wasatch fault zone. We favored the latter in light of recent dates from trenches that suggest overlapping ages for: the youngest events on the Granger fault and the Salt Lake City segment, and the youngest event on the Taylorsville fault and the penultimate event on the Salt Lake City segment (Solomon, 1998; B.D. Black, UGS, written communication, 8-9-99). Steeper dips than typical range-bounding faults were assumed for this intrabasin graben-bounding fault zone. Slip rate distribution is based on data in Keaton et al. (1993) for a variety of time periods.

1. Fault number and nomenclature after Hecker (1993).
2. Measured straight-line, end to end on Hecker (1993) unless noted otherwise.
3. Preferred values estimated using the empirical relation of Wells and Coppersmith (1994) for all fault types. Unless otherwise noted, values are estimated based on maximum surface rupture length.
4. Average crustal dips. Most faults are assumed to be simple planes except those that are italicized, where a curvilinear model was used. Preferred dips are based on available subsurface data for Wasatch Front faults and basin geometries (e.g., Zoback 1983, 1992; Smith and Bruhn, 1984; Bruhn et al., 1992; Mabey, 1992; Mohapatra and Johnson, 1998). Ranges are based on focal mechanisms for large normal faulting earthquakes worldwide (Jackson and White, 1989).
5. Probability of activity, p(a), the likelihood that a fault is an independent seismogenic structure and is still active within the modern stress field.
6. Rates of fault activity are average net slip rates unless noted otherwise. Recurrence models included characteristic, maximum magnitude, and exponential, with weights depending on the type of seismic source and rupture model (as shown in column 3). For longer, segmented faults the distribution is: characteristic – 0.7, maximum magnitude – 0.2, and truncated exponential – 0.1; except when only the recurrence approach was used and then characteristic was weighted 0.8 and maximum magnitude was weighted 0.2. For shorter, single-plane, independent faults the distribution is: characteristic – 0.6, maximum magnitude – 0.2, truncated exponential – 0.2. For faults modeled as zones, characteristic and truncated exponential models are equally weighted (0.5/0.5).
7. Based on the average of expected magnitudes estimated from: surface rupture length, and 3 m of average displacement per event (West, 1994).
8. Based on average of expected magnitudes estimated from: rupture length, and average displacements per event of 0.85 and 1.65 m (McCalpin, 1994).
9. Based on average of expected magnitudes estimated from: rupture length, and inferred average displacements per event of 0.5 to 1.5 m (McCalpin and Forman, 1991) for the southern East Cache fault, and an average displacement per event of 1.8 to 2.4 m for the James Peak fault (Nelson and Sullivan, 1992).
10. Based on average of expected magnitudes estimated from: rupture length, and average displacements per event of 2.6 to 5.6 (McCalpin, 1993)
11. Although displacement data are not available for this segment, maximum magnitudes were estimated similar to the southern segment assuming that behavior is analogous to the southern segment and other active faults in the region that show large displacements relative to segment or fault lengths (McCalpin, 1993).
12. Based on the **M** 6.6 1934 earthquake (Smith and Arabasz, 1991).
13. Based on the average of expected magnitudes estimated from: rupture length, and maximum displacements per event of 2.6 m (McCalpin et al., 1992)
14. Based on the average of expected magnitudes estimated from: rupture length, and average displacements per event of 0.5 to 1.0 m (Sullivan et al., 1988; Sullivan and Nelson, 1992).
15. Based on the average of expected magnitudes estimated from: rupture length, and maximum displacements per event of 2.5 m (McCalpin et al., 1992).
16. Based on the average of expected magnitudes estimated from: rupture length, and average displacements per event of 3.6 m and a maximum displacement per event of 4.5 m (Dinter and Pechmann, 1999).
17. Based on the average of expected magnitudes estimated from: rupture length, and average displacements per event of 2.4 m (Olig et al., 1994).
18. Based on the average of expected magnitudes estimated from: rupture length, and average displacements per event of 1.4 to 2.1 m (Olig et al. 2000).
19. Based on the average of expected magnitudes estimated from: rupture length, and preliminary displacement data of 4.5 m per event, considered as both an average or maximum (Dinter and Pechmann, 1999).
20. Based on the average of expected magnitudes estimated from: rupture length, and preliminary displacement data of 3.6 m per event, considered as both an average or maximum (Dinter and Pechmann, 1999).
21. Based on the average of expected magnitudes estimated from: rupture length, and an average displacement per event of 2 to 3 m (Geomatrix Consultants, 1999).
22. Based on the average of expected magnitudes estimated from: rupture length, and an average displacement per event of 1 to 2 m (Nelson and Van Arsdale, 1986).
23. Based on the average of expected magnitudes estimated from: rupture length, and an average displacement per event of 2 m (Machette et al., 1992).
24. Based on the average of expected magnitudes estimated from: rupture length, and an average displacement per event of 1.8 m (Machette et al., 1992; McCalpin et al., 1994).
25. Based on the average of expected magnitudes estimated from: rupture length, and an average displacement per event of about 2 m (original data from Swan et al., 1981 and Lund and Schwartz, 1987 that is discussed in Black et al., 1996, p.14-15).
26. This estimate is only for the Salt Lake City segment portion of the rupture; maximum magnitudes for the West Valley portion of the rupture are less and depend on the event size on the Salt Lake City segment and slip rates.
27. Based on the average of expected magnitudes estimated from: rupture length, and an average displacement per event of about 1.9 m (Hecker, 1993).
28. Based on the average of expected magnitudes estimated from: rupture length, and a maximum displacement per event of 3.7 m (Black et al., 2000).
29. Based on the average of expected magnitudes estimated from: rupture length, and an average displacement per event of 2.9 m (Black et al., 2000).
30. Based on the average of expected magnitudes estimated from: rupture length, and an average displacement per event of 2.2 m (Black et al., 2000).
31. Based on the average of expected magnitudes estimated from: rupture length, and an average displacement per event of 0.5 to 1.5 m (Solomon, 1998; Keaton et al., 1993).

(1984) proposed that the fault was divided into six segments, but subsequent detailed mapping (Scott and Shroba, 1985; Personius, 1990; Machette, 1992; Personius and Scott, 1992; Nelson and Personius, 1993; and Harty et al., 1997) and dozens of trench investigations (see table 1, Machette et al., 1992, and McCalpin and Nishenko, 1996 for summaries), provide an extensive paleoseismic record of fault behavior that indicates a ten-segment model best fits the data (Machette et al., 1991, 1992). This model is also consistent with statistical analyses of geophysical and geological properties of potential segment boundaries (Wheeler and Krystinik, 1992) that indicate that salients along the Wasatch Range front appear to have formed at persistent segment boundaries between the central most-active segments. Based on these data, we included a segmented model (weighted 0.8) after Machette et al. (1992). We also included an unsegmented model (weighted 0.2) in our analysis (table 1) to account for the possibility of longer multiple-segment ruptures and ruptures that occasionally extend through boundaries. The 1983 **M** 6.8 Borah Peak earthquake is a well-recognized historical analog of such a multiple, partial segment rupture extending through a segment boundary (Crone et al., 1987).

We used curvilinear geometries in our model for four segments near the study area (Brigham City, Weber, Salt Lake City, and Provo). We assumed a preferred dip of 55° for all segments based on available geological and geophysical data along the Wasatch Front (e.g., Zoback, 1983, 1992; Smith and Bruhn, 1984; Bruhn et al., 1992; and Mabey, 1992), and a distribution ranging from 30° to 70° (table 1) based on the range of seismically-determined dips reported by Jackson and White (1989) for 15 worldwide, continental, normal-faulting earthquakes. Our preferred M_{max} for the Wasatch fault ranges from **M** 6.5 to 7.2, depending on available displacement per event data and individual segment lengths (table 1). Minimum and maximum values of M_{max} for the Wasatch fault range from **M** 6.2 to 7.5 (table 1).

Repeated Holocene surface-faulting events are well-documented along the five central, most active segments (Brigham City, Weber, Salt Lake City, Provo, and Nephi) and Holocene vertical slip rates are typically between 0.5 and 1.5 mm/year (Machette et al., 1992). We used McCalpin and Nishenko's (1996) analysis of the extensive available paleoseismic data (summarized in their table 3) to characterize recurrence interval distributions for the central segments. We generally applied results from both their Poissonian group (or fault-specific) and segment-specific models (table 1; also see their table 6). The recurrence interval data and our distributions for the three closest central segments (Salt Lake City, Provo, and Weber) are discussed further below. Additionally, we calculated time-dependent conditional probabilities and equivalent Poisson recurrence intervals for the Salt Lake City and Brigham City segments and these are also discussed.

The northern (Malad City, Clarkston Mountain, and Collinston) and southern (Levan and Fayette) segments of the Wasatch fault are much less active than the central segments as indicated by more subdued and sinuous range fronts, a general lack of Holocene fault scarps, and more discontinuous and degraded fault scarps (Machette et al., 1992). In general, the recency of faulting gets older and cumulative displacements decrease toward the ends of the fault. In our analysis we used slip rates for the four segments lacking detailed trench investigations (Malad City, Clarkston Mountain, Collinston, and Fayette). Due to the sparse data, we used similar distributions for all these segments primarily based on the following: (1) 12 m of surface offset of pre-Bonneville (>> 30 ka) fan deposits at the southern end of the Collinston segment (Personius, 1990), which yields a net slip rate of < 0.5 mm/yr (assuming a 55° dip); (2) small scarps along the Fayette segment that probably formed between 10 to 15 ka (Machette et al., 1992), suggesting net slip rates between 0.1 to 0.2 mm/yr, assuming single-event offsets of 1 to 2 m; and (3) geomorphic expression and range-front morphology which suggest slip rates are likely greater than those of most back valley faults (i.e., > 0.04 mm/yr). There are more paleoseismic data for the Levan segment, including limited recurrence data, so we used recurrence intervals for this segment, but with broader distributions than those used for the central segments (table 1). Data from three trench sites and natural exposures (Schwartz and Coppersmith, 1984; Jackson, 1988; and Machette et al., 1992) indicate that the youngest surface-faulting event occurred around 1 ka and the penultimate event likely occurred in early Holocene to latest Pleistocene time (between 7,000 to 15,000 years) (Machette et al., 1992). Based on the limited data and comparison with distributions for the more active segments, we assigned a distribution of 3,500, 7,000, and 10,000 years (weighted 0.3, 0.4, and 0.3, respectively) for the Levan segment (table 1).

Salt Lake City Segment – This segment bounds the east side of the Salt Lake Valley (Personius and Scott, 1992) and is the most significant seismic source to the Salt Lake Valley. Bounding the graben within the Salt Lake Valley on the west is the West Valley fault zone (figure 1), which is antithetic to, and may or may not be seismogenically dependent on, the Salt Lake City segment (e.g., Youngs et al., 1987; Keaton et al., 1993). We included both possibilities in our model, favoring a dependent or linked rupture model as discussed in table 1 and in the following section on the West Valley fault zone.

The Salt Lake City segment extends for about 46 km from the Traverse Mountains salient north to the Salt Lake salient (Scott and Shroba, 1985; Personius and Scott, 1992; Machette et al., 1992). Holocene fault scarps are prominent along most of the segment and fault trace patterns are very complex, including 2- to 4-km gaps or step-overs, near-right-angle bends, and multiple anastamosing and branching traces. As mapped and described by Scott and Shroba (1985), the Salt Lake City segment includes the Warm Springs fault along the Salt Lake salient, the East Bench fault near downtown Salt Lake City, the Cottonwood section along the southern range front, part of the Fort Canyon fault near the Traverse Mountains salient, and the range-front fault north of Mount Olympus. Except for the last two fault sections, all sections show definitive evidence for repeated Holocene surface-faulting (e.g., Marsell and Threet, 1964; Scott and Shroba, 1985; Personius and Scott, 1992). Based on this, our curvilinear model approximation follows the East Bench fault rather than the overlapping range-front fault north of Olympus Cove.

Similarly, our curvilinear model approximation follows the Warm Springs fault rather than the overlapping, much older bedrock fault splay called Rudy's Flat fault, that lies about 10 km to the east (Personius and Scott, 1992; Nelson and Personius, 1993).

Particularly large scarps are evident along the East Bench fault, reaching heights of 50 m; however, Scott and Shroba (1985) estimated that only about 11 m of displacement has occurred since latest Pleistocene time, yielding a slip rate of about 1 mm/yr. Gilbert (1890) first identified 10- to 14-m-high scarps along the Warms Springs fault that offset post-Bonneville alluvial fans. Unfortunately most of the Warm Springs scarps have been obliterated or altered by quarries and urban development. Scarps measure as high as 30 to 40 m along the Cottonwood fault section, but Scott and Shroba (1985) estimate that probably no more than 15 m of offset has occurred since the Bonneville lake cycle.

Trench studies along the Cottonwood section initially suggested that at least three events occurred during the Holocene (Swan et al., 1981; Schwartz and Lund, 1988; Machette et al., 1992). However, this conclusion was based on an incomplete record as some traces in the zone were not trenched. Subsequent studies identified two additional events and provided a more complete record, indicating that at least five events occurred since 8 to 9 ka and four events occurred since 5.4 ka (Black et al., 1996). McCalpin and Nishenko (1996) estimate the timing of the last four events to be 1.2, 2.5, 3.9, and 5.4 ka (rounded to the nearest century – see their table 3 for standard deviations). However, not all of these events occurred on all of the fault traces within the zone, which raises the question whether all of the events actually ruptured the entire segment length. Large average displacements per event of 2 m (Black et al., 1996) imply large paleomagnitudes (M ≈ 7.2), suggesting that much, if not all, of the full segment length did rupture during these events.

Most recently, deep trenches excavated across two main fault scarps near Little Cottonwood Canyon provide a longer record of faulting (McCalpin and Nelson, 2000). Preliminary results suggest that only three events likely occurred between 6 and 18 ka, rather than the expected 6 to 7 events if recurrence intervals had remained similar to the 1350 ± 200 years (Black et al., 1996) observed for the past 6 ka (McCalpin and Nelson, 2000). These data suggest an average recurrence interval of about 2,800 years for the past 18 ka (18,000-1,230 years/6 intervals; note that 18 ka is the calibrated age for the time of the oldest event, T, which occurred around 15,500 ± 1,000 yr BP, as reported by McCalpin and Nelson, 2000). It is uncertain whether the lower rates between 6 and 18 ka are related to the drying up of Lake Bonneville, but regardless of the cause, a change in behavior appears to have occurred along the Salt Lake City segment during the early to mid-Holocene.

Based on the paleoseismic data for the past 6 ka, McCalpin and Nishenko (1996) calculated a segment-specific repeat time for the Salt Lake City segment of 1,400 years, with a 90% confidence interval of 612 to 4,088 years (assuming a Poisson model and 4 events occurred since 5.6 ka). We rounded these values to the nearest decade to determine the 50th, 95th, and 5th percentiles, respectively, weighted 0.6, 0.2, and 0.2 in our analysis (table 1). We also considered McCalpin and Nishenko's Poissonian group or "fault-specific" model (weighted 0.5). This model assumes that the rates of activity for the central segments are all similar and so a composite recurrence interval distribution best characterizes fault behavior (table 1). Although this may be an oversimplification of actual fault behavior, one advantage to this model is that the much larger dataset provides more stable and robust results. Their mean repeat time for this model is 1,750 years (350 years x 5 segments), with a 90% confidence interval of 1,152 to 2,789 years (230.4 x 5 and 557.8 x 5, respectively). Again, we rounded all values to the nearest decade to determine the 50th, 95th, and 5th percentiles (respectively weighted 0.6, 0.2, and 0.2) (table 1).

Although we calculated time-dependent conditional probabilities and equivalent Poisson recurrence intervals for the Salt Lake City segment (discussed below), the range of these estimates is generally encompassed by our Poisson-based distribution and the average of these estimates is similar to our preferred values. Because of this, and the complexity of including a time-dependent model with the coseismic rupture of the West Valley fault zone, we did not explicitly include a time-dependent approach for the Salt Lake City segment. Finally, we point out that although the preferred values for both the segment-specific and group models are anchored by the data from the past 6 ka, the tails of the distributions are broad and encompass the lower rates of activities suggested for the past 18 ka by the recent McCalpin and Nelson (2000) study.

Our preferred M_{max} of **M** 7.0 for the Salt Lake City segment is based on maximum surface rupture length and average displacement per event (table 1), slightly favoring the former due to the poor-quality data for the latter. The straight-line, end-to-end length is 39 km, yielding an expected **M** 6.9. Unfortunately, displacements per event remain poorly constrained, but estimates average about 2 m (Swan et al., 1981; Lund and Schwartz, 1987; Black et al., 1996), yielding an expected **M** 7.2. These same data formed the basis for our scenario event of a **M** 7.0 earthquake on the Salt Lake City segment.

Provo Segment – This segment lies immediately south of the Salt Lake Valley. It is the longest segment of the Wasatch fault, extending for 70 km (curvilinear trace length) along the eastern margin of Utah Valley, from the Payson salient north to the Traverse Mountains salient (Machette, 1992). The Provo segment is characterized by nearly continuous Holocene fault scarps that show trace patterns almost as complex as the Salt Lake City segment, with near-right-angle bends, multiple overlapping branches, anastomosing splays, step-overs, and gaps.

Holocene and latest Pleistocene slip rate estimates are comparable to estimates for the other central segments of the Wasatch fault. Slip rates range from 0.5 to over 2.5 mm/yr (Swan et al., 1980; Lund et al., 1991; Machette et al., 1992). However, there is also evidence for significant variations in slip rate through time, including very high rates during the Lake Bonneville transgression (as high as 10 mm/yr), and two orders of magnitude lower rates recorded in older deposits

about 130 to 150 ka (between 0.1 and 0.3 mm/yr) (Machette et al., 1992).

Detailed trench investigations at seven trench sites along the Provo segment reveal evidence for at least four events since 8 ka, with events occurring at about 0.5 to 0.6 ka, 2.6 to 3.0 ka, 5.3 ka, and 5.5 to 8.0 ka (Swan et al., 1980; Ostenaa, 1990; Lund et al., 1991; Machette et al., 1992; Lund and Black, 1998). An additional event that occurred after 1.0 ka at the southernmost Water Canyon site (Ostenaa, 1990) may or may not have been associated with "bleed-over" of rupture during the most-recent event on the Nephi segment to the south, which occurred between 300 and 1,200 years ago (Jackson, 1991).

Based on the available paleoseismic data, McCalpin and Nishenko (1996) calculated a segment-specific repeat time for the Provo segment of 1,867 years, with a 90% confidence interval of 723 to 6846 years (assuming a Poisson model and three events since 5.6 ka). We rounded these values to the nearest decade to determine the 50th, 95th, and 5th percentiles, weighted 0.6, 0.2, and 0.2, respectively, in our analysis (table 1). Similar to the Salt Lake City segment, we also included their fault-specific or group model weighted 0.5 (table 1).

Our preferred M_{max} of **M** 7.2 for the Provo segment is based on maximum surface rupture length and average displacement per event (table 1). Along the Provo segment, estimates of net vertical displacement per event range from 0.8 to 3.3 m, but average 2.3 m for six well-constrained measurements and 2.2 m for all of the data (Swan et al., 1980; Lund et al., 1991; Machette et al., 1992; Lund and Black, 1998). These data yield an expected M_{max} of **M** 7.2, consistent with that based on the maximum surface rupture length of 59 km (straight-line, end-to-end) (table 1).

Weber Segment – This segment is located immediately north of the Salt Lake Valley and is the second longest of all the Wasatch fault segments. It extends for 61 km (curvilinear surface trace length) from the Salt Lake salient south of Bountiful, to the Pleasant View salient north of North Ogden (Nelson and Personius, 1993). The segment is geomorphically expressed as nearly continuous fault scarps on Holocene deposits. Nelson and Personius (1993) measured surface offsets across hundreds of topographic profiles, yielding Holocene and latest Pleistocene slip rates of 0.3 to 3.7 mm/year, but values along the central portion of the segment are typically between 0.9 and 1.9 mm/yr. Detailed paleoseismic investigations at three trench sites by several investigators (e.g., Swan et al., 1980; Nelson et al., 1987; Nelson, 1988; Forman et al., 1991; Nelson and Personius, 1993; McCalpin et al., 1994) indicate at least four, and possibly six surface-faulting events occurred since about 6,100 years ago. Two of these events are identified at all three trench sites, including an event around 0.8 to 1.2 ka and one around 2.8 ± 0.7 ka (Machette et al., 1992; McCalpin et al., 1994). However, some of the events apparently did not rupture the entire segment, including a possible event around 0.5 ka suggested at the East Ogden site, and an event that occurred around 1.5 to 2.0 ka at the Garner Canyon site (Machette et al., 1992). Additionally, McCalpin et al. (1994) suggested that a 3.8 to 7.9 ka event at Kaysville does not correlate with a 3.4 to 4.0 ka event at East Ogden, based on their error analysis.

Due to the additional recurrence interval uncertainties related to likely partial segment rupture, problems in event identification and correlation between sites, and the extensive slip rate data for this segment, we used slip rates for this segment (weighted 0.5) instead of segment-specific recurrence rates in our analysis. Our net slip rate distribution of 0.5, 1.5, and 3.5 mm/yr (weighted 0.2, 0.6, and 0.2, respectively) is based on the along-strike surface offset profiles from Nelson and Personius (1993) and net vertical slip rates from trench sites (Swan et al., 1980; Machette et al., 1992; McCalpin et al., 1994). Note that for our analysis we did consider that surface offsets are typically between 60 to 80% of net dip-slip, assuming a 55° fault dip and surface slopes of 5° to 20°. Similar to the Salt Lake City and Provo segments, we also considered McCalpin and Nishenko's Poissonian group or "fault-specific" model for the Weber segment (weighted 0.5) (table 1).

Our preferred M_{max} of **M** 7.1 for the Weber segment is based on maximum surface rupture length and displacements per event (table 1). Along the Weber segment, net vertical displacements per event range from 0.8 to 4.2 m and average about 1.8 m for 11 well-constrained observations (Machette et al., 1992; McCalpin et al., 1994). These data yield an expected **M** 7.1 (Wells and Coppersmith, 1994), consistent with the magnitude estimate based on maximum surface rupture length (56 km straight line, end-to-end; table 1).

Time-Dependent Analysis – Available paleoseismic data for some faults in the Lake Bonneville basin, including some of the most significant faults for this study (e.g., Wasatch and West Valley fault zones), indicate that rates of activity have varied significantly through time, tempting investigators to speculate on possible causal relations between variations in lake level and rates of fault activity (e.g., Machette et al., 1992; McCalpin et al., 1992; Keaton et al., 1993; Olig et al., 1994; McCalpin and Nelson, 2000). This possibility warrants further consideration for this study as the activity rate is the most important fault parameter in the probabilistic hazard analysis. Interestingly, patterns of variation are not consistent in that some faults show evidence for quiescence or slowed rates of activity variously during pluvial periods (e.g., West Valley fault zone), during major regressions following pluvial periods (e.g., Brigham City and Salt Lake City segments of the Wasatch fault zone), or throughout interpluvial periods (e.g., Hansel Valley fault). Similarly inconsistent, some faults show evidence of apparently higher rates of activity during pluvial transgressions (i.e., Provo segment of the Wasatch fault zone and Oquirrh fault), while others show higher rates sometime after regressions and several thousand years into the interpluvial cycle (e.g., Salt Lake City and Brigham City segments). Thus, if a causal relation exists, it must explain these complex patterns of variation. An appropriate approach to systematically consider such effects on rates for the hazard analysis is not readily apparent.

Regardless of its uncertain cause, we have attempted to address the issue of rate variation in two ways in our analysis: (1) by including broad distributions in slip rate and/or recurrence intervals where appropriate (e.g., West Valley and Wasatch fault); and, (2) by including a time-dependent aspect

Table 2. Time-dependent recurrence parameters.

	Salt Lake City Segment:						Brigham City Segment:					
	Shorter Record (past 6 ka)			Longer Record (past 15 ka)			Shorter Record (past 9 ka)			Longer Record (past 15 ka)		
Mean Recurrence	1,350 yrs[1]			2,795 yrs[2,3]			1,280yrs[2]			1,810 yrs[2]		
Elapsed Time	1,230 yrs[1,2]			1,230 yrs[1,2]			2,130 yrs[2]			2,130 yrs[2]		
Covariance	0.3	0.5	0.7	0.3	0.5	0.7	0.3	0.5	0.7	0.3	0.5	0.7
Conditional Probabilities[4]	0.094	0.069	0.057	0.002	0.012	0.019	0.16	0.085	0.059	0.097	0.058	0.044
Equivalent Poisson Recurrence Intervals	510 yrs	700 yrs	850 yrs	23,720 yrs	4,030 yrs	3,610 yrs	280 yrs	560 yrs	820 yrs	490 yrs	830 yrs	1,120 yrs

[1] Based on data from Black *et al.* (1996)
[2] Based on data from McCalpin and Nishenko (1996)
[3] Based on data from McCalpin and Nelson (2000)
[4] For the next 50 years and assuming a lognormal renewal model

to our model. For the latter, we followed the approach of the Working Group on California Earthquake Probabilities (WGCEP, 1999) to calculate conditional probabilities and equivalent Poisson recurrence intervals that could then be incorporated into the hazard analysis. We only calculated conditional probabilities for the Salt Lake City and Brigham City segments (table 2), primarily because we judged these to be the only faults (or fault segments) with long enough paleoseismic records (with data for numerous seismic cycles over the past approximate 15,000 years) to be adequate for a time-dependent analysis. Even so, we readily acknowledge that these datasets may not be complete and large uncertainties exist, particularly for the earlier portion of the records (approximately 6 to 15 ka).

We assumed a lognormal renewal model to calculate conditional probabilities for the next 50 years, the target period of interest for our hazard maps. For comparison, we calculated probabilities using both a longer and shorter paleoseismic record (table 2), due to the uncertainties of the cause(s) in rate variations. We also included a range for the coefficient of variation (COV) of 0.3 to 0.7 due to large uncertainties in this parameter (e.g., Ellsworth et al., 1998; McCalpin and Slemmons, 1998). The COV is a measure of the periodicity of earthquake occurrence equal to the standard deviation of the recurrence interval divided by the mean. Smaller values (< 0.3) indicate more periodic behavior and larger values (> 0.7) indicate non-periodic behavior (N.A. Abrahamson, PG&E, written communication, 2000).

The resulting equivalent Poisson recurrence intervals vary by as much as an order of magnitude, depending on the mean recurrence and COV, with generally lower values calculated for the shorter record as a result of lower mean recurrence intervals (table 2). Values for the Salt Lake City segment vary from 510 to 23,720 years. Except for the case of a COV of 0.3 and mean recurrence of 2,795 years, the spread in these values is similar to the 90% confidence intervals for segment-specific values we used for the Salt Lake City segment (table 1) based on McCalpin and Nishenko's (1996) Poisson model. In contrast, equivalent Poisson recurrence intervals for the Brigham City segment vary from 280 to 1,120 years (table 2) and are all much lower than McCalpin and Nishenko's (1996) mean repeat time of 1,870 years for their segment-specific Poisson model (table 1). Indeed, equivalent Poisson recurrence intervals are all generally much closer to McCalpin and Nishenko's (1996) 95th percentile of 720 years. Due to the much shorter recurrence intervals (and higher implied hazard) suggested by the time-dependent analysis, we included a time-dependent approach (shown in bold italics on table 1) for the Brigham City segment, but only weighted it 0.3 due to the many uncertainties in the model and input parameters.

Oquirrh-East Great Salt Lake Fault Zone

The Oquirrh-East Great Salt Lake fault zone consists of a series of north- to northwest-striking, west-dipping, discontinuous, range-bounding normal faults that extend for 220 km from Rozel Bay in Great Salt Lake, south to Furner Pass west of Nephi. The zone lies 20 to 70 km west of the Wasatch fault zone and is generally west of the study area (figure 1). From north to south, faults comprising the Oquirrh-East Great Salt Lake fault zone are: the Promontory, Fremont Island and Antelope Island segments of the East Great Salt Lake fault, the Oquirrh fault, the South Oquirrh Mountains fault, the Topliff Hills fault, and the East Tintic fault. Based on available geologic and geophysical data, and analogy to the Wasatch fault, previous probabilistic seismic hazard evaluations of the area have combined these faults into one zone that is likely segmented (Youngs et al., 1987; Wong et al., 1995). However, the exact segmentation remains uncertain and so we have included three alternative models in our analysis (table 1). We favor Model B (weighted 0.5) because it best fits recent geophysical and paleoseismic data for the East Great Salt Lake fault (Dinter and Pechmann, 1999, 2000) and the South Oquirrh Mountains fault (Olig et al., 2000).

Available paleoseismic data indicate repeated late Quaternary activity on the fault zone with latest Quaternary offsets on the East Great Salt Lake (Dinter and Pechmann, 1999, 2000), Oquirrh (Olig et al., 1994), South Oquirrh Mountains (Olig et al., 1999b), and possibly the Topliff Hills (Everitt and Kaliser, 1980) faults. Slip rates are highest along the East Great Salt Lake fault, with minimum and maximum vertical estimates of 0.4 ± 0.1 mm/yr (Pechmann et al., 1987) and 0.8 ± 0.3 mm/yr (D.A. Dinter and J.C. Pechmann, University of Utah, unpublished preliminary data, 2000), respectively, compared to vertical estimates of 0.1 to 0.2

mm/yr for other faults to the south (Olig et al., 1994, 1999a, 2000). Recurrence intervals were used to characterize rates for the segments of the East Great Salt Lake fault and are based on recent seismic reflection and drill hole data that indicate at least three events occurred on both the Antelope Island and Fremont Island segments since the Bonneville regression at ~13,500 (± 500) cal yr BP (Dinter and Pechmann, 2000). The Antelope Island segment is the closest to the map area, extending into the northwest corner, and so we have used a curvilinear model for this portion of the Oquirrh-East Great Salt Lake fault in our analysis. Preferred M_{max} for the Oquirrh-East Great Salt Lake fault zone are based on surface rupture lengths and available displacement data. Preferred values range from **M** 6.7 to 7.2 (table 1).

West Valley Fault Zone

The north-south-striking, east-dipping West Valley fault zone extends for about 16 km through the central portion of the study area (figure 1). It consists of two main fault traces, the Taylorsville and Granger faults. These faults lie about 8 to 10 km west of the Salt Lake City segment of the Wasatch fault, forming an inner graben in the Salt Lake Valley (Marine and Price, 1964). Given the similar orientation and close proximity of the Granger and Taylorsville faults to each other, it seems likely that the faults merge at depth. The Granger fault is the farthest from the Wasatch fault and shows the largest cumulative displacement (Keaton et al., 1993), and so we assumed it was the primary fault in our model. The relationship of the West Valley fault zone to the Wasatch fault zone remains unclear and so we have included both independent and dependent (linked) alternatives in our analysis (table 1). We favor the latter (0.7) based on fault geometries and recent paleoseismic data that suggest coseismic rupture of parts of the West Valley fault may have occurred during the past two events on the Salt Lake City segment (Solomon, 1998; B.D. Black, UGS, written communication, 1999). Paleoseismic evidence clearly indicates repeated latest Quaternary activity occurred on the West Valley fault zone, with slip rates that have varied through time from 0.03 to 0.5 mm/yr (Keaton et al., 1993). Due to its location within the map area, we used a curvilinear model for the West Valley fault zone.

Background Seismicity

The hazard from background (floating or random) earthquakes that are not associated with known or mapped faults needs to be incorporated into the probabilistic hazard analysis. Earthquake recurrence estimates in the study region and M_{max} are required to assess the hazard from background earthquakes. In most of the western U.S., particularly the Basin and Range Province, the M_{max} for background earthquakes usually ranges from **M** 6 to 6½. Repeated events larger than these magnitudes probably produce recognizable fault- or fold-related features at the earth's surface (e.g., Doser, 1985; dePolo, 1994). In this study, we adopt a value of **M** 6½ ± ¼.

In addition to the traditional approach of using areal source zones (assuming uniformly distributed seismicity), Gaussian smoothing (Frankel, 1995) was used to address the hazard from background earthquakes in the probabilistic analysis. In this approach, we smoothed the historical background seismicity to incorporate a degree of stationarity, using a spatial window of 15 km.

Using areal source zones, we used a single zone, the Wasatch Front as defined by Pechmann and Arabasz (1995). We weighted the two approaches equally at 0.50. Both approaches were based on a historical catalog of independent mainshocks in the Wasatch Front region from 1962 to 1998, provided to us by Walter Arabasz (UUSS, digital communication, 1999). We assumed that very few of the events in this catalog were associated with the faults included in the hazard analysis (table 1). The range in seismogenic crustal thickness for the background earthquakes was assumed to be the same for the faults.

The earthquake recurrence of the Wasatch Front assumed the truncated exponential form of the Gutenberg-Richter relationship of $\log N = a - bM$. The preferred recurrence parameters a and b were adopted from Pechmann and Arabasz (1995) for the period 1962 to 1994. Because of the limited duration of the historical catalog, we incorporated uncertainties in the recurrence parameters for the background seismicity into the hazard analysis. We used three b-values of 0.62, 0.72, and 0.82 weighted 0.2, 0.6, and 0.2, respectively. An inspection of the resulting recurrence intervals for **M** 5 and 6 and greater events was performed to weight the three b-values. The corresponding a-values defined at $M_{min} = 5.0$ are 0.229, 0.143, and 0.089, respectively.

In figure 4, we show a comparison between the recurrence from the historical seismicity record from Pechmann and Arabasz (1995), the total from all the faults considered in our analysis, the Wasatch fault as characterized in this study, the background seismicity, and the total recurrence from all seismic sources. The agreement between our modeled recurrence and the recurrence from the historical record is quite good at **M** ≥ 6.5 even though the historical record is an extrapolation. At magnitudes of **M** 5.0 to 6.5, however, we are overpredicting the recurrence of moderate-sized events compared to the historical record. This overprediction could stem from our assumptions that the historical seismicity is mainly all background in nature and/or the weighting of the fault recurrence models. For example, increased weighting of the maximum magnitude model and hence decreased weighting of the characteristic model would result in lower recurrence for **M** 5.0 to 6.5 events.

Geologic Site Response Units and Amplification Factors

In order to quantify the site response of soil and unconsolidated sediments, we defined geologic site-response units in terms of a shear-wave velocity (V_S) profile, depth to a reference rock datum, and dynamic degradation curves (both shear modulus reduction and damping). For each unit, we computed frequency- and strain-dependent amplification factors as a function of input ground motions.

Near-Surface Geology

Near-surface geologic conditions in the Salt Lake Valley are dominated by the presence of Lake Bonneville sediments of latest Pleistocene age. The Bonneville Alloformation,

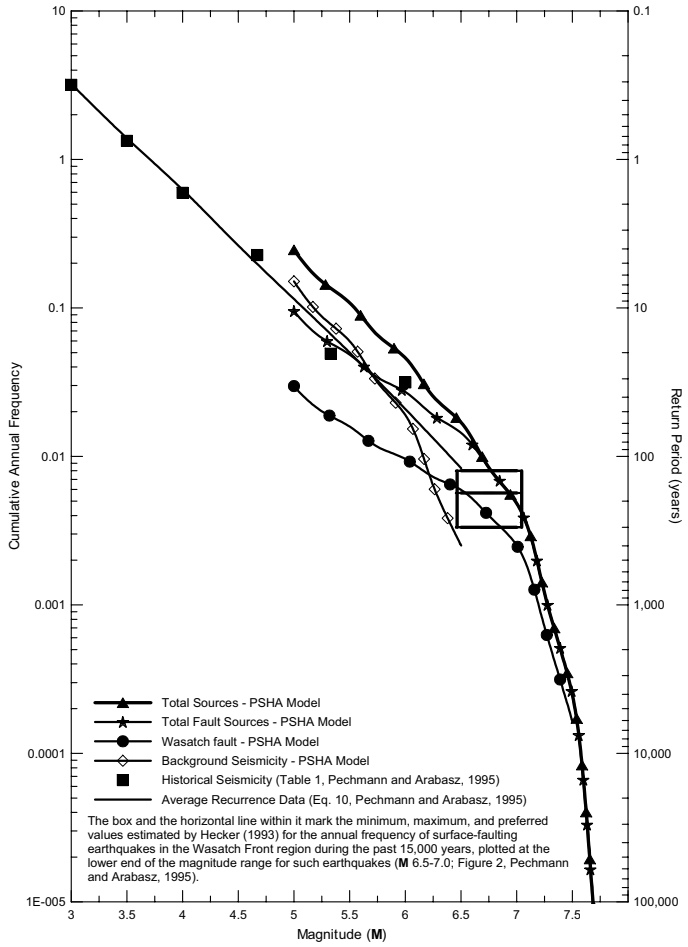

Figure 4. Comparison of the recurrence from the observed historical seismicity and paleoseismic records with that for the seismic sources modeled in the probabilistic seismic hazard analysis.

which lies at the surface over much of the valley, includes a wide variety of soil types and depositional environments. Glacial, stream, alluvial-fan, and colluvial deposits are also locally important. In the southern part of the Salt Lake Valley and along the benches on its eastern edge, surficial deposits (Lake Bonneville deltas, glacial moraines, pre-Bonneville alluvial-fan deposits, late Tertiary/early Pleistocene fanglomerates) are morphologically distinctive and generally thick in areas. In the northern and central parts of the valley, however, Holocene stream alluvium, deltaic deposits, and distal alluvial-fan deposits are generally thin.

Ashland and Rollins (1999) used the Unified Engineering Geology Mapping (UEGM) System (Keaton and DeGraff, 1996), formerly referred to as the Genesis-Lithology-Qualifier (GLQ) System (Keaton, 1984), to regroup traditional surficial-geologic units primarily on the basis of dominant grain size. Other researchers have recognized a correlation between grain size (Kayabelli and West, 1995; Wills and Silva, 1998), void ratio (Aki, 1988), and VS. Thus, the use of the UEGM System directly groups surficial deposits by grain size and likely constrains void ratio, hopefully constraining the site-response characteristics of the near-surface geologic deposits. Based largely on the classification of Ashland and Rollins (1999), we defined five distinct site-response units: lacustrine-alluvial silt and clay, lacustrine sand, lacustrine-alluvial gravel, Parley's Canyon - City Creek Canyon lacustrine-alluvial gravel, and older alluvial-fan/glacial gravel (figure 5).

Bedrock crops out or is buried by shallow surficial deposits along the valley margins, and in the foothills and mountain slopes of the Wasatch, Oquirrh, and Traverse Mountains (figure 5). Ashland and Rollins (1999) regrouped bedrock-geologic units of Salt Lake County and the Wasatch Range (Davis, 1983a,b) to reflect probable V_S characteristics. Only a few V_S measurements exist in the Salt Lake Valley in rock or rock-like material (Tinsley et al., 1991; Adan and Rollins, 1993; Wong and Silva, 1993). Shallow rock-like material that overlies lower-velocity soils (Tinsley et al., 1991) is interpreted to be tufa-cemented soil (Wong and Silva, 1993) associated with valley margin springs or Lake Bonneville shorelines.

Shear-Wave Velocity

We developed representative average near-surface V_S profiles for four of five site response units for which either downhole or surface-wave-based V_S measurements existed (figure 6). Essentially no data were available for the fifth unit, coarse-grained pre-Bonneville alluvial-fan and glacial deposits. Sources of downhole V_S measurements included data from the U.S. Geological Survey (Tinsley et al., 1991) and from unpublished geotechnical reports for various interstate highway and other major construction projects in the valley. Schuster and Sun (1993) determined near-surface V_S to a depth of 40 m using surface wave inversion methods at twenty-eight sites in the Salt Lake Valley. We used selected Schuster and Sun (1993) V_S profiles derived by the inversion of Rayleigh wave dispersion to supplement sparse downhole V_S data in the sand and gravel units. At three selected sites, V_S profiles based on Rayleigh wave-dispersion inversion yielded similar average V_S in the upper 30 m of the soil profile as downhole V_S profiles from nearby boreholes (Tinsley et al., 1991).

Our V_S profiles for each unit were compiled using a 5-m-depth interval. The V_S profiles used to construct the average profiles varied considerably in the level of detail and the depth interval between V_S measurements. Recent V_S profiles for major highway projects commonly used a depth interval less than 5 m and characterized subtle V_S heterogeneity within distinct layers. Other profiles, such as those in Tinsley et al. (1991), show average V_S values of relatively homogeneous distinct layers, some of which exceed 20 m in thickness.

The V_S profiles for the geologic site-response units extended to a maximum depth of only 55 m. The one exception was the lacustrine-alluvial silt and clay category where data were available down to 90 m (figure 6a). To constrain the depth of near-surface geologic units, we plotted contours of the depth of Quaternary valley fill based on well data compiled by Arnow et al. (1970) (figure 5). In the western part of the Salt Lake Valley, the depth of near-surface low-velocity ($V_S < 760$ m/sec) valley fill based on V_S profiles was in agreement with the Arnow et al. (1970) Quaternary valley-fill-thickness data. In the northeastern part of the Salt Lake

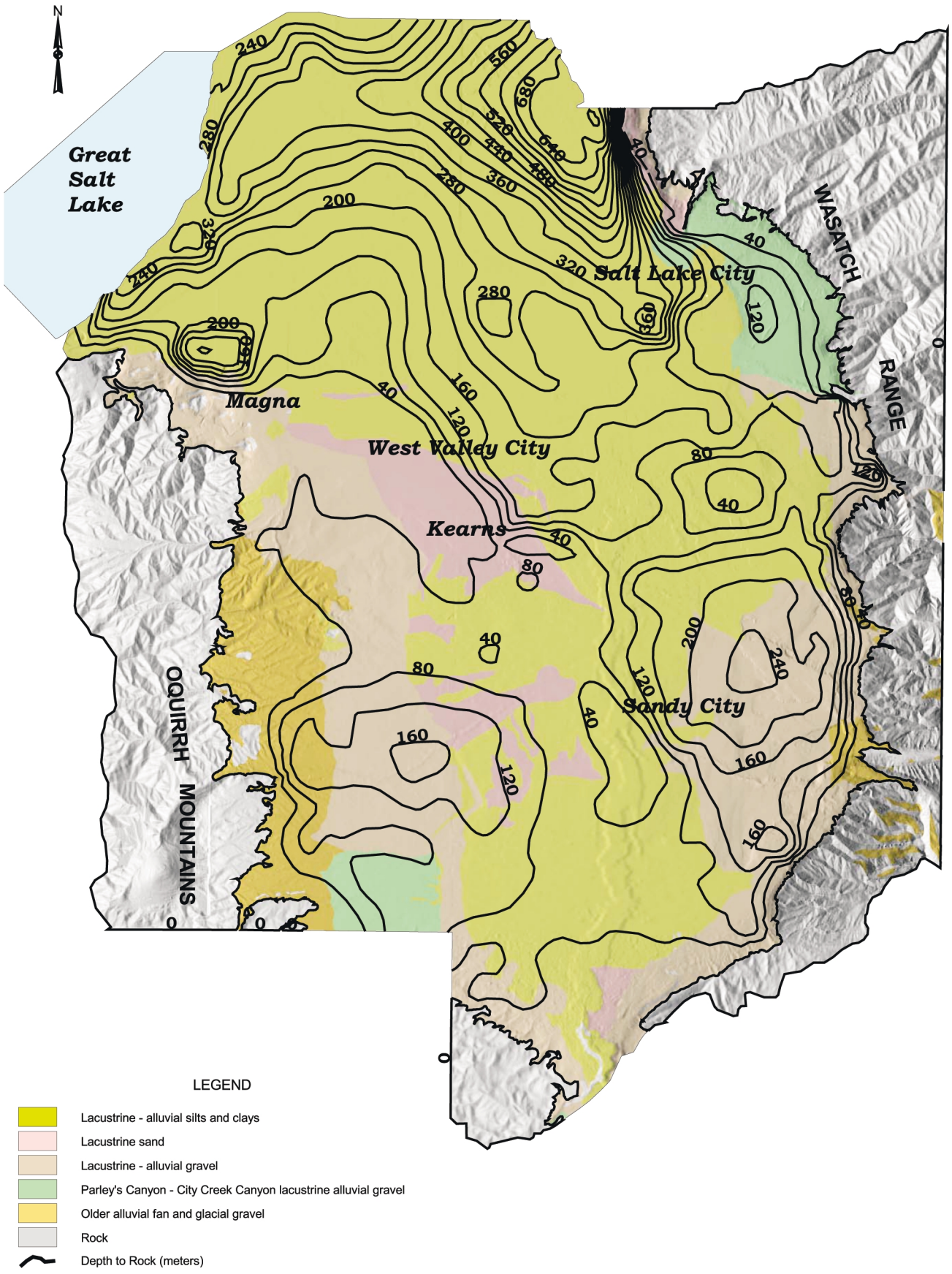

Figure 5. Site-response units and depth to rock in the map area.

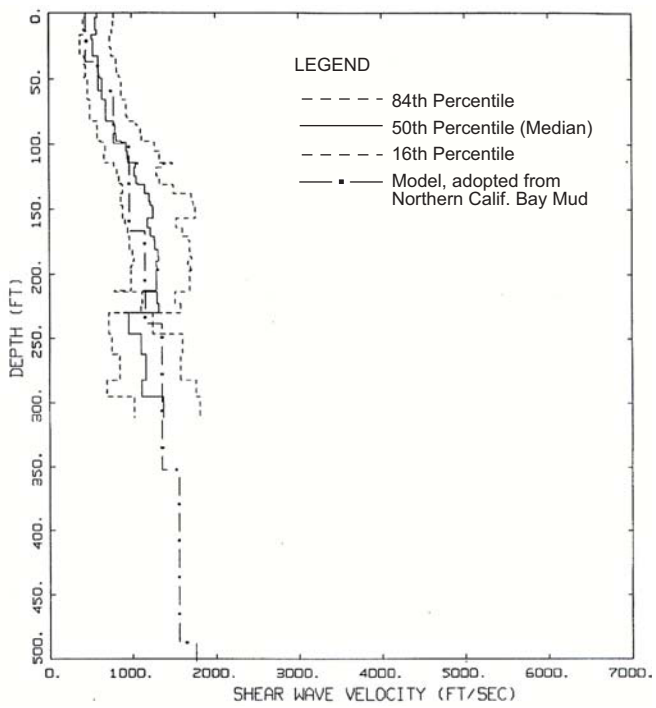

a) Lacustrine-alluvial silt and clay

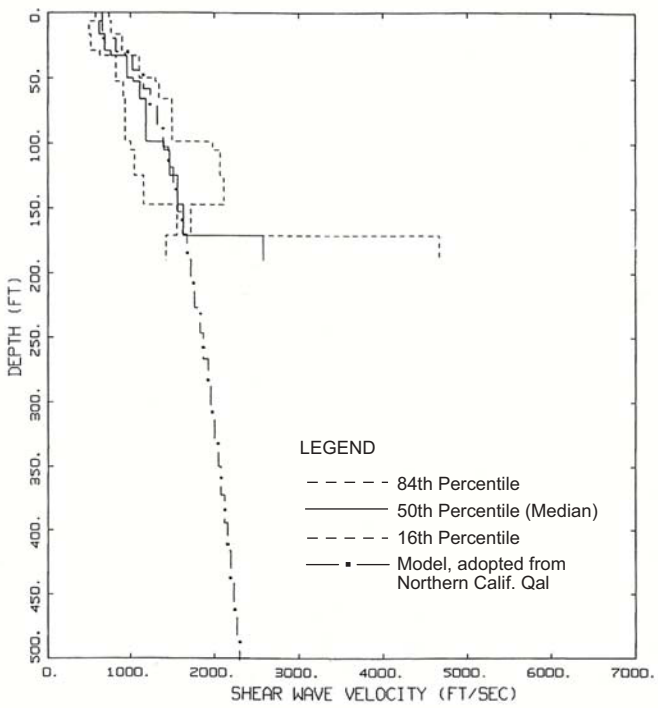

b) Lacustrine sand

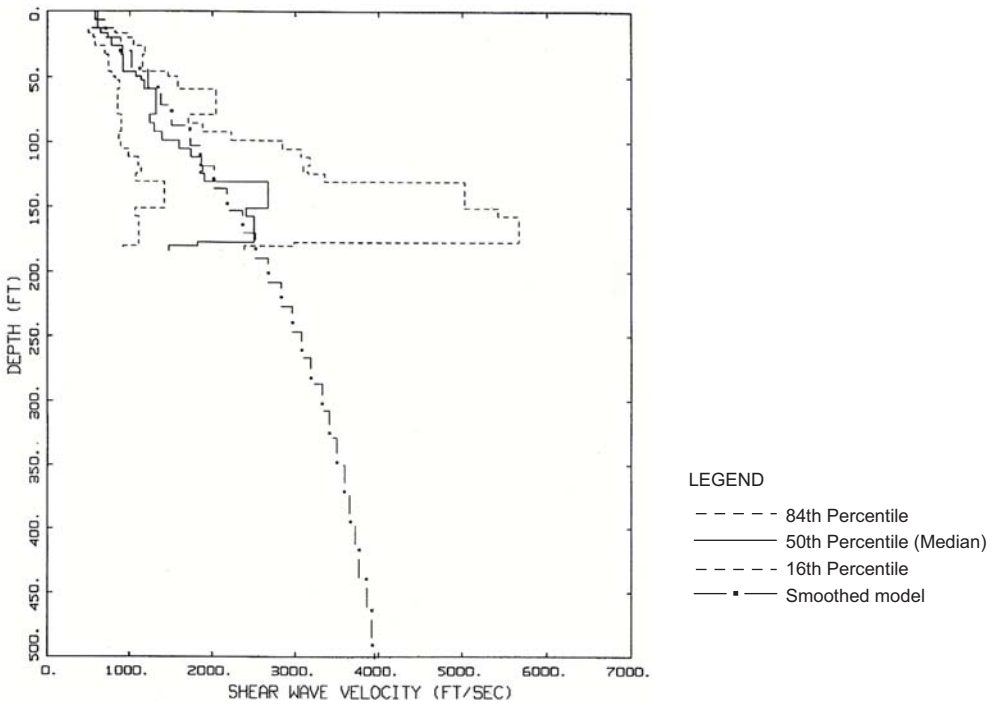

c) Lacustrine-alluvial gravel

Figure 6. Shear-wave velocity profiles for the site-response units.

Valley, high-velocity valley fill (V_S > 760 m/sec) was locally shallower than predicted by the Arnow et al. (1970) data. In the majority of the Salt Lake Valley, Vs profiles do not extend deep enough to validate the Arnow et al. (1970) estimates of Quaternary valley-fill thickness.

Only the upper portion of the profiles are shown on Figure 6, to a depth of 152 m (500 ft), although they extend to 487.7 m (1,600 ft). Below 152 m (500 ft), the velocity profiles exhibit very little or no increase in velocity. Figures 6a, b, and c show the median, 16th, and 84th percentile profiles for the lacustrine-alluvial silt and clay, lacustrine sand, and lacustrine gravel, respectively. In figure 6a, the San Francisco Bay mud velocity profile developed by Silva et al. (1999) is shown for comparison. The median profile for the silt and clay compares very favorably with the Bay mud profile. The latter was used in the computation of the amplification factors because it was based on a much larger database of profiles and was considered to provide a more robust representation of the variability in velocities. Similarly, the profile for northern California Quaternary alluvium (Silva et al., 1999) shown in figure 6b with the profiles for lacustrine sand was used in the calculation of amplification factors. For the lacustrine-alluvial gravels shown in figure 6c, a smoothed velocity profile through the shallow data was computed. The rest of the profile was developed by attaching an average profile appropriate for that lithologic type derived from the database of Pacific Engineering & Analysis. This profile was used for the amplification factors. A single profile from Laird Park (figure 6d; Tinsley et al., 1991) was used for the Parley's Canyon-City Creek Canyon lacustrine-alluvial gravel. A relatively high-velocity tufa (cemented gravel) layer is present in the profile at depths of 9 to 18 m (30 to 60 ft). Finally, because no velocity data were available for the older alluvial fan/glacial gravel, a profile for stiff cohesionless soil from EPRI (1983) was used in the amplification factor calculations.

Amplification Factors

We computed amplification factors as a function of site response unit, ranges in thickness of the unconsolidated sediments, and input rock motion. For computational purposes, we discretized the total thickness of unconsolidated sediments in the Salt Lake Valley into six ranges that covered the full range of thicknesses in the map area based on the Arnow et al. (1970) data: 3.0 to 15.2 m (10-50 ft), 15.2 to 30.5 m (50-100 ft), 30.5 to 61.0 m (100-200 ft), 61.0 to 121.9 m (200-400 ft), 121.9 to 243.8 m (400-800 ft), and 243.8 to 800.0 m (800-2,624 ft). The top of the semi-consolidated sediments (R1) in their model was taken as the bottom of the unconsolidated sediments. In the actual computation of the amplification factors, overlaps in the thicknesses between categories were incorporated into the analysis to accommodate the uncertainties in amplification factors and the estimated thicknesses. Units with thicknesses less than 3 m were considered to be equivalent to rock. For the five site-response units and six thickness categories, a total of 30 subcategories were defined.

Based on each average profile, 30 randomized profiles were computed to account for the horizontal and vertical variability in velocities and these were used in the simulations. The randomization was done using a correlation model for soil velocity profiles developed by Gabriel Toro (Risk Engineering Inc.). Shear modulus reduction and damping curves were assigned to the various site-response units to account for strain-dependent non-linear soil response. For all site-response units except the lacustrine-alluvial silt and clay, both EPRI (1983) curves for cohesionless soils and Peninsular Range, California, curves (Silva et al., 1997) were used to compute the amplification factors. Amplification factors were calculated by enveloping the median factors using each set of degradation curves. The use of both sets of curves captures the uncertainty in non-linear material properties. For the lacustrine-alluvial silt and clay, the EPRI (1983) and Vucetic and Dobry (1998) curves were used depending on depth. Nonlinearity was assumed to a depth of 152 m (500 ft) based on modeling recorded strong ground motions (Silva et al., 1998a).

We used the stochastic numerical ground motion modeling approach coupled with an equivalent-linear methodology (Silva et al., 1998b) to calculate amplification factors for 5% – damped response spectra for each site-category. The point-source stochastic methodology was used to generate rock acceleration response spectra for a **M** 6.5 earthquake, which were then propagated up through the site-category profiles. The **M** 6.5 event was placed at several distances to produce input peak accelerations of 0.05, 0.10, 0.20, 0.40, 0.50, and 0.75 g. Thus the amplification factors (the ratios of the response spectra at the top of the profiles to the input spectra) are a strong function of the reference rock peak acceleration, spectral frequency, and nonlinear soil response. Interpolation was used to obtain amplification factors at other reference rock peak accelerations. The median amplification factors for 0.75 g were used for input motions above that value. An example of the strain-dependent amplification factors is shown in figure 7. At peak horizontal acceleration (100 Hz on figure 7), the median amplification factors ranged from 0.62 to 2.09. At 0.2 and 1.0 sec spectral accelerations, the median factors ranged from 0.50 to 2.19 and 0.94 to 3.13, respectively. For comparison, the site coefficients F_a and F_v in the International Building Code, which are essentially amplification factors, range from 0.9 to 2.5 and 1.3 to 3.5, respectively, for soil site classes C to E. F_a and F_v correspond to the 0.2 sec (short-period) and 1.0 sec period spectral responses, respectively.

Attenuation Characterization

To characterize the attenuation of ground motions in both the scenario and probabilistic analyses, we used empirical attenuation relationships appropriate for soft rock sites in the western U.S. and a stochastic numerical modeling technique (Silva et al., 1998b). An important consideration in the selection of attenuation relationships is that the Wasatch Front is located in the extensional Basin and Range Province where normal faulting predominates. It has been increasingly recognized that earthquakes in extensional tectonic regimes produce lower ground motions than events in compressional/strike-slip regimes for the same magnitude and distance (Wong and Olig, 1998; Spudich et al., 1997; Stepp et al., 2001). We used the

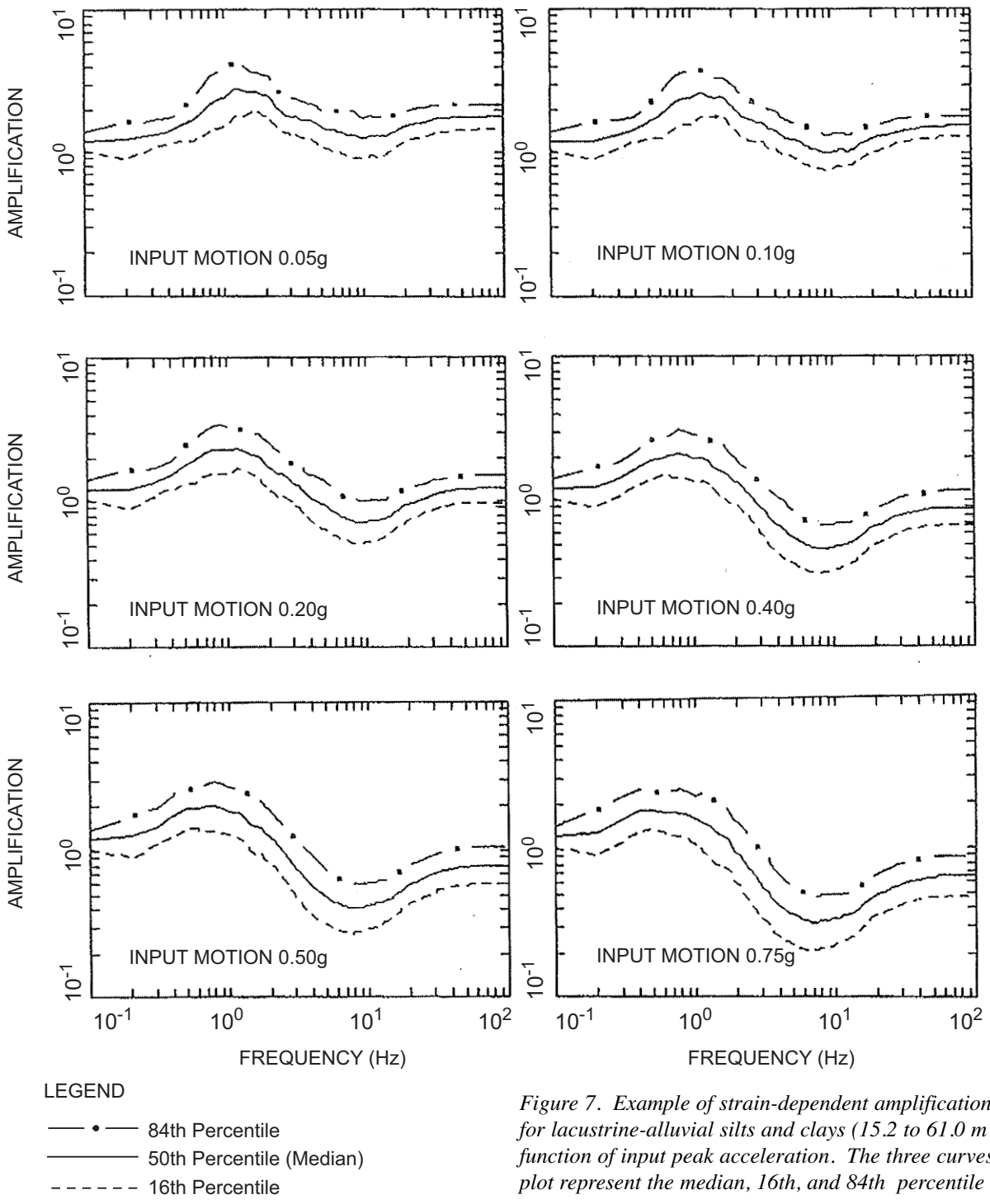

Figure 7. Example of strain-dependent amplification factors for lacustrine-alluvial silts and clays (15.2 to 61.0 m thick) as a function of input peak acceleration. The three curves in each plot represent the median, 16th, and 84th percentile values.

following empirical relationships in this study (figure 8): Abrahamson and Silva (1997), with normal faulting factors (N. Abrahamson, written communication, 1997); Spudich et al. (1999), which was developed from an extensional earthquake strong-motion database; Sadigh et al. (1997); and Campbell (1997). The latter two relationships are based primarily on California strong-motion data and were included to more fully address uncertainty, but assigned a lower weight. None of these relationships are specific to the Salt Lake Valley or the Basin and Range Province due to the absence of strong-motion records. The relationships were weighted 0.40, 0.30, 0.15, and 0.15, respectively, based on our subjective judgment of the applicability of each relationship.

To compensate for the lack of region-specific attenuation relationships, the stochastic ground-motion modeling approach was used to develop such relationships (Wong et al., 1996) (figure 8). The point-source version of the stochastic methodology (Silva et al., 1998b) was used to model earthquakes of **M** 5.5, 6.5, and 7.5 in the distance range of 1 to 400 km. Uncertainties in stress drop, magnitude-dependent focal depths, the crustal attenuation parameters Q_o and η, the near-surface attenuation parameter (kappa), and the rock profile atop the crustal model were included in the computations of the attenuation relationships through parametric variations

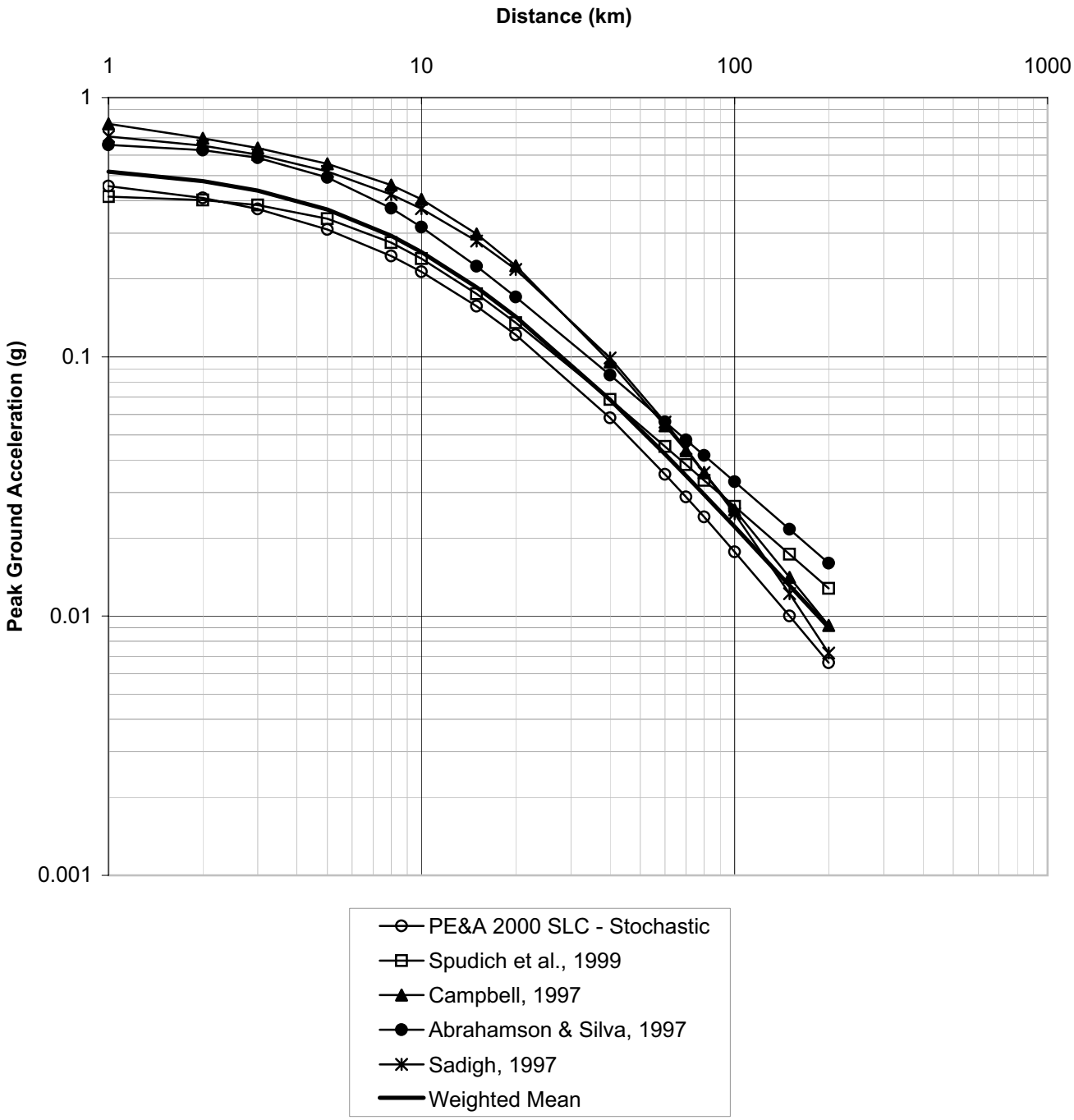

Figure 8. Comparison of rock attenuation relationships for M 7.0.

(Wong et al., 1996) (table 3). A range of magnitude-dependent stress drops appropriate for extensional regimes was used (Silva et al., 1997). The P-wave and S-wave crustal velocity model for the Wasatch Front used in locating earthquakes by the University of Utah Seismograph Stations was adopted in the calculations. Inserted on top of this model is a generic western U.S. soft rock V_S profile developed from the database compiled by Pacific Engineering & Analysis.

Uncertainties in the regression of the simulated data are added to the modeling uncertainty to produce 16th, 50th (median), and 84th percentile attenuation relationships. A total of 30 simulations were made for each magnitude and distance (total of 810), and the results fitted with a functional form which accommodates magnitude-dependent saturation and far-field fall-off (figure 8). The functional form is:

$$\text{Ln } Y = C_1 + C_2 \bullet \mathbf{M} + (C_6 + C_7 \bullet \mathbf{M}) \bullet \text{Ln } [R + \exp(C_4)] + C_{10} \ (\mathbf{M}\text{-}6)^2$$

where Y is the peak ground motion parameter, R is rupture distance, and C_1 through C_{10} are coefficients fit to the data (table 4). The total uncertainty (vector sum of the parametric and modeling uncertainties) is also listed in table 4.

The uncertainty in ground motion attenuation was includ-

Table 3. Input parameters and weights used in development of stochastic attenuation relationships.

Parameter	Values	Standard Errors σ_{ln}
Magnitude (**M**)	5.5, 6.5, 7.5	–
Distance (km)	1, 5, 10, 20, 50, 75, 100, 200, 400	
Source Depth (km)[1]		0.6
M 5.5	7.5 (4, 12)[2]	
M 6.5	7.5 (5, 10)[2]	
M 7.5	7.5 (5, 10)[2]	
Stress Drop (bars)[1]		0.7
M 5.5	60	
M 6.5	45	
M 7.5	36	
Crustal Attenuation[1,3]		0.3
Q_o	400	
η	0.20	–
Kappa (sec)[1,4]	0.04	0.4

[1] Parameters randomly varied where σ_{ln} is based on observations.
[2] Upper- and lower-bound values
[3] Q = Quality Factor = Q *of* $^{\eta}$
[4] Attenuation at zero distance = $e^{-\pi(kappa)f}$

ed in the probabilistic analysis by using the log-normal distribution about the median values as defined by the standard error associated with each attenuation relationship. Three standard deviations about the median value were included in the analysis.

GROUND MOTION CALCULATIONS AND MAP DEVELOPMENT

Ground motions were estimated for both the scenario and probabilistic hazard maps. Peak horizontal acceleration and spectral accelerations at spectral periods of 0.2 and 1.0 sec were calculated using both empirical attenuation relationships and stochastic modeling. The resulting ground motion values were then displayed in map form using GIS.

Scenario Ground Motions

We calculated ground motions for a **M** 7.0 scenario earthquake on the Salt Lake City segment of the Wasatch fault using the stochastic finite fault approach (Silva et al., 1998b). This modeling explicitly incorporates the effects of the seismic source (fault geometry and dip, depth of rupture initiation, and sense of slip) and rupture propagation (e.g., directivity), which are particularly important at close distances to the fault. The scenario earthquake was modeled as a 46-km-long and 19.5-km-wide planar rupture which dips 55° to the west. The modeled rupture extends from the Salt Lake salient south to the Traverse Mountains salient and includes the East Bench fault (figure 1). A total of 30 simulations were made where the slip models and rupture initiation were varied. We used the same values of Q_o and η in the scenario calculations as those assumed for the stochastic attenuation relationships. Because our approach assumes a planar rupture, we adjusted for a curvilinear fault by shifting the computed ground motion values by the shortest distance between the planar and curvilinear faults. Because the finite-fault methodology implicitly assumes stress drops typical of compressional/strike-slip tectonic regimes through use of the Wells and Coppersmith (1994) relationship in defining rupture areas, the stochastic ground motions were adjusted downward to account for the lower stress drops of extensional regime earthquakes. Adjustment factors of 0.74, 0.78, and 0.81 for peak acceleration, and 0.2 and 1.0 sec spectral acceleration, respectively, were derived from the Abrahamson and Silva (1997) normal faulting factors. Scenario ground motion values were calculated by assigning a 0.40 weight to the values from the empirical attenuation relationships and 0.60 weight to the values from the stochastic finite fault model.

Probabilistic Ground Motions

To calculate the probabilistic ground motions, we performed a comprehensive Cornell (1968) hazard analysis using logic trees (figure 3), employing the computer code HAZ32 written by Norm Abrahamson. All known seismic sources, which could generate strong ground shaking in the study area, were incorporated into the probabilistic analysis. Both empirical and stochastic attenuation relationships, weighted 0.40 and 0.60, respectively, were used in the analysis to calculate the ground motion values. The mean probabilistic hazard was calculated for peak horizontal acceleration and 0.2 and 1.0 sec spectral accelerations at return periods of 500 and 2,500 years.

An example of the probabilistic seismic hazard calculations for a single location on the map, in this case, downtown

Table 4. Coefficients and uncertainties for the stochastic attenuation relationships.

Period (sec)	C1	C2	C4	C6	C7	C10	Total Sigma
0.0	2.11611	0.20552	2.60	-2.98853	0.20178	-0.12973	0.7214
0.010	2.07117	0.21210	2.60	-2.99176	0.20229	-0.13295	0.7214
0.020	2.14640	0.20738	2.60	-3.00525	0.20329	-0.13366	0.7244
0.025	2.24628	0.20060	2.60	-3.02424	0.20482	-0.13489	0.7278
0.032	2.36920	0.20057	2.60	-3.04857	0.20555	-0.13868	0.7410
0.040	2.95951	0.17736	2.70	-3.15908	0.21105	-0.14563	0.7580
0.050	3.18765	0.18066	2.70	-3.19780	0.21106	-0.14897	0.7731
0.056	3.37768	0.17344	2.70	-3.22948	0.21281	-0.15052	0.7848
0.0625	4.04963	0.14052	2.80	-3.34773	0.21951	-0.15304	0.8060
0.071	4.23449	0.13580	2.80	-3.36836	0.21976	-0.15113	0.8098
0.083	5.01383	0.08429	2.90	-3.48964	0.22818	-0.14935	0.8178
0.100	5.07446	0.08972	2.90	-3.46592	0.22383	-0.14131	0.8230
0.125	5.58048	0.07191	3.00	-3.51198	0.22307	-0.13153	0.8352
0.143	5.32884	0.10145	3.00	-3.44929	0.21650	-0.13023	0.8328
0.167	5.05552	0.12605	3.00	-3.37517	0.21008	-0.12677	0.8422
0.200	4.10462	0.20177	2.90	-3.17434	0.19370	-0.12138	0.8317
0.250	3.50435	0.26160	2.90	-3.03223	0.17944	-0.11550	0.7887
0.330	2.18045	0.36692	2.80	-2.77044	0.15881	-0.11664	0.7746
0.400	1.17110	0.43911	2.70	-2.59502	0.14636	-0.12177	0.7506
0.500	0.00875	0.52768	2.60	-2.41185	0.13347	-0.13355	0.7542
0.770	-2.55119	0.76351	2.40	-2.05689	0.10491	-0.17699	0.8136
1.000	-4.16777	0.93873	2.30	-1.87090	0.08841	-0.21667	0.8081
1.670	-7.79399	1.34654	2.10	-1.56525	0.06191	-0.32110	0.9347
2.000	-9.29403	1.52258	2.00	-1.45691	0.05256	-0.36517	0.9584
2.500	-11.14149	1.74691	1.90	-1.34389	0.04270	-0.41673	0.9936
5.000	-16.85871	2.44819	1.70	-1.10629	0.02196	-0.55692	1.2241

Note: C_3, C_5, C_8 and C_9 are zero

Salt Lake City, is shown on figure 9. The mean hazard and fractiles are shown. To illustrate the uncertainty in the probabilistic ground motions, one sigma values (15th and 85th percentiles) for peak acceleration at a 2,500-year return period are about 0.45 g and 0.81 g, respectively, with a mean hazard value of 0.67 g. Figure 10 illustrates the deaggregation by seismic source of the mean peak horizontal acceleration hazard for the same location. As expected, the Salt Lake City segment dominates the probabilistic hazard in Salt Lake City except at short return periods of less than 100 years where the background seismicity controls the high-frequency hazard.

Map Development

The ground shaking maps were produced using a vector- and raster-based GIS. Scenario and probabilistic ground motions on rock were calculated for the map area using a grid of points at a 200-m spacing. Each grid point was assigned to a site-response category. The thickness of unconsolidated sediments was estimated for each grid point based on the Arnow et al. (1970) model. Surface ground motions were calculated by multiplying the scenario or probabilistic rock ground motions by the appropriate amplification factors. The amplification factors for each grid point were selected based on the site-response unit, the thickness of the unconsolidated sediments, and the input rock peak acceleration as described above. For each map, the peak or spectral acceleration values were color contoured by interpolation in intervals of 0.10 to 0.30 g. The ground motion values were then spatially smoothed with a circular window of 500-m radius so that no features smaller than this size were present on the maps. The intent was to avoid implying a greater level of resolution and/or accuracy than was possible given the limitations of available geologic data.

MAPS AND RESULTS

The accompanying plates 1 to 9 (on CD in pocket) are the resulting hazard maps at a scale of 1:75,000. Figures 11 to 19 are simplified page-size versions of the plates. To assist the layperson unfamiliar with the mapped ground motion parameters, specifically peak horizontal ground acceleration, we show a correlation between it and Modified Mercalli intensity developed by Wald et al. (1999) on plates 1, 4, and 7, and in table 5. The following are brief general descriptions of the hazard maps.

Wasatch Fault M 7.0 Scenario Maps

The scenario maps are shown on plates 1 to 3 (figures 11 to 13). Examination of plate 1 indicates that high-frequency ground motions, as characterized by peak horizontal acceleration, could exceed 1 g from a **M** 7.0 earthquake occurring on

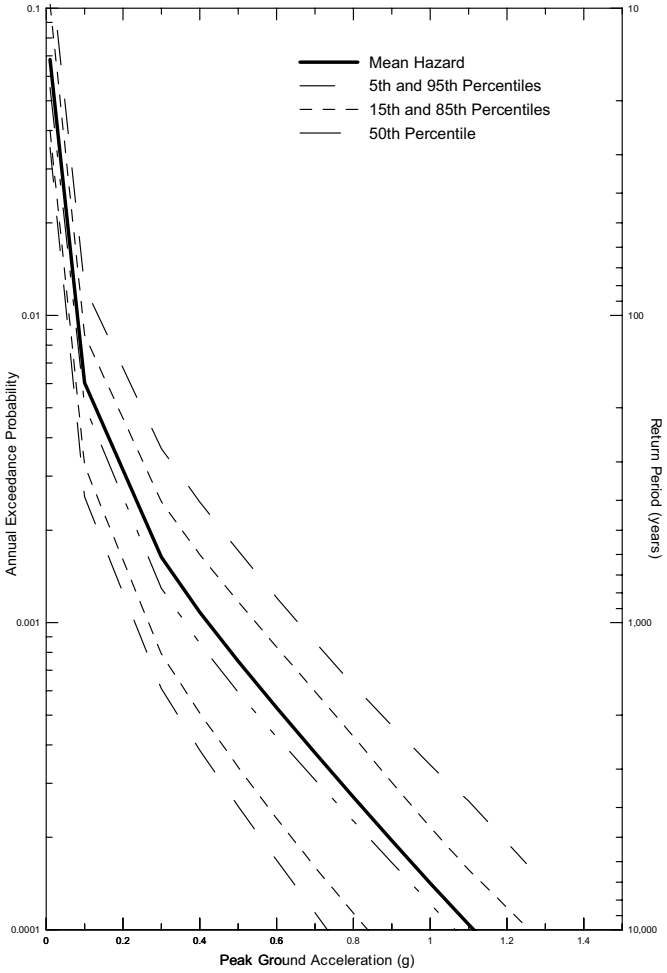

Figure 9. Example of peak horizontal acceleration hazard curves for a site in downtown Salt Lake City.

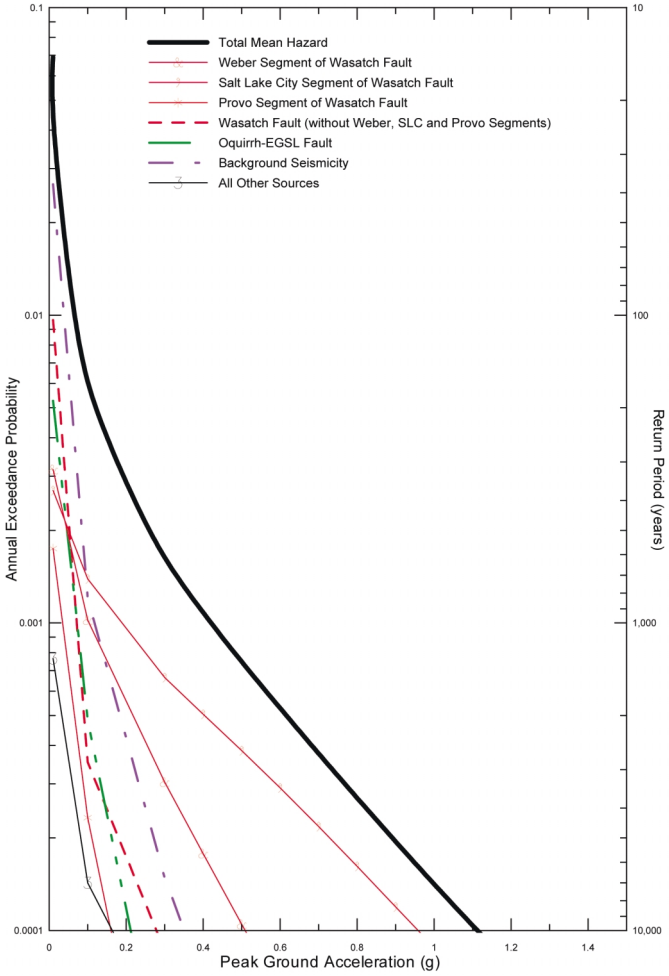

Figure 10. Example of source deaggregation of the mean seismic hazard for peak horizontal acceleration.

the Salt Lake City segment. Note that the rate of decay of ground motions on rock in the footwall (rockmass beneath and east of the west-dipping Wasatch fault) is faster and more uniform than that in the hanging wall (rockmass above and west of the fault). The highest ground motions (> 0.7 g) occur in the stiff gravels and sands adjacent to the fault particularly in the bench areas. In fact, the pattern of high-frequency ground shaking mimics the distribution of site-response units (figure 5). The lower peak accelerations occur over the thick deposits of lacustrine-alluvial silts and clays which are damping out the high-frequency ground motions (plate 1). Site effects appear to be more dominant than the hanging wall effect as illustrated by the high peak accelerations east of the East Bench fault in the footwall.

The pattern of shaking at 0.2 sec resembles that for peak acceleration. The highest shaking occurs in the area east of the East Bench fault, again illustrating the amplification at short to moderate periods (plate 2). In contrast, at long periods (e.g., 1.0 sec spectral acceleration), the correspondence between site-response units and ground motions is not as strong as for the shorter periods. The highest ground motions (> 1.1 g) occur in the deeper portions of the basin, i.e., areas of thick unconsolidated sediments, particularly in the Cottonwood Heights and Olympus Cove areas adjacent to the Wasatch fault (plate 3). Directivity effects, which are long period in nature (> 0.5 sec), are not readily apparent on plate 3 because they have been diluted somewhat by the use of empirical attenuation relationships and/or masked by site effects.

500-Year Probabilistic Maps

Plates 4 to 6 show the probabilistic ground motions at an exceedance probability of 10% in 50 years (500-year return period) (figures 14 to 16). Peak horizontal accelerations range up to 0.5 g. Two localized areas of the highest values (> 0.4 g) are near Kearns in an area of lacustrine sands and along the Warm Springs fault north of downtown Salt Lake City (plate 4). The distribution of peak acceleration greater than 0.3 g corresponds with the occurrence of the lacustrine sands in the valley. The lowest ground motions occur in the bedrock areas of the Wasatch Range and Oquirrh Mountains.

The correlation of site-response units with 0.2 sec spectral acceleration values is most striking (plate 5). The highest motions (> 1.0 g) are again near the Warm Springs fault. Strong moderate-period shaking also occurs in the bench areas east of the East Bench fault, in areas in Kearns and West Valley City, and Point-of-the-Mountain. The lowest 0.2 sec spectral accelerations occur in the bedrock areas and in thick lacustrine-alluvial silts and clays in the central portion of the valley which indicates significant intermediate frequency damping.

Table 5. Relationship of peak horizontal ground acceleration (PGA) to Modified Mercalli (MM) intensity (after Wald et al., 1999).

MM Intensity	Perceived Shaking	Damage	PGA(g)
I	Not felt except by a very few under especially favorable circumstances	None	<<0.01
II	Felt only by a few persons at rest especially on upper floors of buildings.	None	<0.01
III	Felt quite noticeably indoors; especially on upper floors of buildings, but many people do not recognize it as an earthquake.	None	<0.01
IV	During the day felt indoors by many, outdoors by few. At night some awakened.	None	0.01-0.04
V	Felt by nearly everyone, many awakened.	Very light - Some dishes and windows broken; cracked plaster in a few places; unstable objects overturned.	0.04-0.09
VI	Felt by all, many frightened.	Light - Some heavy furniture moved; a few instances of fallen plaster and damaged chimneys.	0.09-0.18
VII	Very strong	Moderate - Damage negligible in buildings of good design and construction; slight to moderate in well built ordinary structures; considerable in poorly built or badly designed structures; some chimneys broken.	0.18-0.34
VIII	Severe-Persons driving cars disturbed.	Moderate to heavy - Damage slight in specially designed structures; considerable in ordinary substantial buildings with partial collapse; great in poorly built structures. Chimneys toppled.	0.34-0.65
IX	Violent	Heavy - Damage considerable in specially designed structures; well designed frame structures thrown out of plumb; great in substantial buildings, with partial collapse. Buildings shifted off foundations.	0.65-1.24
X	Extreme	Very heavy. Some well built wooden structures destroyed; most masonry and frame structures destroyed with foundations.	>1.24
XI	Extreme	Extreme - Few, if any, (masonry) structures remain standing.	>1.24
XII	Extreme	Extreme - Damage total.	>1.24

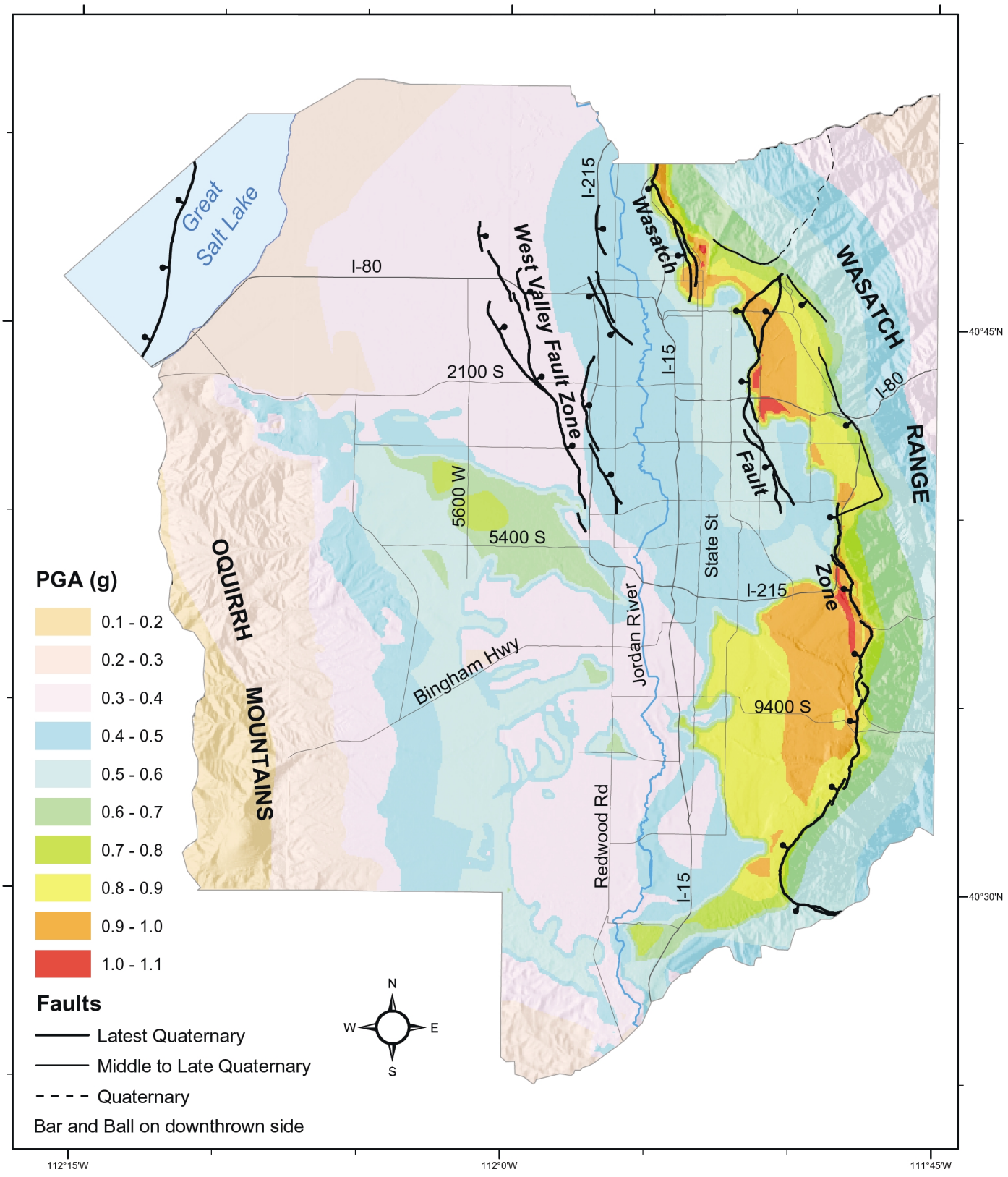

Figure 11. Salt Lake City segment, Wasatch fault M 7.0 earthquake scenario, peak horizontal acceleration (g) at the ground surface. Simplified from Plate 1.

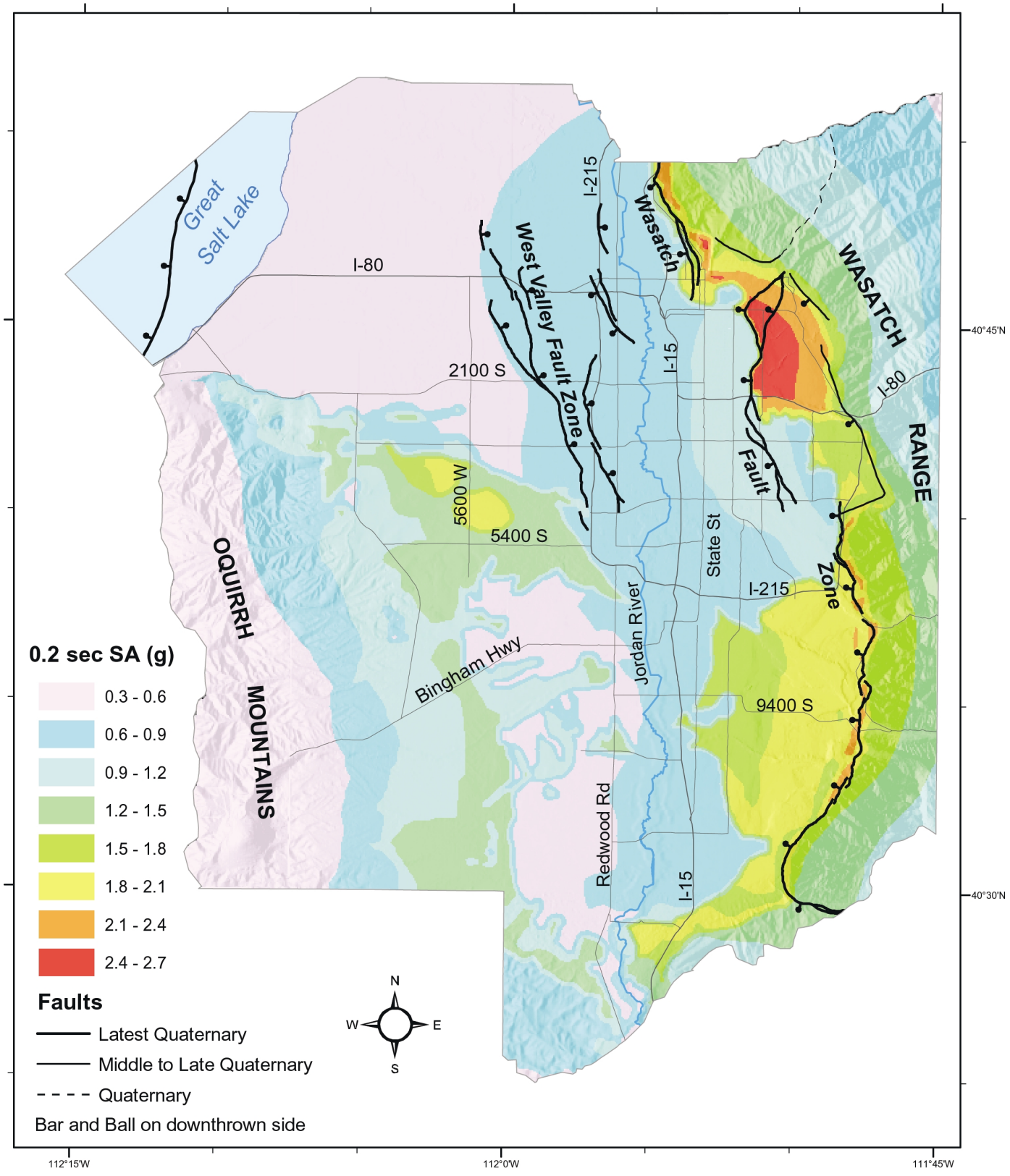

Figure 12. Salt Lake City segment, Wasatch fault M 7.0 earthquake scenario, 0.2 sec spectral acceleration (g) at the ground surface. Simplified from Plate 2.

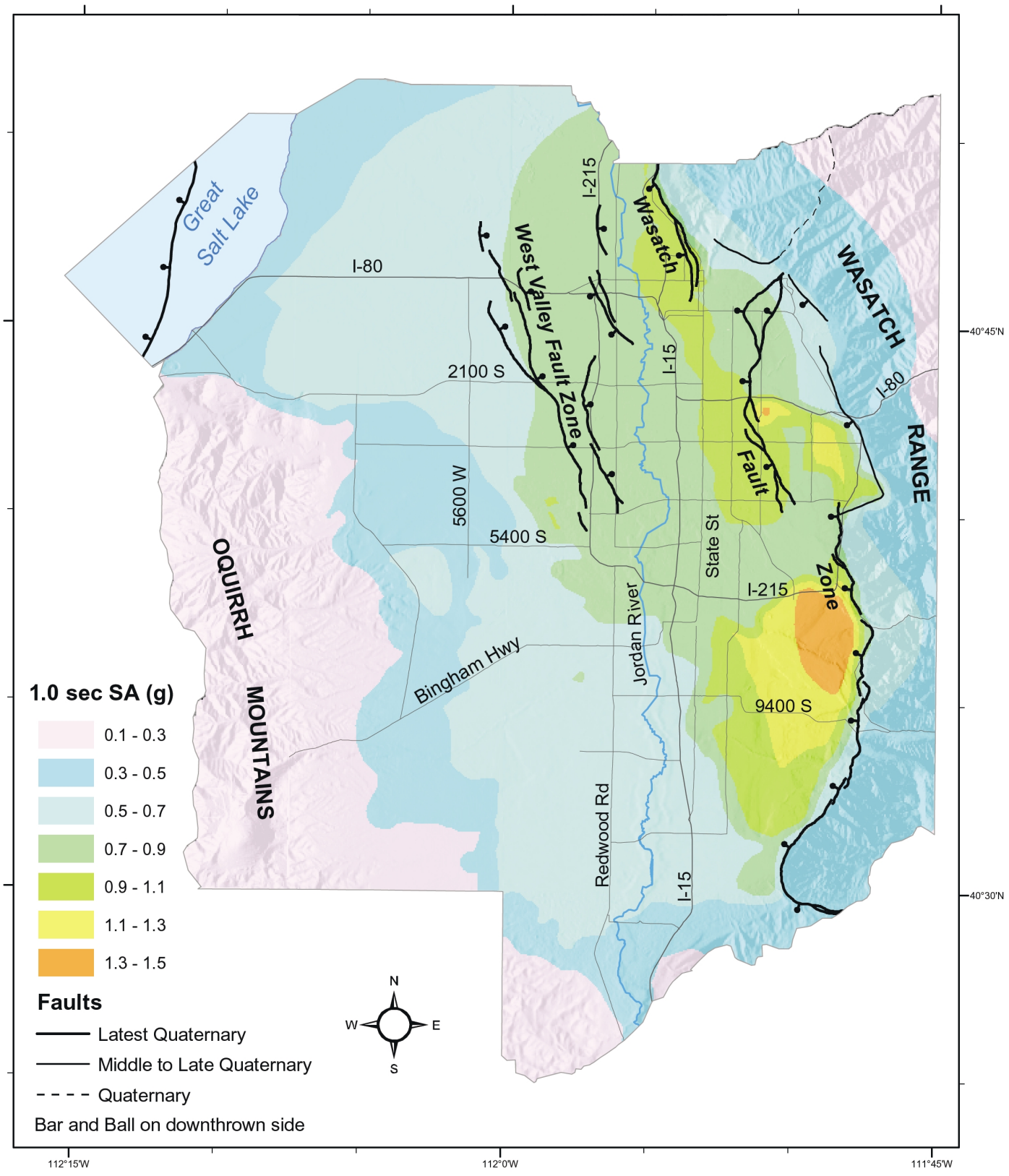

Figure 13. Salt Lake City segment, Wasatch fault M 7.0 earthquake scenario, 1.0 sec spectral acceleration (g) at the ground surface. Simplified from Plate 3.

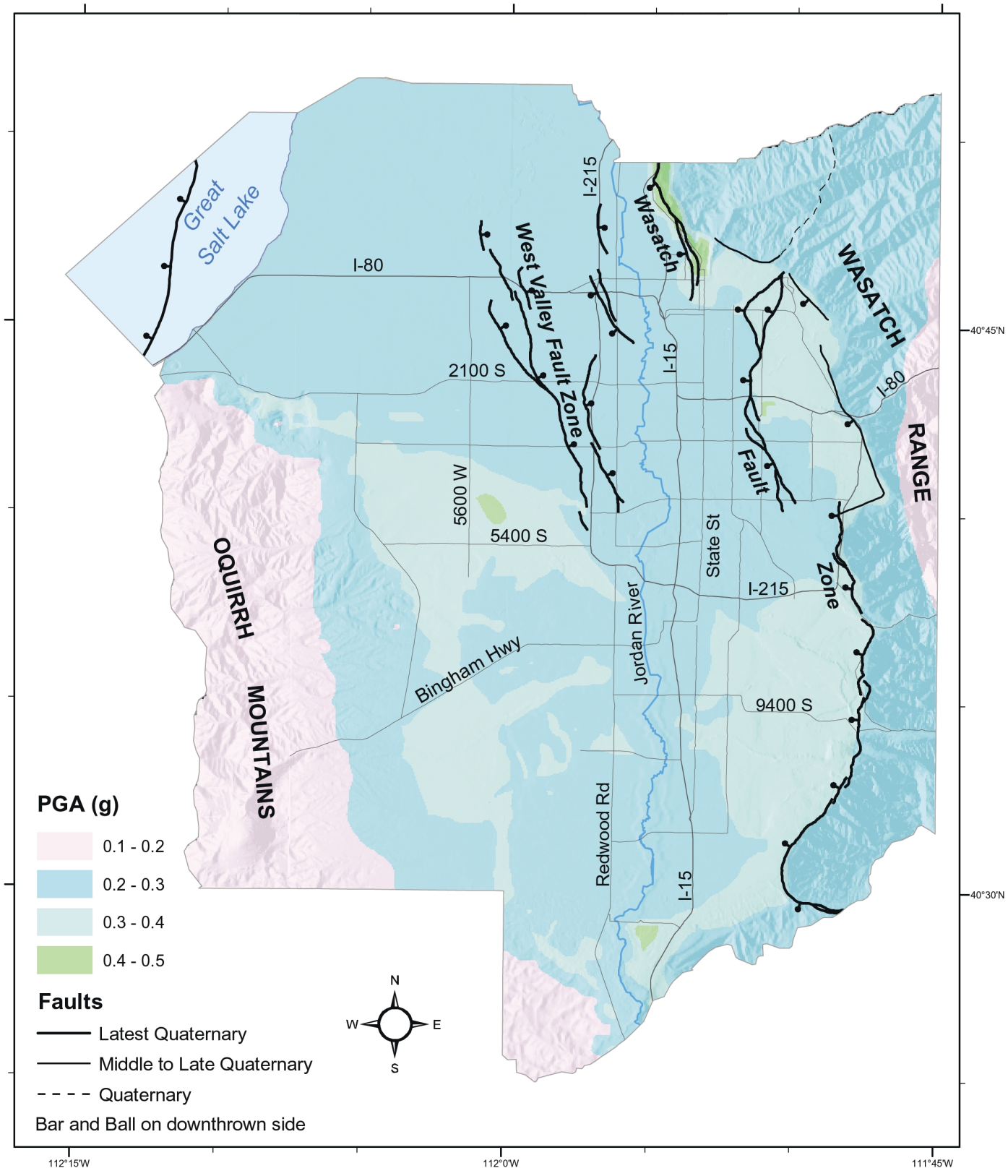

Figure 14. 10% probability of exceedance in 50 years, peak horizontal acceleration (g) at the ground surface. Simplified from Plate 4.

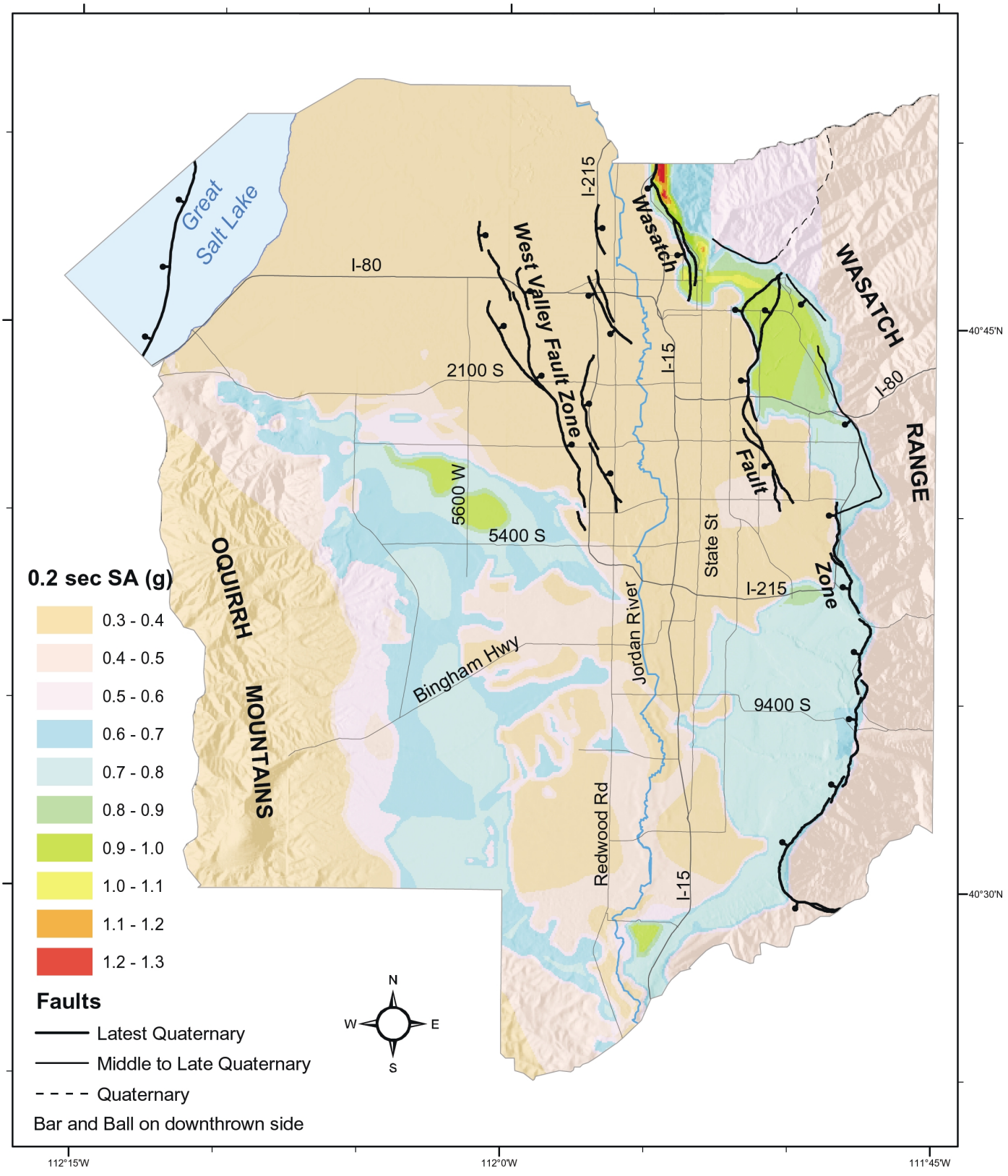

Figure 15. 10% probability of exceedance in 50 years, 0.2 sec spectral acceleration (g) at the ground surface. Simplified from Plate 5.

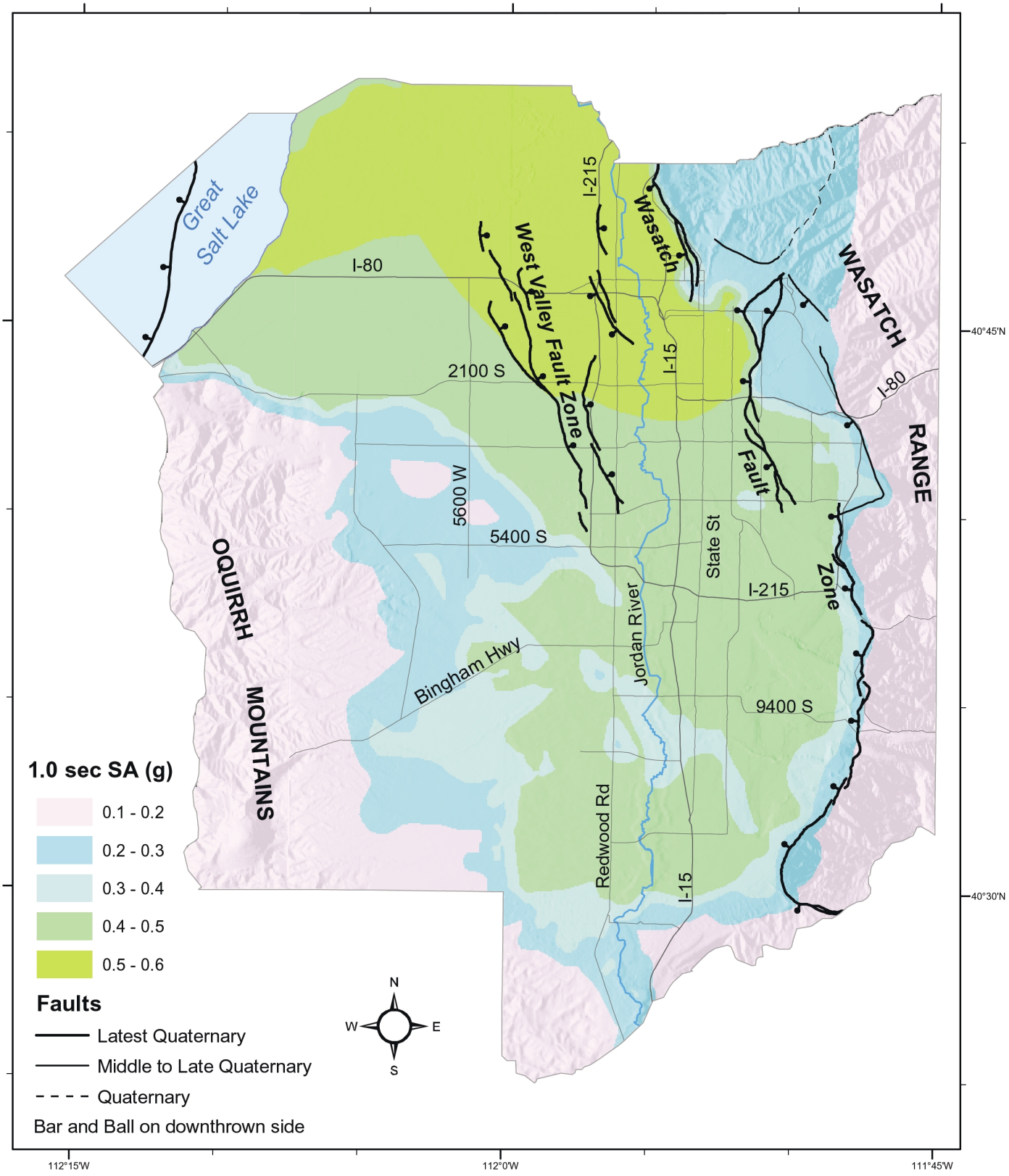

Figure 16. 10% probability of exceedance in 50 years, 1.0 sec spectral acceleration (g) at the ground surface. Simplified from Plate 6.

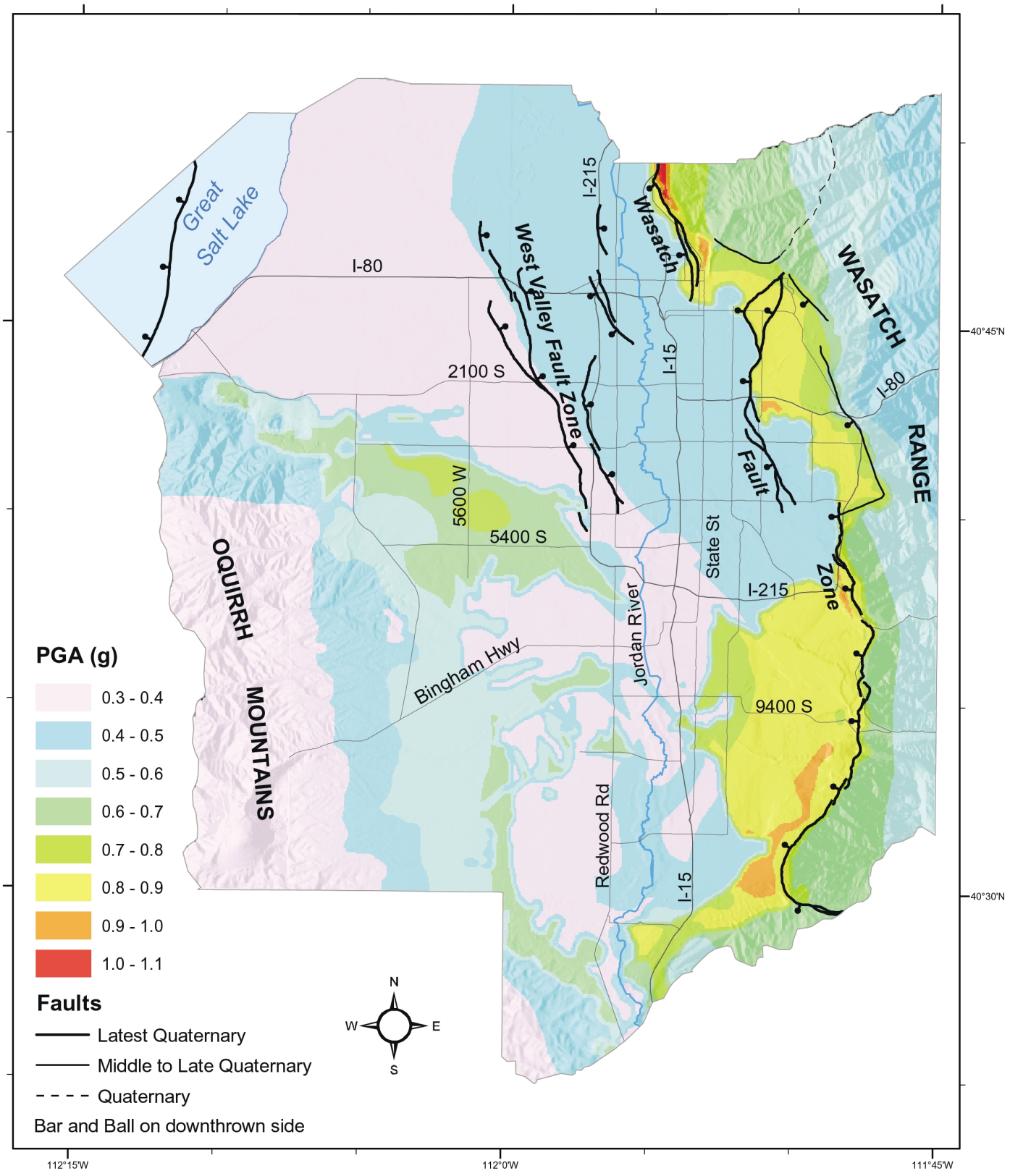

Figure 17. 2% probability of exceedance in 50 years, peak horizontal acceleration (g) at the ground surface. Simplified from Plate 7.

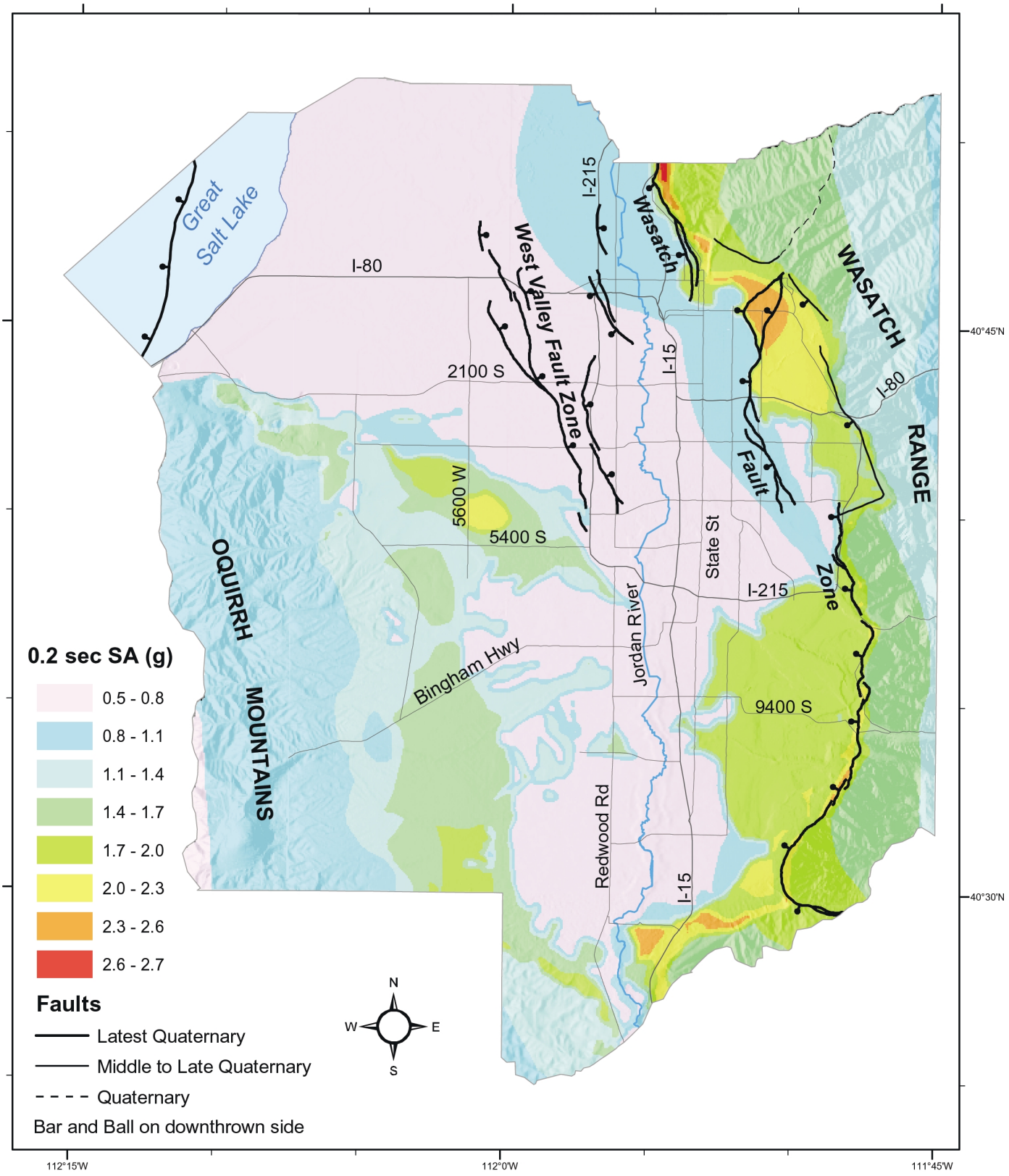

Figure 18. 2% probability of exceedance in 50 years, 0.2 sec spectral acceleration (g) at the ground surface. Simplified from Plate 8.

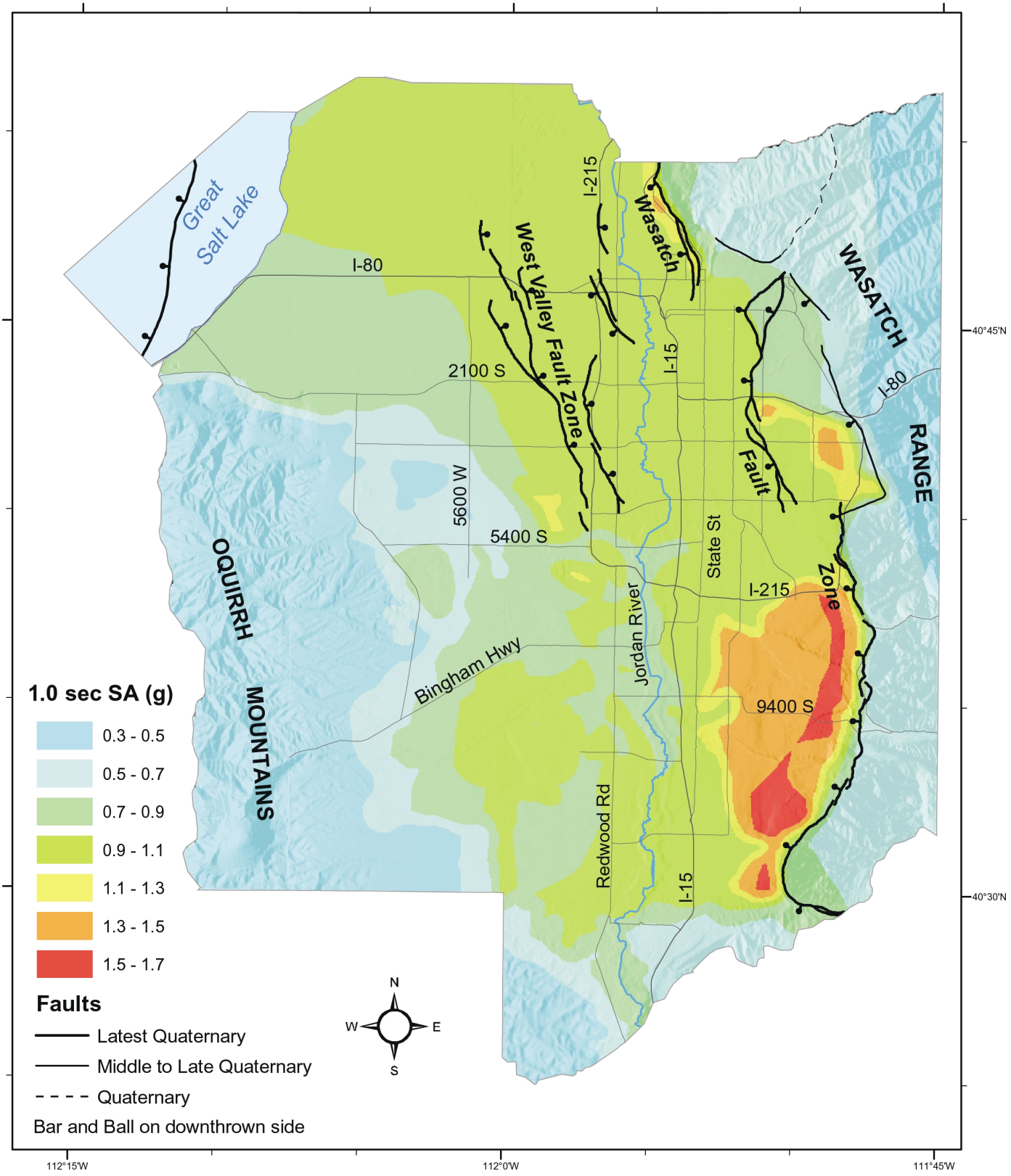

Figure 19. 2% probability of exceedance in 50 years, 1.0 sec spectral acceleration (g) at the ground surface. Simplified from Plate 9.

At 1.0 sec spectral acceleration, the highest motions (> 0.5 g) occur at the very deepest part of the valley (depths greater than 200 m; figure 4) at the north end (plate 6). The lowest long-period ground motions in the valley occur on the west side on lacustrine sands and gravels.

2500-Year Probabilistic Maps

Because of the greater range and higher probabilistic ground motions at the exceedance probability of 2% in 50 years (2,500-year return period), these hazard maps (plates 7 to 9) show more complexity than the 500-year maps. Peak horizontal accelerations exceed 1.0 g in the area of the Warm Springs fault (plate 7). Higher peak accelerations are confined to the areas of lacustrine gravels east of the East Bench fault and the Cottonwood Heights area on the southeastern margin of the valley west of the Wasatch fault. The lowest peak accelerations in the valley occur in the deep lacustrine-alluvial silts and clays in the central portion. The correspondence between peak acceleration and site-response units is dramatic.

The pattern of ground motions at 0.2 sec spectral acceleration (plate 8) is similar to that of peak acceleration. The highest values exceed 2.3 g. At 1.0 sec spectral acceleration, the highest motions (> 1.3 g) are along the eastern margin of the valley in lacustrine gravels that are more than 100 m thick (figure 5). High motions (> 0.9 g) also occur throughout the central deeper portion of the valley.

COMPARISONS WITH BUILDING CODES

In general, our maps cannot be directly compared to seismic design ground-shaking maps because our maps incorporate site effects whereas the former are for rock. Thus, to make a comparison, such as with existing building code maps, we must calculate design ground motions using the appropriate code's site coefficients and then compare these with values shown on our maps.

Currently the 1997 version of the Uniform Building Code governs the design and construction of new facilities in Utah. The seismic coefficient in the code is defined based on peak horizontal accelerations given a 10% in 50 years exceedance probability. The ISB portion of northern Utah including the Salt Lake City metropolitan area has been classified as Seismic Zone 3 with a seismic coefficient (Ca) of 0.3. The coefficient corresponds to an effective peak acceleration. For soil profile types S_C (very dense soil and soft rock) to S_E (soft soil), which occur in the Salt Lake Valley (Ashland and Rollins, 1999), the seismic coefficients range from 0.33 to 0.36. Based on our 500-year return period map for peak horizontal acceleration, most areas in our map area are in this range although some locales adjacent to the Wasatch fault exceed the seismic coefficient of 0.36 (plate 1).

The 1996 national hazard map for a 10% exceedance probability in 50 years developed by the U.S. Geological Survey (Frankel et al., 1996) shows a peak horizontal acceleration up to 0.3 g on soft rock in the Salt Lake City area. For a 2% exceedance probability in 50 years, the maps show peak accelerations up to 1.2 g. These 2,500-year maps are the basis for the design maps in the International Building Code, which is being considered for adoption in Utah. Our 2,500-year map (plate 7) shows peak horizontal accelerations only up to 1.0 g except for some very localized areas adjacent to the Wasatch fault. This difference is due principally to our use of attenuation relationships for extensional regimes compared to the USGS' use of California-based relationships. In only a few areas of the Salt Lake Valley do we believe our ground motions may exceed the USGS 2,500-year return period values.

UNCERTAINTIES

We emphasize that the ground motion values displayed on these maps may have uncertainties as large as a factor of two or more. This is due to significant uncertainties associated with all three primary inputs into the hazard analysis: (1) seismic source characterization, (2) crustal attenuation, and (3) site-response.

The greatest source of uncertainty involves the estimation of rock ground motions through the use of attenuation relationships. These uncertainties reflect the current state-of-practice in ground motion estimation as indicated, for example, in the typical scatter of strong motion data about a median attenuation relationship (see Abrahamson and Shedlock, 1997). Also topographic and basin effects on ground motions have not been addressed in our analyses. Basin effects, which are long-period in nature (> 0.5 sec), may be significant in the Salt Lake Valley (Olsen et al., 1995; 1996). The quantification of site effects is also uncertain although no systematic analyses have been performed, to our knowledge, of the level of the uncertainties. In the development of amplification factors for the San Francisco Bay and Los Angeles areas (Silva et al., 1999) and now the Salt Lake Valley, the uncertainties, as expressed by the standard deviation (σ) in natural log is about 0.3. The σ for attenuation relationships is typically 0.5 or larger.

SUMMARY

The purpose of this study was to quantify the ground shaking that might be experienced in the Salt Lake City metropolitan area in terms of both a possible scenario earthquake and values for two exceedance probabilities of building code relevance. The ground shaking resulting from a future occurrence of a **M** 7.0 earthquake rupturing the Salt Lake City segment of the Wasatch fault will be severe. Based on previous paleoseismic studies of this segment, such an event is expected to occur once on average every 1,350 years, with the most recent event having occurred shortly after 1,200 years ago. High-frequency ground shaking as characterized by peak horizontal acceleration could approach and possibly exceed 1 g in this event. Long-period spectral accelerations, without accounting for possible basin effects, will also be very strong (>1.1 g). The probabilistic maps for the 2,500-year return period are similar to the scenario maps because the Salt Lake City segment dominates the probabilistic hazard. For both the 500-year and 2,500-year return periods, the maximum peak horizontal accelerations occur immediately adjacent to the Warm Springs fault, ranging up to 0.5 g for the 500-year return period and exceeding 1 g for the 2,500-year return period.

Site effects on ground motions are dramatic on all maps

indicating both frequency-dependent amplification and deamplification as a function of sediment type and thickness. Locations in the bench areas near the Wasatch fault exhibit the highest peak accelerations due to high-frequency amplification by the stiff, relatively shallow soils and the proximity to the fault. The areas in the central portion of the valley with deep, soft lacustrine and alluvial silts and clays show lower peak accelerations due to damping, but amplified long-period ground motions at least at 1.0 sec spectral acceleration. Structures such as tall buildings and long highway overpasses, which are sensitive to long-period ground shaking, tend to be concentrated in the center of the Salt Lake Valley.

Both in terms of scenario ground motions and annual probabilities, these maps demonstrate that the Salt Lake City metropolitan area is one of the most hazardous major urban areas in the interior western U.S. We hope that these maps will raise the awareness of Utah's citizens to earthquakes in Utah and that they will assist public officials, engineers, lifeline owners, professionals involved in emergency preparedness and response, urban planners, and the public at large, in mitigating the associated hazards that will accompany future earthquakes.

ACKNOWLEDGMENTS

This study was funded by the U.S. Geological Survey under Award 98HQGR1038. Financial support was also provided by URS Greiner Woodward Clyde, the Utah Geological Survey, and Pacific Engineering & Analysis. We would like to thank many individuals who provided us data, information, and assistance including Norm Abrahamson, Jon Ake, Walter Arabasz, Bill Black, Jim Coogan, Jennifer Helm, Mike Hylland, Jon King, Craig Nelson, Dean Ostenaa, Bob Smith, and Barry Solomon. Our thanks to Fumiko Goss, Melinda Lee, Rachel Griener, Deborah Fournier, Lorraine Nelms, and Neil Storey for assisting in the preparation of this report and maps. The maps and report benefited from reviews by Walter Arabasz, Steve Bartlett, Mike Hylland, and Kimm Harty.

REFERENCES

Abrahamson, N.A. and Shedlock, K.M., 1997, Overview: Seismological Research Letters, v. 68, p. 9-23.

Abrahamson, N.A. and Silva, W.J., 1997, Empirical response spectral attenuation relations for shallow crustal earthquakes: Seismological Research Letters, v. 68, p. 94-127.

Adan, S.M. and Rollins, K.M., 1993, Damage potential index mapping for Salt Lake Valley, Utah: Utah Geological Survey Miscellaneous Publication 93-4, 64 p.

Aki, K., 1988, Local site effects on strong ground motion, *in* J.L. Von Thun (editor), Earthquake Engineering and Soil Dynamics II - Recent Advances in Ground-Motion Evaluation: American Society of Civil Engineers Geotechnical Special Publication 20, p. 103-155.

Arabasz, W.J. and McKee, M.E., 1979, Utah earthquake catalog, 1850-June 1962, *in* Arabasz, W.J., Smith, R.B., and Richins, W.D. (editors), Earthquake Studies in Utah, 1850-1978: University of Utah Seismograph Stations Special Publication, p. 119-121, 133-143.

Arabasz, W.J., Pechmann, J.C., and Brown, E.D., 1992, Observational seismology and the evaluation of earthquake hazards and risk in the Wasatch Front area, Utah, *in* P.L. Gori and W.W. Hays (editors), Assessment of Regional Earthquake Hazards and Risk Along the Wasatch Front, Utah: U.S. Geological Survey Professional Paper 1500-A-J, p. D1-D36.

Arnow, T., Van Horn, R., and LaPray, R., 1970, The pre-Quaternary surface in the Jordan Valley, Utah: U.S. Geological Survey Professional Paper 700, p. D257-D261.

Ashland, F.X. and Rollins, K., 1999, Seismic zonation using geotechnical site-response mapping, Salt Lake Valley, Utah: Utah Geological Survey unpublished Final Technical Report prepared for the U.S. Geological Survey, NEHRP Contract No. 1434-HQ-97-GR-03126, 31 p.

Baker, A.A., 1976, Geologic map of the west half of the Strawberry quadrangle, Utah: U.S. Geological Survey Miscellaneous Investigations Series Map I-931, scale 1:62,500.

Barnhard, T.P. and Dodge, R.L., 1988, Map of fault scarps formed on unconsolidated sediments, Tooele 1° x 2° quadrangle, northwestern Utah: U.S. Geological Survey Miscellaneous Field Studies Map MF-1990, scale 1:250,000.

Bjarnason, I.T. and Pechmann, J.C., 1988, Contemporary tectonics of the Wasatch Front region, Utah, from earthquake focal mechanisms: Bulletin of the Seismological Society of America, v. 79, p. 731-755.

Black, B.D., Giraud, R.E., and Mayes, B.H., 2000, Paleoseismic investigation of the Clarkston, Junction Hills, and Wellsville faults, West Cache fault zone, Utah: Utah Geological Survey Special Study 98, 23 p.

Black, B.D., Hecker, S., Jarva, J.L., Hylland, M.D., and Christenson, G.E., 2000, Quaternary fault and fold database and map of Utah: unpublished Final Technical Report to the U.S. Geological Survey by the Utah Geological Survey, Award No. 98HQGR1029, unpaginated.

Black, B.D., Lund, W.R., Schwartz, D.P., Gill, H.E., and Mayes, B.H., 1996, Paleoseismic investigation of the Salt Lake City segment of the Wasatch fault zone at the South Fork Dry Creek and Dry Gulch sites, Salt Lake County, Utah: Utah Geological Survey Special Study 92, 22 p.

Brimhall, W.H. and Merritt, L.B., 1981, The geology of Utah Lake-implications for resource management: Great Basin Naturalist Memoirs Number 5, p. 24-42.

Bruhn, R.L., Gibler, P.R., Houghton, W., and Parry, W.T., 1992, Structure of the Salt Lake segment, Wasatch normal fault zone: implications for rupture propagation during normal faulting, *in* P.L. Gori and W.W. Hays (editors), Assessment of Regional Earthquake Hazards and Risk Along the Wasatch Front, Utah: U.S. Geological Survey Professional Paper 1500-A-J, p. H1-H25.

Bryant, B., 1990, Geologic map of the Salt Lake City 30' x 60' quadrangle, north-central Utah, and Uinta County, Wyoming: U.S. Geological Survey Miscellaneous Investigations Series Map I-1944, scale 1:100,000.

Campbell, K.W., 1997, Empirical near-source attenuation relationships for horizontal and vertical components of peak ground acceleration, peak ground velocity, and pseudo-absolute acceleration response spectra: Seismological Research Letters, v. 68, p. 154-179.

Coogan, J.C. and King, J.K., 1999, Progress report – geologic map of the Ogden 30' x 60' quadrangle, Utah and Wyoming, Year 2 of 3: Utah Geological Survey Open-File Report 365.

Cornell, C.A., 1968, Engineering seismic risk analysis: Bulletin of the Seismological Society of America, v. 58, p. 1583-1606.

Crone, A.J., Machette, M.N., Bonilla, M.G., Lienkaemper, J.J., Pierce, K.L., Scott, W.E., and Bucknam, R.C., 1987, Surface faulting accompanying the Borah Peak earthquake and segmentation of the Lost River fault, central Idaho: Bulletin of the Seismological Society of America, v. 77, p. 739-770.

Davis, F.D., compiler, 1983a, Geologic map of the central Wasatch Front, Utah: Utah Geological and Mineral Survey Map 54-A, scale 1:100,000.

Davis, F.D., compiler, 1983b, Geologic map of the southern Wasatch Front, Utah: Utah Geological and Mineral Survey Map 55-A, scale 1:100,000.

dePolo, C.M., 1994, The maximum background earthquake for the Basin and Range Province, western North America: Bulletin of the Seismological Society of America, v. 84, p. 466-472.

Dinter, D.A. and Pechmann, J.C., 1999, Multiple Holocene earthquakes on the East Great Salt Lake fault, Utah: Evidence from high resolution seismic reflection data (abs.): EOS Transactions AGU, v. 80, p. F734.

Dinter, D.A. and Pechmann, J.C., 2000, Paleoseismology of the East Great Salt Lake fault: U.S. Geological Survey, National Earthquake Hazards Reduction Program Summary Technical Report, Award No. 98HQGR1013, published on the web at http://erp-web.er.usgs.gov/reports/annsum/vol42/ni/g1013.pdf, 6 pp.

Doser, D.I., 1985, The 1983 Borah Peak, Idaho and 1959 Hebgen Lake, Montana earthquakes—Models for normal fault earthquakes in the Intermountain Seismic Belt, *in* R.S. Stein and R.C. Bucknam (editors), Proceedings of Workshop XXVIII on the Borah Peak, Idaho, Earthquake: U.S. Geological Survey Open-File Report 85-290, p. 368-384.

Ellsworth, W.L., Matthews, M.V., Nadeau, R.M., Nishenko, S.P., Reasenberg, P.A., and Simpson, R.W., 1998, A physically-based earthquake recurrence model for estimation of long-term earthquake probabilities: Proceedings of the Second Joint Meeting of the UJNR Panel on Earthquake Research, p. 135-149.

Electric Power Research Institute, 1993, Guidelines for determining design basis ground motions: EPRI TR-102293, v.1.

Evans, J.P., 1991, Structural setting of seismicity in northern Utah: Utah Geological Survey Contract Report 91-5, 37 p.

Evans, J.P. and Oaks, R.Q., Jr., 1996, Three-dimensional variations in extensional fault shape and basin form: The Cache Valley basin, eastern Basin and Range Province, United States (abs): Geological Society of America Bulletin, v. 108, p. 1580-1593.

Everitt, B.L., 1995, Activity classification of the Saleratus Creek fault: Utah Division of Water Resources Memorandum dated January 3, 1995 to Dennis Strong, 5 p. plus figures.

Everitt, B.L. and Kaliser, B.N., 1980, Geology for assessment of seismic risk in the Tooele and Rush Valleys, Tooele County, Utah: Utah Geological and Mineral Survey Special Study 51, 33 p.

Forman, S.L., Nelson, A.R., and McCalpin, J.P., 1991, Thermoluminescence dating of fault-scarp-derived colluvium—deciphering the timing of paleoearthquakes on the Weber segment of the Wasatch fault zone, north-central Utah: Journal of Geophysical Research, v. 96, no. B1, p. 595-606.

Frankel, A., 1995, Mapping seismic hazard in the central and eastern United States, Seismological Research Letters, v. 66, p. 8-21.

Frankel, A., Mueller, C., Barnard, T., Perkins, D., Leyendecker, E.V., Dickman, N., Hanson, S., and Hopper, M., 1996, National seismic-hazard maps: Documentation June 1996, U.S. Geological Survey Open-File Report 96-532.

Geomatrix Consultants, Inc., 1999, Fault evaluation study and seismic hazard assessment, Private Fuel Storage Facility, Skull Valley, Utah: unpublished report prepared for Stone & Webster Engineering Corp., three volumes, variously paginated.

Gilbert, G.K., 1890, Lake Bonneville: U.S. Geological Survey Monograph 1, 438 p.

Harty, K.M., Mulvey, W.E., and Machette, M.N., 1997, Surficial geologic map of the Nephi segment of the Wasatch fault zone, eastern Juab County, Utah: Utah Geological Survey Map 170, scale 1:50,000.

Hecker, S., 1993, Quaternary tectonics of Utah with emphasis on earthquake-hazard characterization: Utah Geological Survey Bulletin 127, 157 p., map scale 1:500,000.

Helm, J.M., 1995, Quarternary faulting in the Stansbury fault zone, Tooele County, Utah, *in* Lund, W.R., (editor), Environmental and Engineering Geology of the Wasatch Front Region: Utah Geological Association Publication 24, p. 31-44.

Hopper, M.G., 2000, Isoseismals of some historical earthquakes affecting the Wasatch Front area, Utah, *in* Gori, P.L. and Hays, W.W. (editors), Assessment of Regional Earthquake Hazards and Risk Along the Wasatch Front,

Utah: U.S. Geological Survey Professional Paper 1500 K-R, p. Q1-Q25.

Hylland, M.D., Lowe, M., and Bishop, C.E., 1995, Engineering geologic map folio, Western Wasatch County, Utah: Utah Geological Survey Open-File Report 319, scale 1:24,000.

Jackson, M. E., 1988, Thermoluminescence dating of Holocene paleoseismic events on the Nephi and Levan segments, Wasatch fault zone, Utah: Boulder, University of Colorado, unpublished M.S. thesis, 149 p.

Jackson, M.E., 1991, The number and timing of Holocene paleoseismic events on the Nephi and Levan segments, Wasatch fault zone, Utah: Utah Geological Survey Special Study 78, 23 p.

Jackson, J.A., and White, N.J., 1989, Normal faulting in the upper continental crust: Observations from regions of active extension: Journal of Structural Geology, v. 11, p. 15-36.

Kayabelli, K. and West, T.R., 1995, Prediction of site-response of surficial deposits in Evansville, Indiana: Environmental & Engineering Geoscience, v. I, p. 191-206.

Keaton, J.R., 1984, Genesis-Lithology-Qualifier (GLQ) system of engineering geology mapping symbols: Bulletin of the Association of Engineering Geologists, v. XXI, p. 355-364.

Keaton, J.R., Currey, D.R., and Olig, S.J., 1993, Paleoseismicity and earthquake hazards evaluation of the West Valley fault zone, Salt Lake City urban area: Utah Geological Survey Contract Report 93-8, 55 p.

Keaton, J.R. and DeGraff, J.V., 1996, Surface observation and geologic mapping, *in* A.K. Turner and R.L. Schuster (editors), Landslides - Investigation and Mitigation: National Research Council, Transportation Research Board Special Report 247, p. 178-230.

Keefer, D.I. and Bodily, S.E., 1983, Three-point approximations for continuous random variables: Management Science, v. 26, p. 595-609.

Lund, W.R. and Black, B.D., 1998, Paleoseismology of Utah, volume 8 - Paleoseismic investigation at Rock Canyon, Provo segment, Wasatch fault zone, Utah County, Utah: Utah Geological and Mineral Survey Special Study 75, 41 p.

Lund, W.R. and Schwartz, D.P., 1987, Fault behavior and earthquake recurrence at the Dry Creek site, Salt Lake City segment, Wasatch fault zone, Utah (abs.): Geological Society of America Abstracts With Programs, v. 19, p. 317.

Lund W.R., Schwartz, D.P., Mulvey, W.E., Budding, K.E., and Black, B.D., 1991, Paleoseismology of Utah, volume 1- fault behavior and earthquake recurrence on the Provo segment of the Wasatch fault zone at Mapleton, Utah County, Utah: Utah Geological and Mineral Survey Special Studies 75, 41 p.

Mabey, D.R., 1992, Subsurface geology along the Wasatch Front, *in* P.L. Gori and W.W. Hays (editors), Assessment of Regional Earthquake Hazards and Risk Along the Wasatch Front, Utah: U.S. Geological Survey Professional Paper 1500-A-J, p. C1-C16.

Machette, M.N., 1992, Surficial geologic map of the Wasatch fault zone, eastern Utah Valley, Utah County and parts of Salt Lake and Juab Counties, Utah: U.S. Geological Survey Miscellaneous Investigations Series Map I-2095, scale 1:50,000.

Machette, M. N., Personius, S.F., and Nelson, A.R., 1992, Paleoseismology of the Wasatch fault zone – A summary of recent investigations, conclusions, and interpretations, *in* P.L. Gori and W.W. Hays (editors), Assessment of Regional Earthquake Hazard and Risk along the Wasatch Front, Utah: U. S. Geological Professional Paper 1500, p. A1-A71.

Machette, M.N., Personius, S. F., Nelson, A. R., Schwartz, D.P., and Lund, W. R., 1991, The Wasatch fault zone, Utah - segmentation and history of Holocene earthquakes: Journal of Structural Geology, v. 13, p. 137-149.

Marine, I.W. and Price, D., 1964, Geology and ground-water resources of the Jordan Valley, Utah: Utah Geological and Mineral Survey Water-Resources Bulletin 7, 63 p.

Marsell, R.E. and Threet, R.L., 1964, Geologic map of Salt Lake County, Utah, *in* Crawford, A.L. (editor), Geology of Salt Lake County: Utah Geological and Mineral Survey Bulletin 69, scale 1:63,360.

McCalpin, J.P., 1993, Neotectonics of the northeastern Basin and Range margin, western USA: Zeitschrift fuer Geomophologie N. Folge, v. 94, p. 137-157.

McCalpin, J.P., 1994, Neotectonic deformation along the East Cache fault zone, Cache County, Utah: Utah Geological Survey Special Study 83, 37 p.

McCalpin, J.P. and Forman, S.L., 1991, Late Quaternary faulting and thermoluminesence dating of the East Cache fault zone, north-central Utah: Bulletin of the Seismological Society of America, v. 81, p. 139-161.

McCalpin, J.P., Forman, S.L., and Lowe, M., 1994, Reevaluation of Holocene faulting at the Kaysville site, Weber segment of the Wasatch fault zone, Utah: Tectonics, v. 13, p. 1-16.

McCalpin, J.P. and Nelson, C.V., 2000, Long recurrence records from the Wasatch fault zone, Utah: U.S. Geological Survey, National Earthquake Hazards Reduction Program Final Technical Report, Contract No. 99HQGR0058, 61 p.

McCalpin, J.P. and Nishenko, S.P., 1996, Holocene paleoseismicity, temporal clustering, and probabilities of future large (M>7) earthquakes on the Wasatch fault zone, Utah: Journal of Geophysical Research, v. 101, p. 6,233-6,253.

McCalpin, J.P., Robison, R.M., and Garr, J.D., 1992, Neotectonics of the Hansel Valley-Pocatello Valley corridor, northern Utah and southern Idaho, *in* Gori, P.L. and Hays, W.W. (editors), Assessment of Regional Earthquake Hazards and Risk Along the Wasatch Front, Utah: U.S. Geological Survey Professional Paper 1500, p. G1-G18.

McCalpin, J.P. and Slemmons, D.B., 1998, Statistics of paleoseismic data: unpublished Final Technical Report submitted to U.S. Geological Survey by GEO-HAZ Consulting, Inc., Contract 1434-HQ-96-GR-02752, March 20, 1998, 62 p.

Meibos, L.C., 1983, Structure and stratigraphy of the Nephi NW 7 1/2-minute quadrangle, Juab County, Utah: Brigham Young University Geology Studies, v. 30, pt. 1, p. 37-58.

Mohapatra, G.K. and Johnson, R.A., 1998, Localization of listric faults at thrust ramps beneath the Great Salt Lake Basin, Utah: Evidence from seismic imaging and finite element modeling: Journal of Geophysical Research, v. 103, p. 10,047-10,063.

Nelson, A.R., 1988, The northern part of the Weber segment of the Wasatch fault zone near Ogden, Utah, *in* M.N. Machette (editor), In the Footsteps of G.K. Gilbert-Lake Bonneville and Neotectonics of the Eastern Basin and Range Province: Utah Geological and Mineral Survey Miscellaneous Publication 88-1, p. 33-37.

Nelson, A.R., Klauk, R.H., Lowe, M., and Garr, J.D., 1987, Holocene history of displacement on the Weber segment of the Wasatch fault zone at Ogden, northern Utah: Geological Society of America Abstracts with Programs, v. 19, p. 322.

Nelson, A.R. and Martin, R.A., Jr., 1982, Seismotectonic study for Solider Creek Dam, Central Utah Project: U.S. Bureau of Reclamation Seismotectonic Report 82-1, p. 115.

Nelson, A.R. and Personius, S.F., 1993, Surficial geologic map of the Weber segment, Wasatch fault-zone, Weber and Davis Counties, Utah: U.S. Geological Survey Miscellaneous Investigations Series Map I-2199, 1:50,000 scale, 22 p.

Nelson, A.R. and Sullivan, J.T., 1992, Late Quaternary history of the James Peak fault, southernmost Cache Valley, north-central Utah, *in* Gori, P.L. and Hays, W.W. (editors), Assessment of Regional Earthquake Hazards and Risk Along the Wasatch Front, Utah: U.S. Geological Survey Professional Paper 1500, p. J1-J13.

Nelson, A. R. and Van Arsdale, R.B., 1986, Recurrent late Quaternary movement on the Strawberry normal fault, Basin and Range – Colorado Plateau transition zone, Utah: Neotectonics, v. 1, p. 7-37.

Olig, S.S., Gorton, A.E., Black, B.D., and Forman, S.L., 2000, Evidence for young, large earthquakes on the Mercur fault: Implications for segmentation and evolution of the Oquirrh-East Great Salt Lake fault zone, Wasatch Front, Utah: Geological Society of America Abstracts with Programs, v. 32, p. A-120.

Olig, S.S., Gorton, A.E., and Chadwell, L., 1999a., Mapping and Quaternary fault scarp analysis of the Mercur and West Eagle Hill faults, Wasatch Front, Utah: unpublished technical report submitted to the U.S. Geologic Survey NEHRP Award No. 1434-HQ-97-GR-03154.

Olig, S.S., Gorton, A.E., and Chadwell, L.C., 1999b, Quaternary behavior along the southern Oquirrh fault zone, Utah (abs.): Association of Engineering Geologists Program with Abstracts, p. 80.

Olig, S.S., Lund, W.R., and Black, B.D., 1994, Large mid-Holocene and late Pleistocene earthquakes on the Oquirrh fault zone, Utah: Geomorphology, v. 10, p. 285-315.

Olsen, K.B., Pechmann, J.C., and Schuster, G.T., 1995, Simulation of 3-D elastic wave propagation in the Salt Lake Basin: Bulletin of the Seismological Society of America, v. 85, p. 1688-1710.

Olsen, K.B., Pechmann, J.C., and Schuster, G.T., 1996, An analysis of simulated and observed blast records in the Salt Lake Basin: Bulletin of the Seismological Society of America, v. 86, p. 1061-1076.

Ostenaa, D., 1990, Late Holocene displacement history, Water Canyon site, Wasatch fault zone [abs.]: Geological Society of America Abstracts with Programs, v. 22, p. 42.

Pechmann, J. C. and Arabasz, W. J., 1995, The problem of the random earthquake in seismic hazard analysis: Wasatch Front Region, Utah, *in* W. R. Lund (editor), Environmental and Engineering Geology of the Wasatch Front Region, 1995 Symposium and Field Conference: Utah Geological Association Publication 24, p. 77-93.

Pechmann, J.C., Nash, W.P., Vivieros, J.J., and Smith, R.B., 1987, Slip rate and earthquake potential of the East Great Salt Lake fault, Utah (abs.): EOS Transactions, v. 68, p. 1369.

Personius, S.F., 1990, Surficial geologic map of the Brigham City segment and adjacent parts of the Weber and Collinston segments, Wasatch fault zone, Box Elder and Weber Counties, Utah: U.S. Geological Survey Miscellaneous Investigations Map I-1979, scale 1:50,000.

Personius, S.F. and Scott, W.E., 1992, Surficial geologic map of the Salt Lake City segment and parts of adjacent segments of the Wasatch fault zone, Davis, Salt Lake, and Utah Counties, Utah: U.S. Geological Survey Miscellaneous Investigations Map I-2106, scale 1:50,000.

Richins, W.D., 1979, Earthquake data for the Utah region, 1850 to 1978, *in* W.J. Arabasz, R.B. Smith, and W.D. Richins (editors), Earthquake Studies in Utah, 1850-1978: University of Utah Seismograph Stations Special Publication, p. 57-251

Sadigh, K., Chang, C.-Y., Egan, J.A., Makdisi, F., and Youngs, R.R., 1997, Attenuation relationships for shallow crustal earthquakes based on California strong motion data: Seismological Research Letters, v. 68, p. 180-189.

Schuster, G.T. and Sun, Y., 1993, Surface wave inversion of near-surface shear-wave velocities in Salt Lake Valley: University of Utah unpublished Final Technical Report prepared for the U.S. Geological Survey, NEHRP Contract No. 1434-92-G-2175, 31 p.

Schwartz, D.P. and Coppersmith, K.J., 1984, Fault behavior and characteristic earthquakes - examples from the Wasatch and San Andreas fault zones: Journal of Geophysical Research, v. 89, p. 5681-5698.

Schwartz, D.P. and Lund, W.R., 1988, Paleoseismicity and

earthquake recurrence at Little Cottonwood Canyon, Wasatch fault zone, Utah, *in* Machette, M. N. (editor), In the Footsteps of G.K. Gilbert—Lake Bonneville and Neotectonics of the Eastern Basin and Range Province: Utah Geological and Mineral Survey Miscellaneous Publication 88-1, p. 82-85.

Scott, W.E. and Shroba, R.R., 1985, Surficial geologic map of an area along the Wasatch fault zone in the Salt Lake Valley, Utah: U.S. Geological Survey Open-File Report 85-448, pamphlet, 2 pls., scale 1:24,000.

Silva, W.J., Abrahamson, N.A., Toro, G., and Constantino, C., 1997, Description and validation of the stochastic ground motion model: unpublished report prepared for the Brookhaven National Laboratory.

Silva, W.J., Costantino, C., and Li, S., 1998, A quantification of nonlinear soil response for the Loma Prieta, Northridge, and Imperial Valley California earthquakes *in* Irikura, Kudo, Okada & Sasatani (editors), The Effects of Surface Geology on Seismic Motion.

Silva, W.J., Li, S. Darragh, R.B., and Gregor, N., 1999, Surface geology based strong motion amplification factors for the San Francisco Bay and Los Angeles areas: A PEARL report to PG&E/CEC/CalTrans, Award No. SA212059652.

Silva, W.J., Wong, I.G., and Darragh, R.B., 1998b, Engineering characterization of earthquake strong ground motions in the Pacific Northwest, *in* A.M. Rogers, T.J. Walsh, W.J. Kockleman, and G.R. Priest (editors), Assessing Earthquake Hazards and Reducing Risk in the Pacific Northwest: U.S. Geological Survey Professional Paper 1560, v. 2, p. 313-324.

Smith, R.B. and Arabasz, W.J., 1991, Seismicity of the Intermountain seismic belt, *in* D.B. Slemmons, E.R. Engdahl, M.D. Zoback, M.L. Zoback, and D. Blackwell (editors), Neotectonics of North America: Geological Society of North America, SMV V-1, p. 185-228.

Smith, R.B. and Bruhn, R.L., 1984, Intraplate extensional tectonics of the eastern Basin-Range: inferences on structural style from seismic reflection data, regional tectonics, and thermal-mechanical models of brittle-ductile deformation: Journal of Geophysical Research, v. 89, p. 5733-5762.

Solomon, B. J., 1996, Surficial geology of the Oquirrh fault zone, Tooele County, Utah, *in* W.R. Lund (editor), The Oquirrh Fault Zone, Tooele County, Utah: Surficial Geology and Paleoseismicity: Utah Geological Survey Special Study 88, p. 1-17.

Solomon, B.J., 1998, New evidence for the age of faulting on the West Valley fault zone: Survey Notes, Utah Geological Survey, v. 30, p. 8-13.

Solomon, B.J., 1999, Surficial geologic map of the West Cache fault zone and nearby faults, Box Elder and Cache Counties, Utah: Utah Geological Survey Map 172.

Sorensen, M.L. and Crittenden, M.D. Jr., 1979, Geologic map of the Huntsville quadrangle, Weber and Cache Counties, Utah: U.S. Geological Survey Geologic Quadrangle Map GQ-1503, 1:24,000.

Spudich, P., Fletcher, J.B., Hellweg, M., Boatwright, J., Sullivan, C., Joyner, W.B., Hanks, T.C., Boore, D.M., McGarr, A., Baker, L.M., and Lindh, A.G., 1997, SEA96-A new predictive relation for earthquake ground motions in extensional tectonic regimes: Seismological Research Letters, v. 68, p. 190-198.

Spudich, P., Joyner, W.B., Lindh, A.G., Boore, D.M., Margaris, B.M., and Fletcher, J.B., 1999, SEA99 – A revised ground motion prediction relation for use in extensional tectonic regimes: Bulletin of the Seismological Society of America, v. 89, p. 1156-1170.

Stirling, M.W., Wesnousky, S.G., and Shimazaki, K., 1996, Fault trace complexity, cumulative slip, and the shape of the magnitude-frequency distribution for strike-slip faults: A global survey: Geophysical Journal International, v. 124, p. 833-868.

Stepp, J.C., Wong, I., Whitney, J., Quittmeyer, R., Abrahamson, N., Coppersmith, K., Toro, G., Youngs, R., Savy, J., Sullivan, T., and Yucca Mountain PSHA Project Members, 2001, Probabilistic seismic hazard analyses for ground motions and fault displacement at Yucca Mountain, Nevada: Earthquake Spectra, v. 17, p.113-151.

Sullivan, J.T., Foley, L.L., Baltzer, E.M., and Krinsky, C.K., 1987, Seismic sources, maximum credible earthquakes, and related seismic hazards for Monks Hollow damsite: U.S. Bureau of Reclamation Seismotectonic Report 87-2, 35 p.

Sullivan, J.T. and Nelson, A.R., 1992, Late Quaternary displacement on the Morgan fault, a back valley fault in the Wasatch Range of northeastern Utah, *in* Gori, P.L., and Hays, W.W. (editors), Assessment of Regional Earthquake Hazards and Risk along the Wasatch Front: U.S. Geological Survey Professional Paper 1500, p. I1-I19.

Sullivan, J. T., Nelson, A.R., LaForge, R.C., Wood, C.K., and Hansen, R.A., 1988, Central Utah regional seismotectonic study: U. S. Bureau of Reclamation Seismotectonic Report 88-5, 65 p.

Swan, F.H., III, Hanson, K.L., Schwartz, D.P., and Black, J.H., 1981, Study of earthquake recurrence intervals on the Wasatch fault at the Little Cottonwood Canyon site, Utah: U.S. Geological Survey Open-File Report 81-450, 30 p.

Swan, F.H., III, Schwartz, D.P., and Cluff, L.S., 1980, Recurrence of moderate to large magnitude earthquakes produced by surface faulting on the Wasatch fault zone, Utah: Bulletin of the Seismological Society of America, v. 70, p. 1431-1462.

Tinsley, J.C., King, K.W., Trumm, D.A., Carver, D.L., and Williams, R., 1991, Geologic aspects of shear-wave velocity and relative ground response in Salt Lake Valley, Utah, *in* J.P. McCalpin (editor), Proceedings of the 27th Symposium on Engineering Geology and Geotechnical Engineering, p. 25-1 to 25-9.

Vivieros, J.J., 1986, Cenozoic tectonics of the Great Salt Lake

from seismic reflection data: M.S. Thesis, University of Utah, 99 p.

Vucetic, M. and Dobry, R., 1998, Degradation of marine clays under cyclic loading: Journal of Geotechnical Engineering, ASCE, v. 114, p. 133-149.

Wald, D.J., Quitoriano, V., Heaton, T.H., and Kanomori, H., 1999, Relationships between peak ground acceleration, peak ground velocity, and Modified Mercalli intensity in California: Earthquake Spectra, v. 15, p. 557-564.

Wells, D. and Coppersmith, K.J., 1994, New earthquake magnitude and fault rupture parameters, correlations among earthquake magnitude, rupture length, and fault displacement: Bulletin of the Seismological Society of America, v. 84, p. 974-1002.

Wesnousky, S.G., 1986, Earthquakes, Quaternary faults, and seismic hazard in California: Journal of Geophysical Research, v. 91, p. 12,587-12,631.

Wesnousky, S.G., 1990, Seismicity as a function of cumulative geologic offset: Some observations from southern California: Bulletin of the Seismological Society of America, v. 80, p. 1374-1381.

Wesnousky, S.G., 1994, The Gutenberg-Richter or characteristic earthquake distribution: Which is it?: Bulletin of the Seismological Society of America, v. 84, p. 1940-1959.

Wesnousky, S.G., Scholz, C.H., Shimazaki, K., and Matsuda, T., 1983, Earthquake frequency distribution and the mechanics of faulting: Journal of Geophysical Research, v. 88, p. 9331-9340.

West, M.W., 1994, Seismotectonics of north-central Utah and southwestern Wyoming: Utah Geological Survey Special Study 82, 93 p.

Westaway, R. and Smith, R.B., 1989, Strong ground motion in normal-faulting earthquakes: Geophysical Journal, v. 96, p. 529-559.

Wheeler, R.L. and Krystinik, K.B., 1992, Persistent and non-persistent segmentation of the Wasatch fault zone, Utah: Statistical analysis for evaluation of seismic hazard: U. S. Geological Survey Professional Paper 1500, p. B1-B47.

Wills, C.J. and Silva, W.J., 1998, Shear-wave velocity characteristics of geologic units in California: Earthquake Spectra, v. 14, p. 533-556.

Wong, I.G. and Olig, S.S., 1998, Seismic hazards in the Basin and Range Province: Perspectives from probabilistic analyses, in Western States Seismic Policy Council, Proceedings Volume, Basin and Range Province Seismic-Hazards Summit, W.R. Lund (editor): Utah Geological Survey Miscellaneous Publication 98-2, p. 110-127.

Wong, I., Olig, S., Green, R., Moriwaki, Y., Abrahamson, N., Baures, D., Silva, W., Somerville, P., Davidson, D., Pilz, J., and Dunne, B., 1995, Seismic hazard evaluation of the Magna tailings impoundment *in* W.R. Lund (editor), Environmental and Engineering Geology of the Wasatch Front Region: Utah Geological Association Publication 24, p. 95-110.

Wong, I., Olig, S., Thomas, P., Dober M., and Gerth, R., 2001a, Probabilistic seismic hazard analysis and safety evaluation earthquake ground motions, Pineview Dam, Ogden River Project, north-central Utah: unpublished final report prepared for U. S. Bureau of Reclamation.

Wong, I., Olig, S., Thomas, P., Dober M., and Gerth, R., 2001b, Probabilistic seismic hazard analysis and safety evaluation earthquake ground motions, Deer Creek Dam, Provo River Project, north-central Utah: unpublished final report prepared for U. S. Bureau of Reclamation.

Wong, I.G. and Silva, W.J., 1993, Site-specific strong ground motion estimates for the Salt Lake Valley, Utah: Utah Geological Survey Miscellaneous Publication 93-9, 34 p.

Wong, I.G., Silva, W.J., Youngs, R.R., and Stark, C.L., 1996, Numerical earthquake ground motion modeling and its use in microzonation, Proceedings, 11th World Conference on Earthquake Engineering: Pergamon (CD-ROM).

Woodward-Clyde Federal Services, 1998, Preliminary geologic hazards survey of existing, proposed, and related properties for the Metropolitan Water District of Salt Lake City: unpublished report prepared for Carollo Engineers.

Working Group on California Earthquake Probabilities (WGCEP), 1999, Earthquake probabilities in the San Francisco Bay Region: 2000 to 2030 - A summary of findings: U.S. Geological Survey Open-File Report 99-517, 34 p.

Young, G.H., 1978, Geology of the Billies Mountain Quadrangle, Utah County, Utah: Brigham Young University Geology Studies, v. 24, pt.1, p. 205-280.

Youngs, R.R. and Coppersmith, K.J., 1985, Implications of fault slip rates and earthquake recurrence models to probabilistic seismic hazard estimates: Bulletin of the Seismological Society of America, v. 75, p. 939-965.

Youngs, R.R., Swan, F.H., Power, M.S., Schwartz, D.P., and Green, R.K., 1987, Probabilistic analysis of earthquake ground shaking hazard along the Wasatch Front, Utah, *in* P.L. Gori and W.W. Hays (editors), Assessment of Regional Earthquake Hazards and Risk Along the Wasatch Front, Utah: U.S. Geological Survey Professional Paper 1500 K-R, p. M1-M110.

Zoback, M.L., 1983, Structure and Cenozoic tectonism along the Wasatch fault zone, Utah, *in* D.M. Miller, V.R. Todd, and K.A. Howard (editors), Tectonics and Stratigraphy of the Eastern Great Basin: Geological Society of America Memoir 157, p. 3-27.

Zoback, M.L., 1992, Superimposed late Cenozoic, Mesozoic, and possible Proterozoic deformation along the Wasatch fault zone in central Utah, *in* P.L. Gori and W.W. Hays (editors), Assessment of Regional Earthquake Hazards and Risk Along the Wasatch Front, Utah: U.S. Geological Survey Professional Paper 1500-A-J, p. E1-E20.

Miscellaneous Publication 02-5
UTAH GEOLOGICAL SURVEY
a division of
Utah Department of Natural Resources

ISBN 1-55791-666-7